GAS ANALYSIS OF FLUID INCLUSIONS:
APPLICATION TOWARD PRECIOUS METAL EXPLORATION,
STEEPLE ROCK MINING DISTRICT, GRANT COUNTY,
NEW MEXICO

By

Randy K. Ruff

Submitted in Partial Fulfillment of the

Requirement for the Degree of Master of Science

in Geochemistry

New Mexico Institute of Mining and Technology

Socorro, New Mexico

September 9, 1993

ABSTRACT

Fluid inclusion studies of ore deposits show gas-rich fluids, H_2S and CO_2 in particular, are associated with ore formation. These gases may form a gas-rich halo around ore deposits, and in epithermal environments, rise above a boiling zone and become trapped in fluid inclusions to provide evidence of an otherwise blind ore body. In order to test the use of fluid inclusion gas analysis for use in the exploration of precious metal deposits, 149 surface samples were systematically collected over about 35 mi^2 in the Steeple Rock mining district, New Mexico.

The Steeple Rock mining district is host to scattered epithermal-vein, volcanic-hosted, Au-Ag-base metal deposits. Extensive areas of acid-sulfate alteration and silicification along the northwest striking Summit-East Camp fault has maintained an exploration interest in the district. Steeple Rock offers excellent exposure of apparent barren mineralization and mineralization associated with mines. Fluid inclusions are analyzed by crushing the sample under a high vacuum, releasing the volatiles directly into a fast-scanning quadrupole mass spectrometer. Methane, H_2O, H_2S, Ar, C_nH_n, CO_2, and SO_2 were analyzed with a lower detection range of about 5 ppm (molar) for trace gases. The concentration range of minor and trace gases exhibit a sample to sample variation of 2 to 3 orders of magnitude.

Statistical treatment of fluid inclusion gas data

defines anomalous concentrations and indicates ratios involving combinations of CH_4, CO_2, H_2S, and SO_2 concentrations are the most useful gases for defining anomalies. Ternary composition plots of CO_2, CH_4, and total S suggest boiling is the dominant factor controlling gas compositions. Sulfur dioxide is detected in most of the analyses SO_2/H_2S ratios > 2 in about 15% of the analyses. District-scale contour plots of gas ratios show that well constrained anomalies occur along the Summit vein, Telephone Ridge - Raeburn Hills, and East Camp mine along the Summit-East Camp fault. These anomalies represent degassed S-rich upwelling fluids with marginal CO_2-rich fluids. The upwelling S-rich fluids are spacially proximal to or coincident with known precious metal mineralization. The largest anomaly occurs at Telephone Ridge in the center of the district and does not include the adjacent base-metal-rich Carlisle-Center mine group. This spacial relationship may suggest fluid mixing with marginal fluids may be important in the formation of base-metal rich ore.

PREFACE

Gas analysis of fluid inclusions as part of detailed studies of ore deposits can be useful in developing genetic models for ore deposition. Recent advancements in the sensitivity and speed of quadrupole mass spectrometers facilitate rapid analysis of fluid inclusions and suggest a

potential application toward the exploration for ore deposits. At present commercial labs do not offer fluid inclusion gas analysis; however, the cost of such analysis would be comparable to standard lithogeochemical analysis. This document presents results from a project designed to test the applicability of fluid inclusion gas analysis for exploration of epithermal precious metal ore deposits.

Chapter 1 is an introduction to gases in geothermal and epithermal systems. Geothermal systems are shown to have discrete fluid-gas regimes. Dissolved gases are shown to have active roles in metal solubilities and may provide a geochemical signature in fluid inclusions well above an ore zone.

Chapter 2 presents the results of a case study from the Steeple Rock and Duncan mining districts. An exploration approach is taken in which fluid inclusion gases are analyzed from surface samples collected throughout the Steeple Rock and Duncan districts. Minimal sample preparation and utilization of a fast-scanning quadrupole mass spectrometer allow relatively rapid acquisition of fluid inclusion gas analysis. The results from this study suggest fluid inclusion gas analysis does have potential for exploration use. As a tool for exploration, fluid inclusion gas analysis may be most advantageous when used in epithermal systems with shallow erosional levels.

TABLE OF CONTENTS

LIST OF FIGURES

LIST OF TABLES

LIST OF FIGURES IN APPENDICES

LIST OF TABLES IN APPENDICES

ACKNOWLEDGEMENTS

CHAPTER 1

INTRODUCTION TO GASES IN GEOTHERMAL AND

EPITHERMAL SYSTEMS

INTRODUCTION

The gas geochemistry of near-surface hydrothermal fluids reflect the deep reservoir pH and redox conditions, along with the effects of boiling and/or mixing during their ascent. Studies of the gas compositions of volcanic emissions (Gerlach, 1980a, 1980b, 1982; Giggenbach, 1982), oil field brines (Sverjensky, 1987), and geothermal systems (Giggenbach, 1980; Giggenbach and Glover, 1992), indicate that fluids from these very different geologic settings have distinct gas compositions. Studies of metal transport and precipitation suggest gas chemistry plays an important role in ore formation. Microscopic samples of hydrothermal fluids are trapped in imperfections in precipitating minerals as vapor and liquid inclusions. Analysis of gases in fluid inclusions may provide insight into the unique chemistry and/or processes required to form an ore deposit.

The analysis of gases in fluid inclusions is hindered by the small size of fluid inclusions (typically < 20 micron diameter) and their resulting small sample sizes (10^{-5} – 10^{-6} micromoles for typical crush analysis). In addition, gases of interest are commonly present in the ppm (by moles) concentration range. The instrument of choice for measuring fluid inclusion gases is the quadrupole mass spectrometer (QMS). The QMS can scan a broad AMU (AMU = atomic mass unit or mass/e^{-} ratio) range and is sensitive enough to measure ppm concentrations.

Epithermal mineralization is favorable for the study of fluid inclusion gases for two reasons: 1) The study of active geothermal systems provides a basic analog for fluid chemistry and processes in the near-surface environment and 2) the dramatic effect of chemical and physical processes that occur in the near-surface environment should be reflected by the distribution of fluid inclusion gas compositions.

ROLE OF GASES FOR METAL SOLUBILITIES

Studies of epithermal ore deposits and active geothermal systems suggests ore formation involves deep upwelling fluids that boil and/or mix with cooler marginal or shallow waters in the near-surface environment (< 2 km). Thermodynamic modelling of ore fluids illustrate the importance of dissolved gases (i.e. CO_2, H_2S) on mineral solubilities and the active role gases play for the precipitation of minerals during boiling (Drummond and Ohmoto, 1985; Reed and Spycher, 1985). The pH and redox conditions of deep geothermal fluids represent mineral-fluid equilibria in a reservoir (Giggenbach, 1980). As these fluids ascend toward the near-surface environment, redox and pH changes due to mixing, and more dramatically, boiling are viable ore deposition mechanisms (Drummond and Ohmoto, 1985; Reed and Spycher, 1985). Mixing, which can be considered a dilution process in most cases, of deep-upwelling fluids

with more oxidized surface waters will destabilize Cl⁻ base-metal complexes through cooling, which is a more important factor than dilution or oxidation. Temperature has little effect on gold bisulfide (HS^-) complexes, however oxidation of HS^- to sulfate (SO_4^{2-}) can destabilize Au, Ag, or Cu HS^- complexes (Reed and Spycher, 1985). Sulfide-rich fluids are capable of carrying gold from the deep reservoir up to the hot-spring environment if cooling and some boiling are the dominant processes affecting the fluid. Boiling strongly partitions the acid-forming gas CO_2 and into the vapor phase and thus increasing the pH of the fluid according to the following reaction (Drummond and Ohmoto, 1985; Reed and Spycher, 1985):

$$HCO_{3\,(aq)}^- + H^+_{(aq)} \longrightarrow H_2O_{(aq)} + CO_{2(g)}$$

Upon further boiling significant amounts of H_2S partition to the vapor phase destabilizing HS^- complexed metals (Drummond and Ohmoto, 1985; Reed and Spycher, 1985):

$$HS^-_{(aq)} + H^+_{(aq)} \longrightarrow H_2S_{(g)}$$
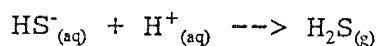
Boiling and mixing can result in cooling, which destabilizes chloride complexes (Cl⁻) and causes sulfide and carbonate minerals to precipitate; two examples follow:

$$Zn^{2+}_{(aq)} + HS^-_{(aq)} \longrightarrow ZnS_{(s)} + H^+_{(aq)}$$

$$Ca^{2+}_{(aq)} + HCO_{3\,(aq)}^- \longrightarrow CaCO_{3(s)} + H^+_{(aq)}$$
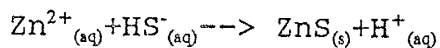
(Reed and Spycher, 1985). Gold is thought to be transported as a HS^- complex even in acidic and saline fluids with the

solubility best expressed by:

$$Au_{(s)}+2H_2S_{(aq)}=Au(HS)^-_{2(aq)}+.5H_{2(g)}+H^+_{(aq)}$$
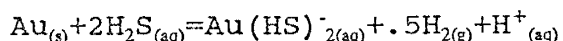
(Hayashi and Ohmoto, 1990). The above reaction indicates that upon boiling, increasing pH and H_2S partitioning to vapor are competing effects on the stability of $Au(HS)^-_2$. Models of the effect of boiling on Au solubility indicates Au solubility increases initially followed by a sharp decrease as H_2S is degassed and/or fixation of HS^- into Cl^- complexed metals (Drummond and Ohmoto, 1985; Reed and Spycher, 1985).

GAS-FLUID REGIMES IN GEOTHERMAL SYSTEMS

Studies of the shallow parts of active geothermal systems defines three end-member type fluids: deep upflow fluids, CO_2- rich marginal fluids, and acidic steam-heated surface waters (Hedenquist, 1989,1991; Henley, 1985; Glover, 1970). The deep upflow fluids would be expected to have equilibrium gas compositions representative of the reservoir conditions only if they have not boiled assuming steam separation occurs (Giggenbach, 1980). As fluids ascend and boil, gases partition to the vapor phase at different rates according to Henry's Law which describes gas solubilities. The more volatile gases partition into the vapor phase at a faster rate than the more soluble gases for example N_2 (less soluble) is followed by CH_4, CO_2, H_2S, SO_2 (more soluble)

(Drummond and Ohmoto, 1985). Giggenbach and Glover (1992) find a systematic variation in gas compositions of deep-upwelling fluids that reflect the degree of degassing and gas solubilities with distinctive fluids containing "late" vapor with a higher proportion of the more soluble gases (i.e. H_2S) relative to fluids containing "early" vapor. This observation suggests that as ascending fluids boil, vapor may rise independently of the fluid. CO_2-rich waters are also HCO_3^--rich, and may mix with deep-upwelling fluids to deposit metalliferous ore and gangue calcite (Hedenquist, 1990). Surface steam-heated waters can be acidic from oxidation of H_2S in the vadose zone and would be expected to have a N_2/Ar ratio equivalent to air-saturated meteoric water (Giggenbach, 1980). These acidic and oxidizing fluids may mix with deep-upflow fluids to deposit ore (Spycher and Reed, 1989) although deep downward circulation of surface-waters is problematic given the hydrologic recharge and discharge anatomy of many active geothermal systems (Hedenquist, 1991). Fluid inclusion freezing point depression (T_m) and temperature of homogenization (T_h) data in authegenic minerals from the Broadlands-Ohoaki geothermal system suggests that boiling and dilution patterns from the past are similar to those present today, providing an indication of steady-state behavior for thermal and salinity fluid characteristics (Brown, et al., 1976; Hedenquist, 1990).

FLUID INCLUSION GAS ANALYSIS

Fluid inclusion gas analysis is a relatively recent field of study that has advanced beyond the experimental stage. A recent volume of the Journal of Exploration Geochemistry is dedicated to the current state of the art applications of gas analysis of fluid inclusions to ore deposit studies (Jor. Expl. Geochem., 1991, v.42, No.1). Gas analysis of fluid inclusions from epithermal mineralization demonstrate a positive correlation between H_2S/CO_2 ratios and proximity to ore mineralization (Landis and Hofstra, 1991; Norman et al., 1991; Graney, et al., 1991). Anomalous N_2 and CO_2 in fluid inclusions above ore mineralization has been cited as evidence for boiling and an indicator of ore deposition at depth (Norman et al., 1991; Kesler, et al., 1986). Graney et al. (1991) analyzed jasperoid-hosted fluid inclusions from the Carlin and Standard deposits in Nevada and found N_2/Ar ratios of air-saturated meteoric water that suggests meteoric waters were involved in ore deposition.

Fluid inclusion gas analysis may provide evidence for a magmatic component to mineralizing fluids in epithermal environments where dilution with meteoric water hinders isotopic interpretations. Hedenquist's (1991, 1993) study of geothermal systems in Japan and New Zealand suggests that hot magmatic fluids may be a required metal source which then must interact with meteoric water and undergo focused

flow to form suitable conditions for an ore deposit to form. Analysis of fumarole vapors indicate that certain gases, such as CO_2, H_2, SO_2, HCl, and HF, are part of a distinct magmatic assemblage (Gerlach, 1980a, 1980b, 1982; Giggenbach, 1982; Marty and Giggenbach, 1990). Giggenbach and Glover (1992) use relative N_2, Ar, and He concentrations to discriminate between "rift"-type and "arc"-type tectonic settings for geothermal systems in the Taupo Volcanic Zone, New Zealand. Their study implies a magmatic component to these geothermal systems and that the difference between basaltic and andesitic contributions can be discerned. Magro and Pennisi (1991) document relative changes in noble gases and N_2 concentrations over a 10 year period from Vulcano, Italy, showing a trend from magmatic-dominated vapors to increasing atmospheric contributions from air-saturated meteoric water. Further studies of fluid inclusion gases that focus on unreactive species may be able to discriminate source components in hydrothermal fluids (i.e. magmatic component).

Recent advancements in the speed and sensitivity of Quadrupole mass spectrometers (QMS) now enables gas analysis of individual or small numbers of fluid inclusions (Landis and Hofstra, 1991; Jones and Kesler, 1992). This allows more paragenetic control of analyses and possibly better chemical characterization of ore-bearing fluids. Studies of unreactive gases in volcanic emissions, geothermal systems,

and in fluid inclusions may provide insight into the source
of various components of ore deposits. Fluid inclusion gas
analysis, in the context of detailed study of epithermal ore
deposits, contribute to the development of conceptual ore
deposit models (Landis and Hofstra, 1991; Norman, et al.,
1991). These ore deposit models can then be used in
exploration programs. Empirical studies of fluid inclusion
gases, comparing barren mineralization to known ore
mineralization, can define guidelines but often do not
provide "vectorable" results (Haynes and Kesler, 1988;
Graney, et al., 1991). In Chapter 2, results from a
district-scale study of fluid inclusion gases are presented
in the context of an exploration perspective.

CHAPTER 2

A PAPER TITLED "GAS ANALYSIS OF FLUID INCLUSIONS: APPLICATION TOWARD PRECIOUS METAL EXPLORATION, STEEPLE ROCK MINING DISTRICT, GRANT COUNTY, NEW MEXICO

INTRODUCTION

Epithermal mineralizing systems commonly contain broad areas of alteration and mineralization with ore mineralization more limited in areal and vertical extent. In epithermal mineralizing systems, structural control and dynamic physio-chemical processes affect hydrothermal fluids in the near-surface environment and may prevent development of a broad lithogeochemical anomaly. Deep reservoir fluids boil and mix as they ascend to the near-surface environment. Thermodynamic models of ore fluids illustrate the effectiveness of boiling as an ore depositing process (Drummond and Ohmoto, 1985; Reed and Spycher, 1985). As a fluid boils gases partition to the vapor phase and may rise well above the ore horizon. Fluid inclusions are microsamples of hydrothermal fluids and vapor trapped in precipitating minerals. Gas analysis of fluid inclusions provides direct evidence of fluid chemistry and/or processes and may provide evidence of otherwise blind boiling zones.

Fluid inclusion gases can be quantitatively analyzed using a quadrupole mass spectrometer (QMS). A QMS is sensitive and stable over a broad AMU range. Previous studies have measured CO_2, N_2, Ar, CH_4, H_2S, SO_2, and H_2O among other gases in fluid inclusions. Advancements in the sensitivity and speed of QMS now enable analysis of single or small numbers of inclusions. In this study a fast-scanning QMS, with an attached manifold of three sample crushers is utilized

to analyze fluid inclusion gases using a method that facilitates rapid data acquisition.

Epithermal mineralization may provide the optimum setting to test fluid inclusion gas analysis as a tool for exploration because; (1) studies of active geothermal systems provide analogs of fluid-gas regimes and (2) rapid physical and chemical changes in the near-surface environment affect gas compositions. Studies of active geothermal systems suggest boiling strongly influences gas compositions and distributions in the shallow parts of geothermal systems, typically creating degassed H_2S-rich upflow zones and marginal CO_2-rich fluids (Hedenquist, 1991; Giggenbach and Glover, 1992). Fluid inclusion gas analysis may be able to delineate fluid-gas regimes in epithermal mineralization by locating zones of deep upwelling fluids which would be favorable settings for ore deposition.

The Steeple Rock mining district in southwest New Mexico, is comprised of scattered epithermal vein-hosted precious and base-metal ore deposits hosted in Tertiary volcanics. Extensive areas of acid-sulfate alteration and silicification proximal to vein deposits have maintained exploration interest for bulk-mineable ore potential. Steeple Rock offers excellent exposure of apparent barren mineralization and mineralization related to ore deposits.

GEOLOGIC SETTING

REGIONAL GEOLOGY

The Steeple Rock mining district is located in the Summit Mountains, near the southwest boundary of the Mogollon-Datil volcanic field and southern Basin and Range province (Fig. 1). The Mogollon-Datil volcanic field is part of a discontinuous belt of silicic volcanic fields that extends from the Sierra Madre-Occidental of Mexico to the San Juan volcanic field of Colorado (Ratte', et al., 1989). The Summit Mountains are comprised of flows, ash-flow tuffs, and vents of Oligocene calc-alkaline rocks intruded by Miocene high-silica rhyolites (Wahl, 1980; Mclemore and Clark, 1993). The volcanic section rests on early Tertiary- upper- Cretaceous volcaniclastic sequence that uncoformably overlies upper Cretaceous Colorado Formation and Beartooth Quartzite (Hedlund, 1990b). The Beartooth Quartzite lies unconformably on Precambrian granite at Riley Peaks, approximately 12 km south of the Steeple Rock mining district (Hedlund, 1990b).

The extensional structural fabric of the Mogollon-Datil volcanic field differs from that of the Southern Basin and Range in that it is less systematically oriented (Chapin and Seager, 1975; McIntosh et al., 1992). This suggests extension in the Mogollon-Datil volcanic field was inhomogenously distributed and of less magnitude relative to extension in the southern Basin and Range (Chapin and Seager, 1975; McIntosh, 1992). Structure in the Steeple Rock mining district is
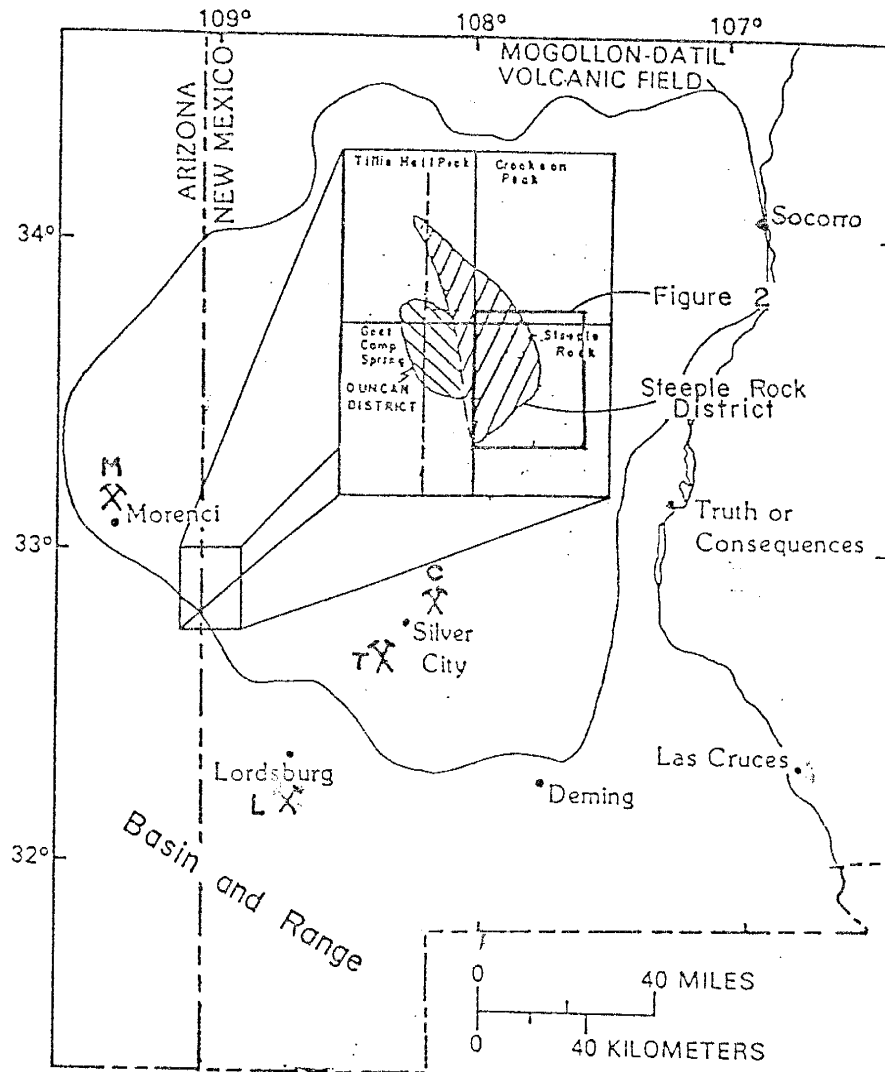
FIGURE 1. Location map for the Steeple Rock and adjacent
Duncan fluorspar mining districts. Most of the precious metal
mineralization occurs in the area of the box labelled Figure
2. Fluorite veins occur in the Duncan district and in the
north part of the Steeple Rock district. The box labelled
Figure 2 is the area of interest for this study and is
enlarged in Figure 2. M, T, and C represent the Morenci,
Tyrone, and Chino copper porphyrys respectively. L is the
Lordsberg Au-Cu vein district. Boundary for the Mogollon-
Datil volcanic field is from Ratte' et al. (1989).

dominated by northwest striking normal faults that are concordant with the structural fabric of the southern Basin and Range. The region surrounding the Steeple Rock mining district includes the Morenci, Tyrone, and Chino Cu-porphyrys. The Lordsberg district is comprised of Cu-Au vein deposits (Fig. 1).

GEOLOGY OF THE STEEPLE ROCK MINING DISTRICT

Volcanic flows, flow breccias, and intrusives of with interbedded ash-flow tuffs and localized volcaniclastic rocks comprise the bulk of outcrops in the Steeple Rock mining district. Hedlund (1990a) divides the rocks into two general map units: the Dacite of Summit Mountain, dated at 31-32 Ma (K-Ar), which is overlain by the Basaltic and Andesitic Rocks of Dark Thunder Canyon and Interlayered Silicic Tuffs. Both map units have localized sandstone members and interbedded ash-flow tuffs. Distinctive ash-flow tuffs are useful in recognizing rotated and repeated sections. The Bloodgood Canyon Tuff, dated at 28.05 ±0.04 Ma (Ar-Ar) (McIntosh, et al., 1992), is the most confidently correlated and is interbedded in the Dacite of Summit Mountain. Rhyolite dikes and plugs (18-21 Ma; zircon fission tracks, Hedlund, 1990) have intruded along northwest striking faults at various localities throughout the Steeple Rock mining district and are more densely exposed in the western part.

Northwest striking normal faults bound half-grabens that

dip 10°-20° northeast. The most prominent of these structures is the Summit-East Camp fault with a northwest strike and is traceable for 29 km with a splayed northern terminus (Fig. 2). The Carlisle fault is a west-northwest striking fault in the center of the district near the Summit-East Camp fault. The largest base- and precious- metal deposits occur along the Summit-East Camp and Carlisle faults. Discrete areas of acid-sulfate alteration also occur proximal to the Summit-East Camp fault (Fig. 2).

MINERALIZATION AND ALTERATION

The Steeple Rock mining district has produced precious- and base- metals from vein deposits almost continously from 1880 to 1992. Approximately total production as reported by McLemore (in prep., 1993) is as follows: 1,200,000 lbs Cu, 151,000 oz Au, 3,400,000 oz Ag, 5,000,000 lbs Pb, and 4,000,000 oz Zn from 365,000 short tons of ore. The Carlisle-Center group of mines on the Carlisle fault, and the East Camp group of mines have dominated production in the Steeple Rock mining district (Fig. 2). The Carlisle-Center mine group is base-metal rich (Cu, Pb, Zn) with Au and Ag ore. The Summit mine and East Camp mines (Fig. 2) located northwest and southeast respectively from the Carlisle-Center mine group, have lower base-metal grades. Discrete areas of advanced argillic alteration and silicification, located along the Summit-East Camp fault, have been drilled and found to contain

Figure 2 (next page). Map of the Steeple Rock mining district showing faults, mines, sample locations, and areas of acid sulfate alteration. Fault locations are taken from Hedlund (1990b). Abbreviations are: NYG= New Years Gift mine; A= Alabama mine; C-C= Carlisle Center mine group; TR= Telephone Ridge; RH= Raeburn Hills; S= Summit mine; S-EC Fault= Summit - East Camp fault, and EC= East Camp mine.

109°00'

108°54'48"

32°53'07"

N

S

RH

Bluebell vein

TR

S-EC Fault

C-C

EC

NYG

A

Steeple Rock
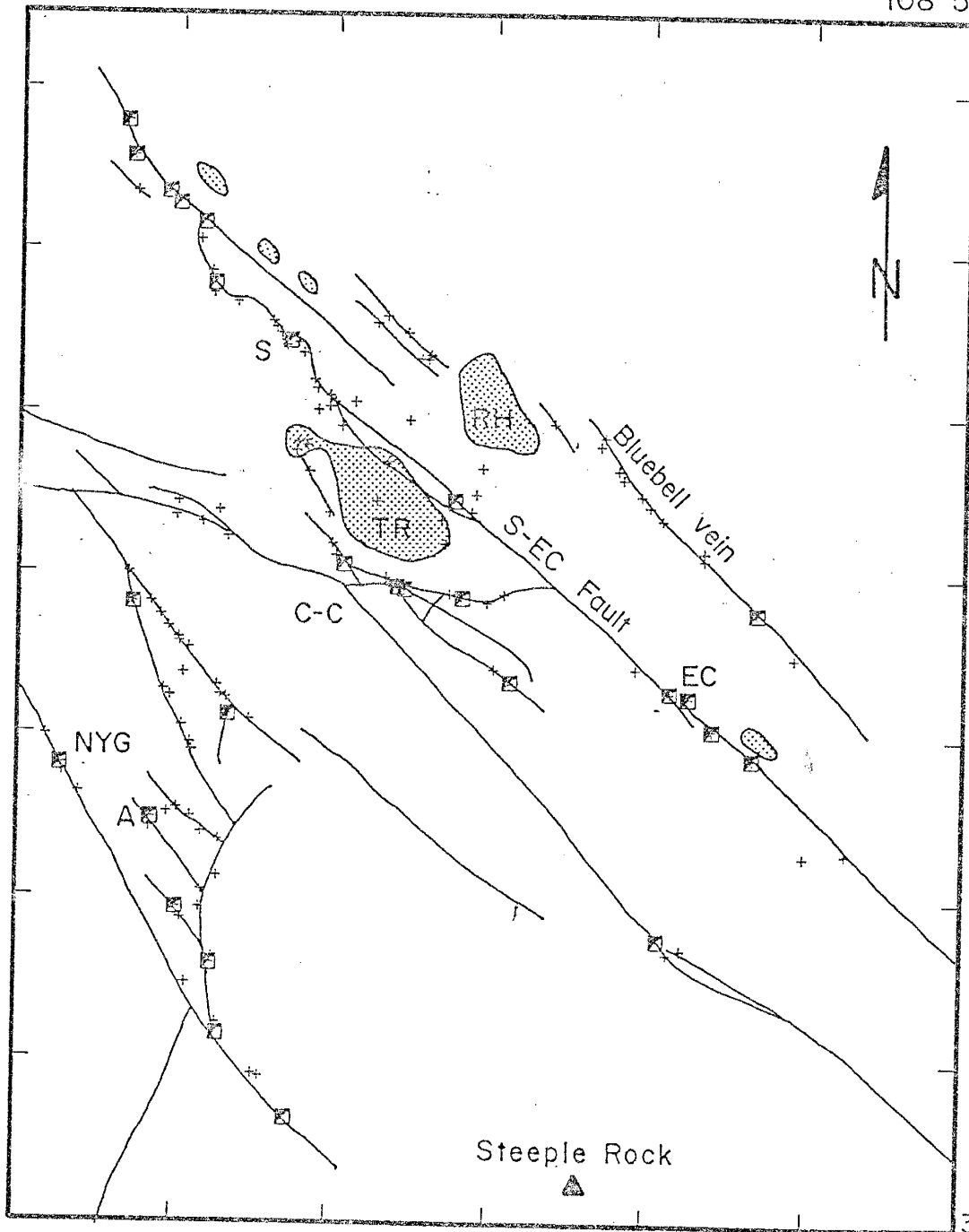
32°47'36"

Legend

Fault

Mine

+ Sample Location

Acid Sulfate Alteration

Scale

0 1 2 mi

0 1 2 3 km
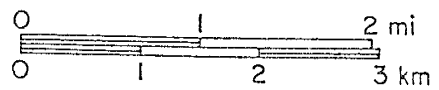
anomalous but uneconomic Au grades (Fig. 2). A Biron Bay Resources Ltd.-Nova Gold exploration and drilling program conducted during 1988-1992 have reported discovery of a 1 M st deposit of 0.18 oz/st Au and 11.6 oz/st Ag at depth on the Summit Vein and a parallel vein.

Veins in the Steeple Rock mining district are structurally controlled by northwest striking, and in the case of the Carlisle-Center vein, west-northwest striking faults (Fig. 2). Rhyolite dikes and plugs are also structurally controlled and often host veins in brecciated margins. Veins throughout the district exhibit textures characteristic of epithermal mineralization; vuggy open space fillings, brecciation and crustification, coxcomb quartz with fine-grained encrusted sulfides, multiple banding of successive quartz generations often including chalcedony, quartz replacements of bladed calcite, and late-stage vein filling calcite and vug-filling amethystine quartz. Veins exhibit crystalline quartz occurring as intersecting blades up to 2 cm in length at several localities in the Steeple Rock mining district. This texture is commonly observed in epithermal mineralization. Simmons and Christenson (1990) studied bladed calcite from the Broadlands-Ohaaki geothermal system, New Zealand, and suggest that initial boiling and CO_2 degassing causes rapid precipitation of bladed calcite. Further boiling and cooling may saturate the fluid with respect to quartz and increase the solubility of calcite leading to calcite

replacement by quartz (Simmons and Christensen, 1990).

Gangue minerals include quartz, pyrite, chlorite, calcite, and locally illite/smectite and adularia (McLemore and Clark, 1993). Ore minerals are galena, sphalerite, chalcopyrite, bornite, and various Au and Ag minerals (McLemore and Clark, 1993). McLemore and Clark (1993) report fluid inclusion homogenization temperatures 288°-325° C for inclusions in sphalerite and 180°-310° C homogenization temperatures from quartz-hosted inclusions. Fluid inclusions from one sample of quartz associated with sulfides from the Imperial Mine contain liquid + vapor inclusions that homogenize to liquid at an average of 250° C. Cutting the primary inclusions is a plane of pseudo-secondary vapor-filled inclusions that suggest a boiling event. Wahl (1983) reports a date of 18 Ma (K-Ar) from an adularia-rich sample from the East Camp vein suggesting vein formation closely followed rhyolite dike intrusion.

Veins or vein segments display distinctive structures and textures systematically distributed throughout the district. The Carlisle-Center vein and the East Camp vein are 10 - 15 m thick at the surface and comprised of massive quartz, commonly vuggy, with zones of brecciation and abundant host-rock clasts. Griggs and Wagner (1966) describe an apparent vertical metal zonation of the Carlisle mine with the best Au-Ag grades occurring the vuggy top part of the veins above base-metal-rich ores (0.7% Cu, 3% Pb, 3% Zn). The Au-Ag

mineralization may not be related to the same mineralizing event responsible for the deeper base-metal mineralization (Griggs and Wagner, 1966). The Summit and Bluebell veins have vein segments with colloform banded chalcedony and quartz with late vein-filling calcite. The veins at the north end of the Summit-East camp structure are in shears and breccias within broad zones of massive silicification. At the Alabama Mine area, in the western part of the district, the veins are commonly hosted in the brecciated margins of rhyolite dikes with a late hematite-quartz matrix common.

Alteration associated with the veins is propylitic to argillic and a non-uniform sericitic alteration that ranges from 0-2 m from the vein (Hedlund, 1990b; Mclemore and Clark, 1993). Discrete areas of advanced-argillic alteration and silicification are distributed along the Summit-East Camp structure (Fig. 2). Veins and vein alteration appear to cut the advanced-argillic alteration. Detailed work by Mclemore and Clark (1993) on the advanced-argillic alteration and silicification at the Telephone Ridge defines an apparent vertical (up) and inward zonation from illite/smectite to kaolinite-illite to kaolinite to pyrophyllite-diaspore-kaolinite to alunite-kaolinite to quartz-kaolinite with local anatase and pyrophyllite. This mineral assemblage is classified as an acid-sulfate alteration in which H_2SO_4 is the acidic component causing extreme base leaching of the host rock (Knight, 1977; Rye, et al., 1992). The rocks at

Telephone Ridge in the central part of the district, have been acid-sulfate altered and are capped by highly silicified rocks (Fig. 2). Where relict textures are preserved, breccias, clastic units, and rare lava flows were the host rock for silicification and appear to exhibit a stratigraphic control. Many of the altered areas along the Summit-East Camp structure are capped by silicified rocks with apparent stratigraphic control. Bazrafshan and Norman (unpublished report, 1988, with permission) measured temperature of homogenization and freezing point depressions of 110 fluid inclusions from 12 samples of quartz from the silicified cap on Telephone Ridge. Temperature of homogenization range 215°-299° C with a median at 246° C and a mean equivalent weight % NaCl of 0.58.

DUNCAN FLUORSPAR DISTRICT

Significant fluorite occurs in veins in the northern-most part of the Steeple Rock mining district and to the west in the Duncan Fluorspar district. The Duncan Fluorspar district is a group of small mines 3.5-8.5 km west of the Steeple Rock mining district with limited historic fluorite production (Fig. 1). North and northwest striking faults host fluorite and quartz veins with trace sulfides reported (Hedlund, 1990b). Veins are locally hosted in rhyolite dike margins. In the vicinity of Goat Camp Spring, intense acid sulfate alteration is present and cut by fluorspar veins. Hedlund (1990b) and McLemore and Clark (1993) propose fluorite vein

formation was contemporaneous with, or late stage to, precious metal mineralization at Steeple Rock.

ANALYTICAL METHODS

Fluid inclusion gas analysis can be a time-intensive laboratory procedure involving thermal decrepitation or mechanical crushing in a high-vacuum extraction line and a Quadrupole mass spectrometer (QMS) to quantitative analyze the gas mixtures. One method involves cryogenically separating gas fractions and water, whereupon each gas fraction is analyzed separately (Norman and Sawkins, 1987). Modern fast-scanning quadrupole mass spectrometers (QMS), have increased sensitivity and scan speeds of milliseconds per AMU that enables real-time analysis of released fluid inclusion volatiles from single or small numbers of inclusions (Jones and Kesler, 1992; and Landis and Hofstra, 1991). In this study, rapid analysis of fluid inclusion volatiles are obtained by crushing samples in modified MDC high-vacuum valves and releasing the fluid inclusion volatiles directly into a fast-scanning QMS. A manifold with three crushers, all with equal path-lengths to the ion source, decreases the overall pump-down time per sample. Analyses are made under dynamic pumping conditions and without a leak valve between the crushers and the QMS to maximize vacuum conductance. The manifold and crushers are kept at lab-temperature except during pump-down. Routine

crush analysis give a lower limit in the 5 ppm range for trace gases. This method gives a bulk analysis of fluid inclusions that may include inter-granular inclusions, and desorbed gas release (see below) in addition to primary and secondary inclusions. Mechanical crushing to release fluid inclusion volatiles avoids the potential of thermal decomposition of host or included minerals, high-temperature gas reactions, and pyrolysis that may occur with thermal decrepitation release methods. In addition, vapor-filled inclusions with shallow sloped isochores that may not decrepitate can be analyzed by crushing.

A Balzers model QMG 125 QMS equipped with a secondary electron multiplier (SEM) detector is used to analyze the fluid inclusion gases. The QMS is computerized for instrument control and data acquisition. The ion source is set at 100 EV and the SEM operated at 1900 volts. Up to 16 user specified AMUs that can be independently set to various scan-speeds with a maximum speed of 0.5 millisecond/AMU. To decrease cycle time, 9-12 AMUs were selected with scan speeds set at 5-50 milliseconds/AMU depending on the abundance of the gas species. Each sample is crushed and recrushed a total of three times during 500 cycles which last from 1 to 2 minutes depending on the scan speed. An actual computer graphics display is shown in Figure 3 with AMU intensities of 18, 34, and 44, the major peaks for H_2O, H_2S, and CO_2 respectively, plotted against cycles (time) for
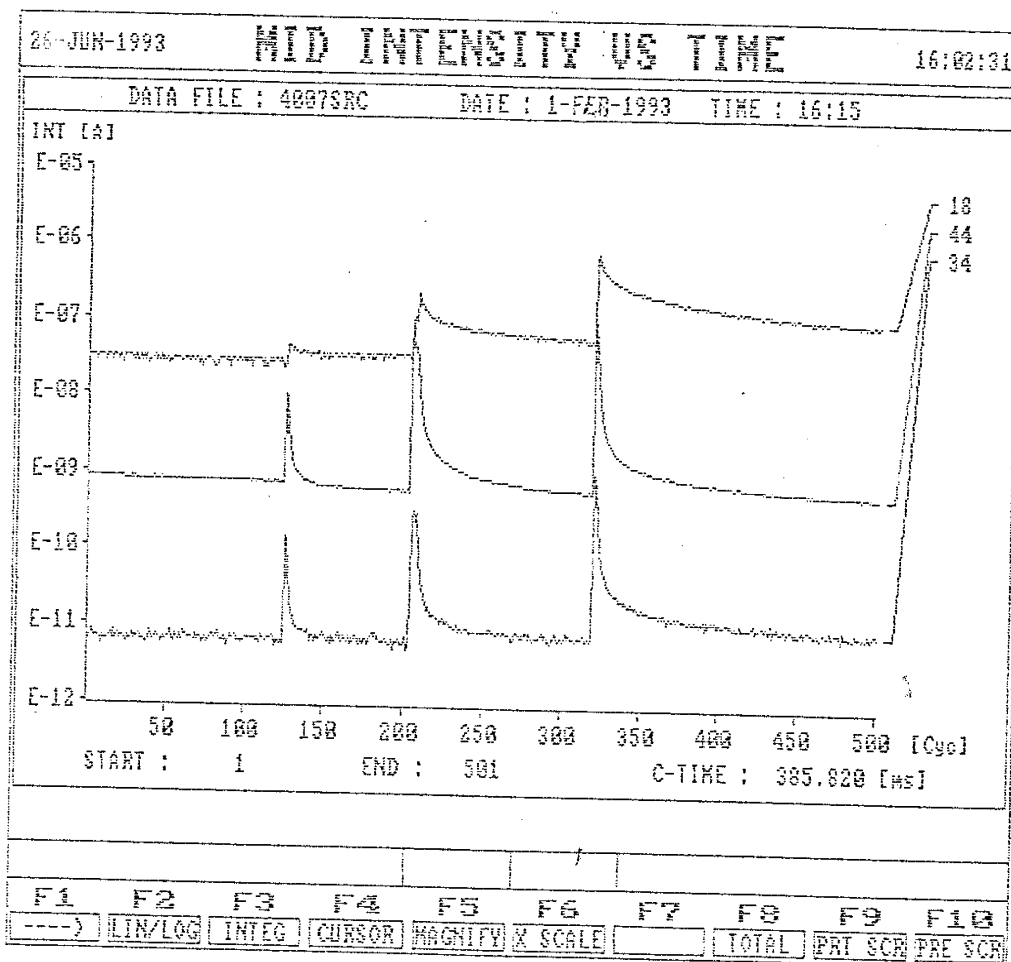
FIGURE 3. Computer graphic display of quadrupole response to a typical crush release fluid inclusion gases. The y-axis is logarithmic current intensity of the SEM and the x-axis is time represented by 500 measurement cycles. Each peak represents a crush of sample SR-142. AMU 18,44, and 34 are the major peaks for H_2O, CO_2, and H_2S respectively.

three crushes of sample SR-142. Intensity peaks are integrated and an equal number of cycles from just before the crush are integrated and subtracted from the peak area to give net peak intensity. AMU intensities (I) are related to pressure (P) by

$$I = P * S$$

where S is the sensitivity of the gas. For gas mixtures, matrix algebra is used to simultaneously solve for the partial pressures. In matrix terms,

$$|I|^m * |S|^{-1} = |P|^n$$

where $|P|^n$ is the n vector (partial pressure for n gas species) and $|I|^m$ is the m vector (column matrix) of AMU intensities and $|S|^{-1}$ is the inverted matrix of m * n (AMU * gas species) and $|P|^n$ is the resultant column matrix of gas species partial pressures for n gas species. $|S|$ combines cracking outlines and sensitivity factors for n gas species relative to N_2 (see Appendix A for description of $|S|$). The cracking outlines and sensitivity factors are determined by analyzing prepared reference gases. In this study the AMU intensities of 15, 18, 28, 32, 34, 40, 43, 44, and 64 are used to solve for CH_4, H_2O, N_2, O_2, H_2S, Ar, C_nH_n (short-chain hydrocarbons) CO_2, and SO_2. The 43 AMU peak is used to analyze for short-chain hydrocarbons and mostly comprised of propane (C_3H_8) and butane (C_4H_{10}). In the early part of the study, the 4 AMU peak was measured to detect He. However, resolution of the 4 AMU peak is difficult due to a large 2

AMU peak that is probably a fragment of H_2O and thus unreliable. About halfway through the study, the 40 AMU peak was measured for detecting Ar.

Adsorption/desorption effects can be seen in the peak shapes in Figure 3 with H_2O partial pressure slowly decaying relative to CO_2 and H_2S. This could be problematic when comparing results from variable sample sizes in that the gases with a greater tendency to adsorb would be under-represented in small samples. To evaluate this effect, Hansonberg Fluorite (HF-1) was analyzed 19 times, manually varying the amount of crushing to give a range of sample sizes. HF-1 is cleaned and hand-picked fluorite collected from the Hansonberg Mining district, NM, which hosts stratiform lead-fluorite-barite deposits (Putnam, et al., 1983). Numerous microthermometric measurements and bulk gas analysis of fluid inclusions in HF-1 have demonstrated a relatively homogenous fluid inclusion composition with respect to decrepitation analysis of 1 gram or larger samples. From these analyses, sample size, considered to be the sum of AMU intensities, is plotted against a specific gas-species/CO_2 ratios. Most gases except H_2O display relatively confined gas-species/CO_2 variance suggesting sample size has little effect on adsorption relative to CO_2 (see Appendix B for plots of other gases). H_2O/CO_2 ratios however, show a positive slope with increasing sample size and apparent clustering of peak 18/peak 44 ratios near the

maximum sample size (Fig. 4). This relationship suggests that small samples have a higher proportion of H_2O adsorbing than larger samples which could introduce a systematic bias. A simple calibration factor for H_2O is derived that incrementally adds H_2O to smaller H_2O peaks (see Appendix B for details).

Several fluid inclusion gas analyses of samples from the Steeple Rock mining district contained anomalously high N_2 and O_2. Splits from two of these samples were baked overnight at 100° C in a high-vacuum line then removed and loaded into crushers for repeat analysis. Results show 50% less N_2 and 30% less O_2 from the repeat crushes suggesting the prior analyses were air contaminated. The air may be trapped in fractures or in surface oxides then released upon crushing. Jones and Kesler (1992) report similar air contamination from crushes of barite. To compensate for this effect, all O_2 is assumed to be air contamination and appropriate proportions of N_2 and Ar, based on ratios of subtracted gas components to O_2, are subtracted from the analysis which is then re-normalized to 100% (see Appendix C for details).

Sampling procedure emphasized collection of representative samples. Samples are comprised predominantly of quartz varieties collected from rock chip traverses across veins. Where late-stage calcite vein fillings occur, late calcite was sampled separately. Fluorite and quartz
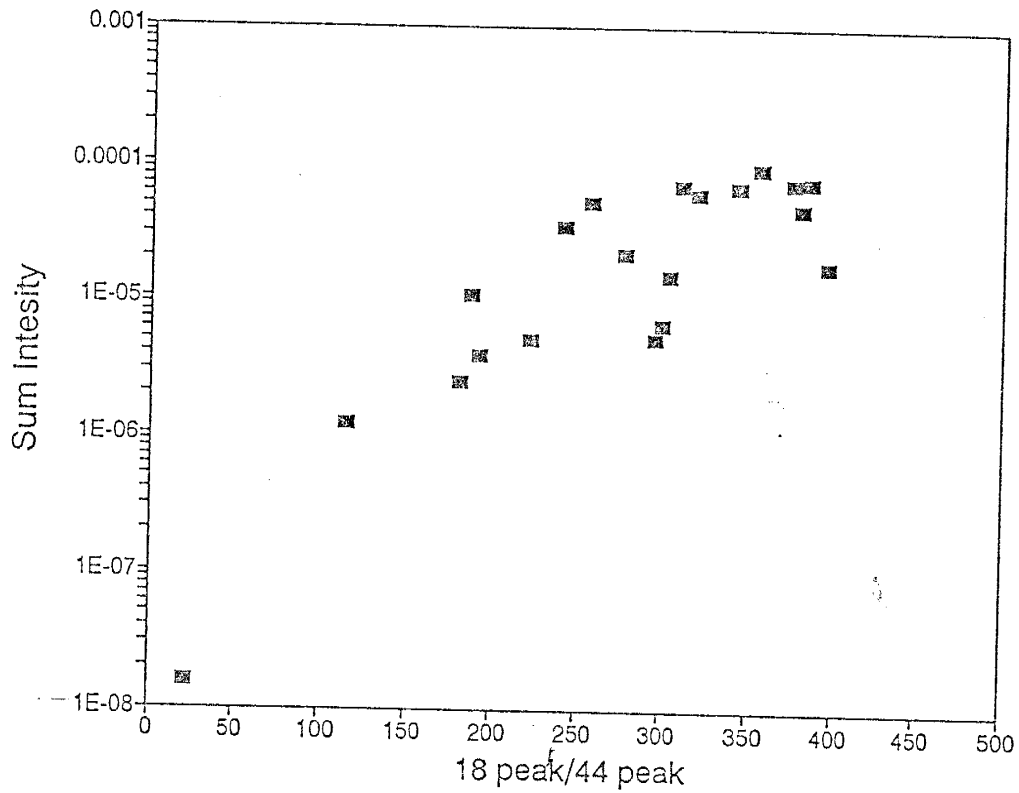
FIGURE 4. Sum intensity vs 18 peak/44 peak for repeats of HF-1 from the crush analysis method. Sum intensity is proportional to sample size and the 18 AMU and 44 AMU are the major peaks for H_2O and CO_2 respectively. The positive slope suggests that smaller sample sizes have a greater proportion of H_2O absorbing relative to CO_2.

from veins in the north end of the Steeple Rock mining
district and the Duncan Fluorspar district were sampled
separately. Each entire sample was machine ground to -10
mesh. The samples were screened to +10 to -40 mesh and
split to around 10 grams. Samples were cleaned by rinsing
in 40% HCl acid, with exception of the calcite bearing
samples, followed by soaking in 0.1 molar NaOH. The
samples are then thoroughly rinsed in deionized water,
drained, and oven dried at about 80° C. Approximately 3
grams of sample is placed in the crusher for analysis. The
crushing process breaks a small number of the grains loaded
into the crusher.

PRECISION AND SAMPLE HETEROGENEITY

The determination of precision and accuracy for methods
of measuring fluid inclusion volatiles is hindered by the
absence of a suitable and/or accepted geologic standard.
Calculations of a typical sample size released by crushing
in this study, show that it could be contained in 2.6 ten
micron diameter H_2O filled inclusions or 106 H_2O vapor-filled
10 micron diameter inclusions with some combination likely
in most analysis. These sample size calculations use
density of liquid and vapor H_2O at 250° C and hydrostatic
pressure conditions. The possibility of unrepresentative
sampling of the bulk fluid inclusion composition is
suggested by the small numbers of inclusion analyzed. The

results from 19 repeat analyses of HF-1 demonstrate a large
compositional variance between individual crushes (see Table
1). However, if the mean composition from crush analysis is
compared to the best known bulk composition from thermal
decrepitation, the agreement is much better for H_2O, CO_2,
H_2S, and N_2 than suggested by the relative standard deviation
of individual crushes. This suggests that individual
crushes are partially discriminating fluid inclusion types,
but when averaged together give a representative
composition. Table 1 also lists Steeple Rock repeat
analysis which have comparable or larger relative standard
deviation than repeats of HF-1. Fluid inclusions with
known compositions were fabricated utilizing a high-vacuum
extraction-line. Nitrogen, CO_2, H_2S, and SO_2 were mixed to
similar proportions measured in fluid inclusions. This gas
was then trapped in a capillary and heat-sealed into
segments containing appropriate sample sizes. The
capillaries were then loaded in the crushers and analyzed to
define the precision of the crush method. The results and
relative standard deviations (Table 1.) demonstrate a
variance near but slightly less than repeats of Steeple Rock
samples. It is unclear if this variation is due to
incomplete mixing, and/or unmixing during capillary filling
and sealing or adsorption processes. In this study, trace
gas species concentrations can vary 2-3 orders of magnitude
from sample to sample and major gas species vary about 1

Table 1. Means and % relative standard deviation (one sigma) for Steeple Rock, HF-1, and lab mixture repeats.+ Means and %RSTD are for "dry gas" concentrations.

		SR-24 n=9	SR-33 n=9	SR-61 n=9	SR-97 n=13	HF-1 n=19	HF-1*	Lab Mix n=10
H_2O	%RSTD	5.3	2.6	3.5	7.0	0.2		2.2
	mean	92.2	96.9	95.7	89.8	99.7	99.57	94.3
N_2	%RSTD	28.3	39.1	21.5	33.9	88.6		20.2
	mean	51.80	45.80	59.57	46.83	16.48	15.81	66.72
CO_2	%RSTD	38.6	32.0	35.5	29.9	32.7		35.7
	mean	46.48	42.85	35.67	50.79	62.63	41.86	10.07
H_2S	%RSTD	108.6	63.0	101.4	59.6	83.8		83.9
	mean	0.0606	0.1786	0.2169	0.0140	7.6592	6.0465	0.8661
SO_2	%RSTD	107.4	155.7	43.0	75.8	63.2		74.8
	mean	0.5662	0.7376	0.0272	0.0037	0.3993		0.0529
CH_4	%RSTD	83.9	57.5	65.4	57.2	47.6		62.5
	mean	7.533	9.507	6.998	2.146	16.539	27.907	20.698
C_nH_n	%RSTD	57.5	49.4	55.1	26.2	39.3		51.2
	mean	0.570	0.323	0.188	0.249	1.178	7.674	0.159
Ar	%RSTD	76.5	33.8	41.4		71.8		99.6
	mean	0.2207	0.3057	0.4295		0.3516	0.00165	0.3499

(+) Mean and standard deviation determined using robust statistics described by the Analytical Methods Committee (1989).
(*) Thermal decrepitation analysis of Hansonberg Fluorite.

order of magnitude. Because of quality control problems in testing the precision, the relative standard deviations listed in Table 1 should be considered the maximum possible variability. In spite of a precision such as ±23% for N_2 and ±79% for SO_2 (Table 1) the wide ranging compositions would still allow anomalous samples to be differentiated. Steeple Rock analyses are the average of a minimum of three crushes per sample giving a much more representative result as shown by averaging repeats of HF-1 (see Table 1).

RESULTS

Mineralization in the Steeple Rock mining district occurs over about 70 km². Samples were collected from all known veins at multiple sites along strike (Fig. 2). Analyses from 134 samples from the Steeple Rock district and 15 samples from the from the Duncan fluorspar district are presented in this paper (see Appendix D for list of analyses for each sample). The Duncan fluorspar district analyses are included with Steeple Rock samples for univariate analysis, regression analysis, and scatter plots, but not plotted on contour maps because of limited sample site control. Appendix B is a list of the gas analysis for each sample.

Histograms and probability plots of gas concentrations for each measured gas species display varying degrees of normal or lognormal shapes with exception of H_2O (Fig. 5).

Gas concentrations are expressed as mole % of the "dry gas" (- H_2O) fraction to avoid uncertainty in the measurement of H_2O mole %. Methane was detected in all samples. A histogram and probability plot of CH_4 concentrations displays a lognormal and bimodal distribution plot with population modes separated by a factor of 4 (Fig. 5). These modes occur at approximately 30 and 85 percentile. The total range of CH_4 concentrations is slightly over one order of magnitude. The frequency distribution of H_2O concentrations do not show a normal or lognormal distribution (Fig. 5). Water concentrations range from slightly less than 100 to 83 mole %. Fifty percent of the samples have < 97.5 mole % H_2O. Nitrogen was measured in 143 samples and not detected in 6 samples. Nitrogen concentrations range almost one order of magnitude and have a broad and poorly defined normal distribution (Fig. 5). The probability plot for N_2 (Fig. 5) contains an inflection point at the 40 percentile that may suggest a bimodal distribution.

Hydrogen sulfide was detected in 147 samples and not detected in two samples. The concentration range for H_2S is about 2.5 orders of magnitude. The histogram and probability plot for H_2S displays a broad lognormal distribution (Fig. 5). Argon was detected in 63 samples out of the 65 samples analyzed for Ar. A histogram and probability plot of Ar concentrations display a narrow range

FIGURE 5 (next 4 pages). A series of histograms and probability plots for CH_4, H_2O, N_2, H_2S, Ar, C_nH_n, CO_2, SO_2, S/CO_2, and N_2/Ar. Note that CH_4, H_2S, Ar, C_nH_n, SO_2, and S/CO_2 are log values. Gases are expressed as "dry gas" mole % with exception of H_2O. See text for description of each distribution.
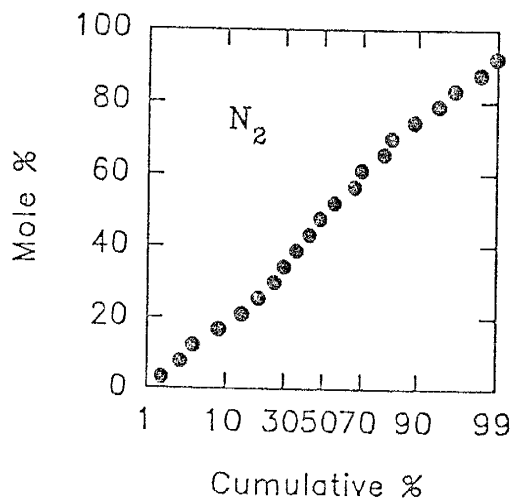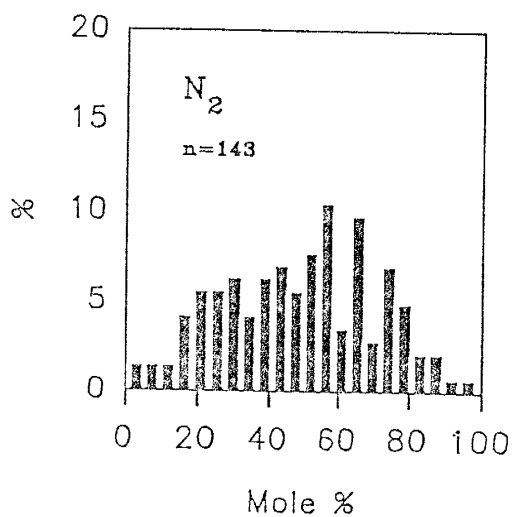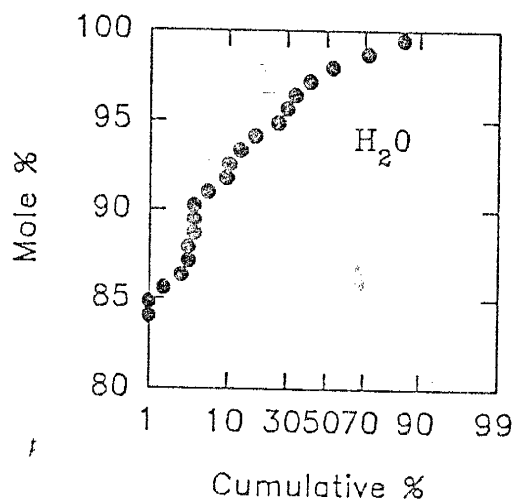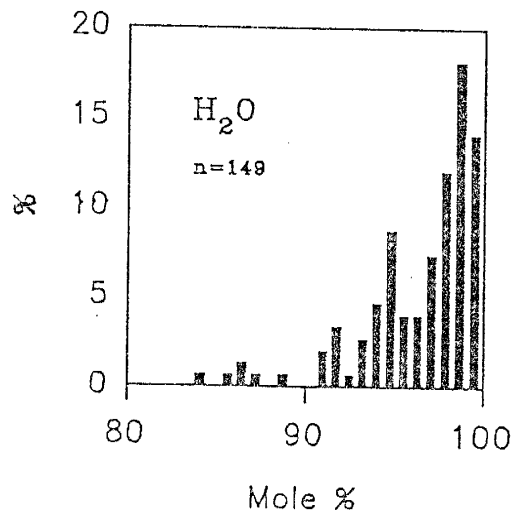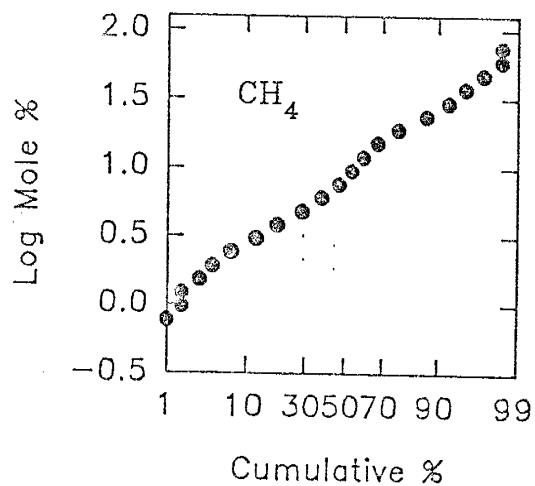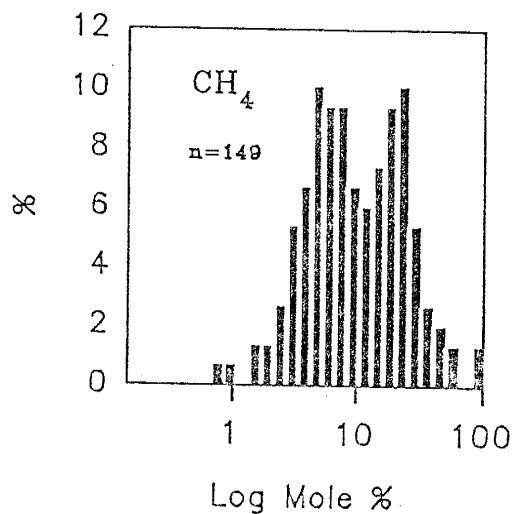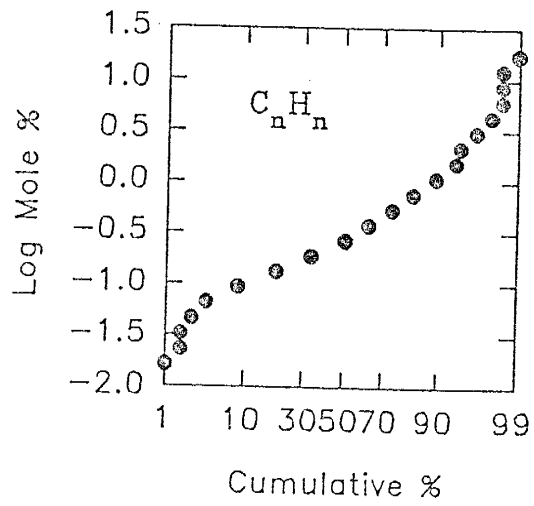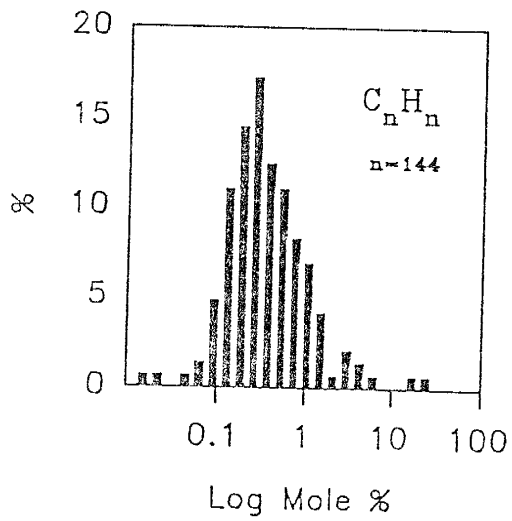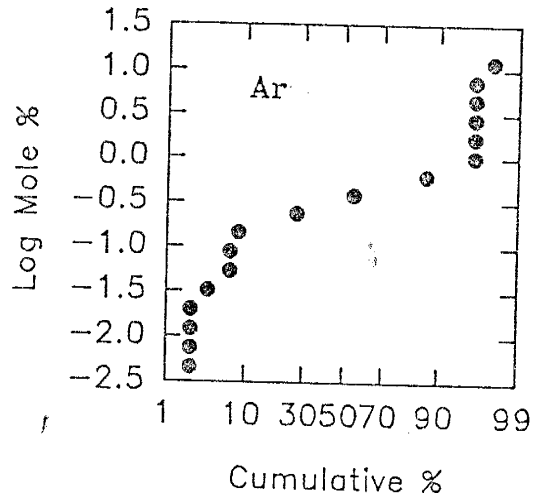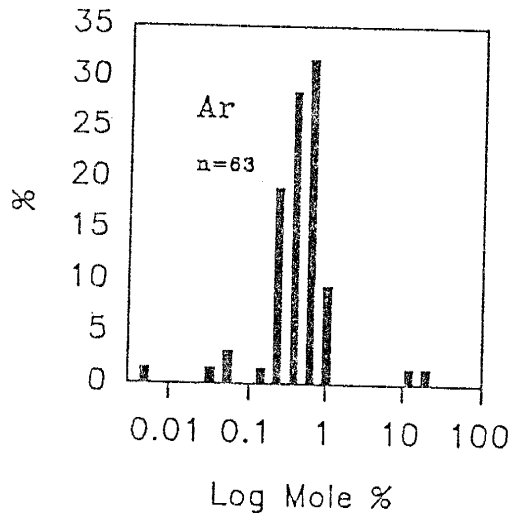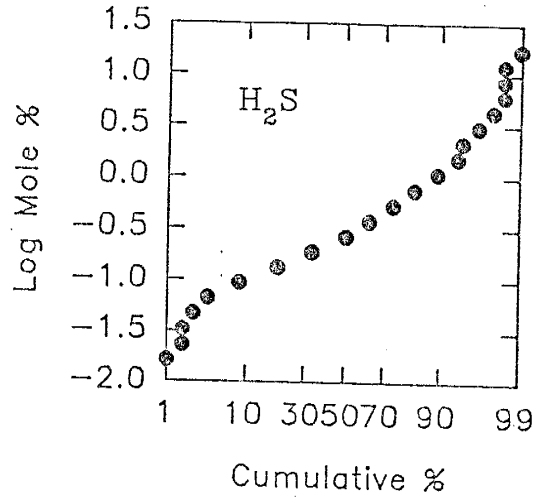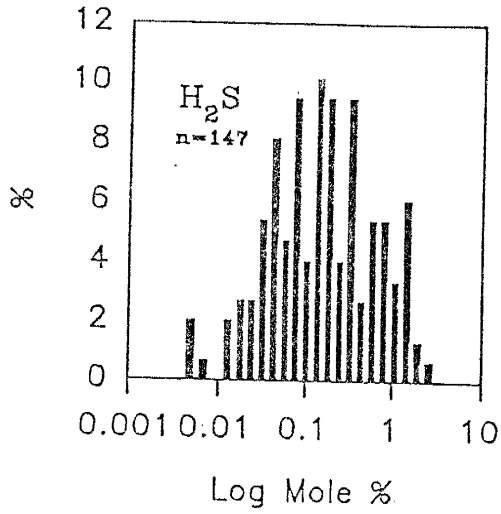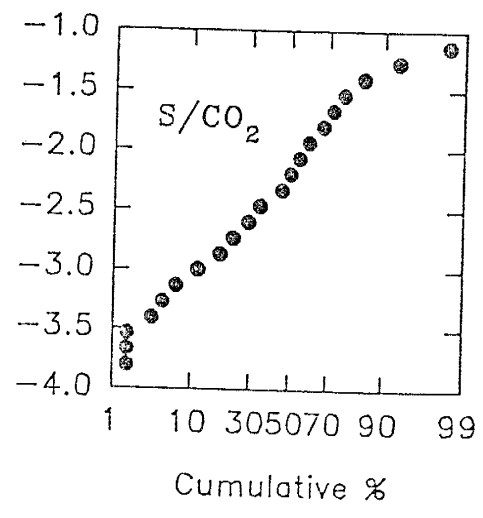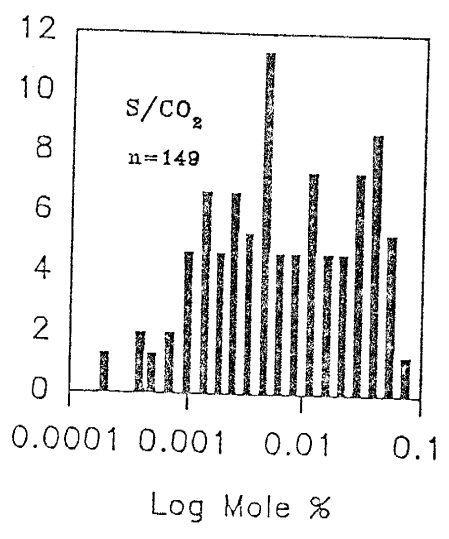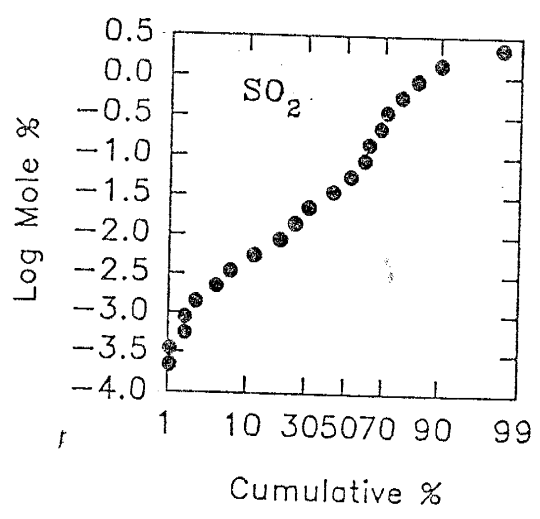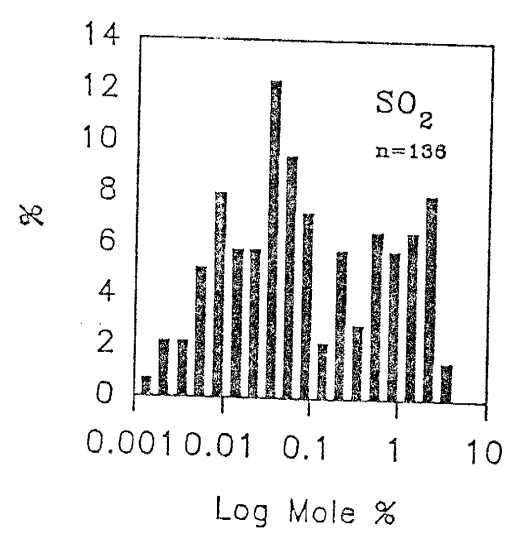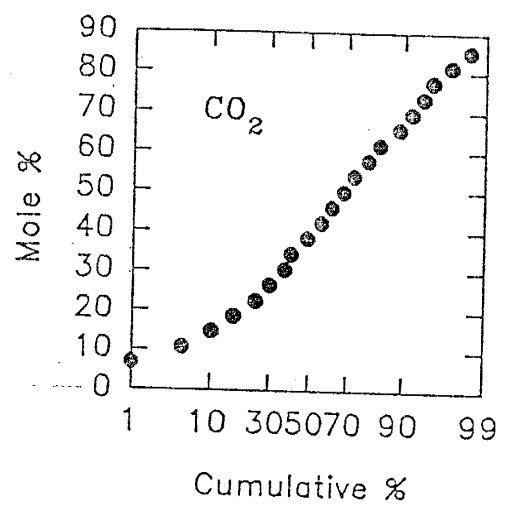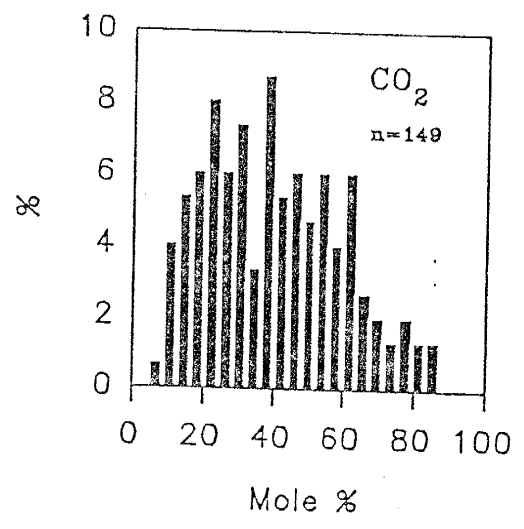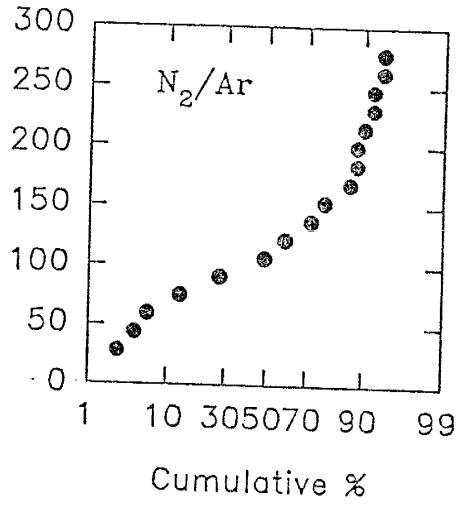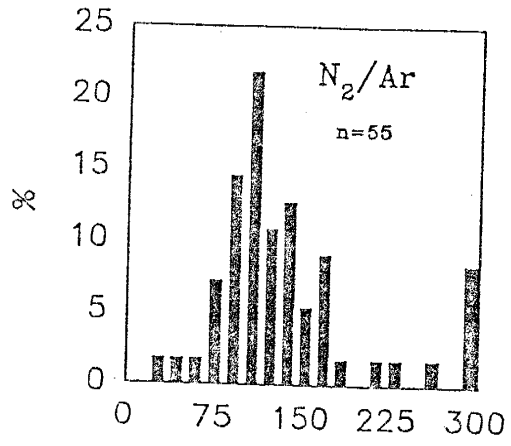
in which 88.9% of the samples occur within 0.24 to 1.70 mole % Ar (Fig. 5). Short chain hydrocarbons (C_nH_n, mostly C_3H_8 and C_4H_{10}) were measured in 144 samples and not detected in three samples and not measured in two samples. A histogram of C_nH_n concentrations displays a log normal shape with a slight positive skewness and a few outliers (Fig. 5). Carbon dioxide was measured in all samples with concentrations ranging from 7 to 85 mole %. A histogram of CO_2 concentrations shows a broad normal distribution and positive skewness (Fig. 5). Sulfur dioxide was measured in 136 samples and was not detected in 5 samples, and not measured in 8 samples. The compositional range of SO_2 is greater than all other measured gases ranging from 0.0001 to 3.5 mole %. The histogram and probability plot for SO_2 display lognormal and bimodal distributions. The population modes occur at about 43 and 85 percentile and are separated by > 1 order of magnitude (Fig. 5).

Carbon dioxide and H_2S are common constituents in hydrothermal fluids. In Figure 5, log S/CO_2 ratios are plotted on a histogram and probability plot. The ratios range over 3 orders of magnitude and appear to have lognormal and bimodal distribution. An inflection point on the probability plot occurs at 50 percentile and the two modes are separated by about one order of magnitude. The N_2/Ar ratios from 55 samples are plotted on a histogram and probability plot in Figure 5. The histogram of ratios

displays a relatively narrow range of 75 to 168 and a median of 109.

Multivariate regression analysis reveals mostly poor correlations between gas species (Table 2). The CH_4, H_2S, C_nH_n, and SO_2 concentrations were transformed to log values before the regression analysis. The best correlation coefficient is for N_2 and CO_2 at -0.81. Nitrogen and CO_2 are the major gas components in all analyses and their negative correlation is at least partly an induced correlation caused by normalization of each analysis to 100 mole %. The next best correlation is between H_2S and SO_2 with a 0.7 correlation coefficient. Figure 6 is a scatter plot of SO_2 and H_2S with a line of slope = 1 plotted for reference. The SO_2/H_2S ratios increase from < 1 at low S concentrations to > 1 at relatively high S concentrations. Concentrations of CH_4 and C_nH_n are poorly correlated with each other. Water concentrations are best correlated with CH_4 at a 0.46 correlation coefficient. Nitrogen is negatively correlated with all other measured gases (Table 2) with the exception of Ar. A Scatter plot of Ar vs N_2 (Fig. 7) displays a linear and positive correlation. Also plotted in Figure 7 are lines representing the N_2/Ar ratio of air at 84 and air saturated meteoric water at 38. The data from Steeple Rock plot close to the N_2/Ar line for air with some deviation toward greater N_2/Ar ratios for samples with higher N_2 concentrations. These relationships suggest

	CH₄	N₂	H₂S	Ar	CₙHₙ	CO₂	SO₂	H₂O
CH₄	1.00	-.03	-.03	.18	.02	-.17	-.05	.46
N₂	-.35	1.00	-.26	.37	-.31	-.81	-.29	-.31
H₂S	-.03	-.26	1.00	-.04	.24	.28	.73	.38
Ar	.18	.37	-.04	1.00	-.20	-.55	-.07	.07
CₙHₙ	.02	-.32	.24	-.20	1.00	.25	.26	.21
CO₂	-.17	-.81	.28	-.55	.24	1.00	.30	.09
SO₂	-.05	-.29	.73	-.07	.26	.30	1.00	.27
H₂O	.46	-.31	.38	.07	.21	.09	.27	1.00

Table 2. Correlation coefficient matrix for 149 sample from the Steeple Rock mining district. "Dry gas" concentrations are used. The concentrations for CH_4, H_2S, C_nH_n, and SO_2 are converted to log values before regression analysis.
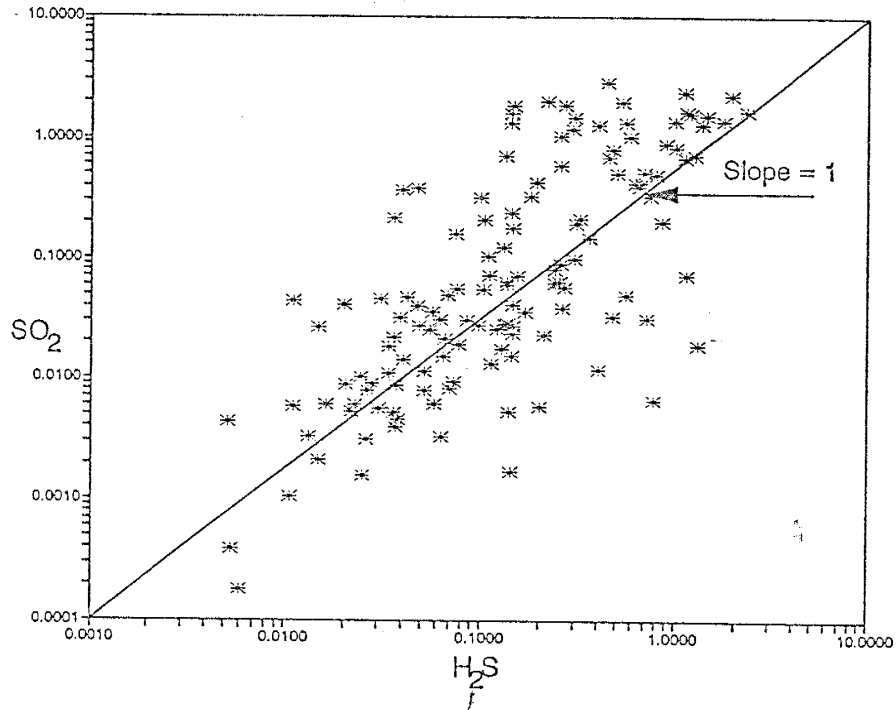
FIGURE 6. Scatter plot of SO_2 and H_2S "dry gas"
concentrations from fluid inclusion gas analysis. Note the
relatively S-rich samples have greater SO_2/H_2S ratios.
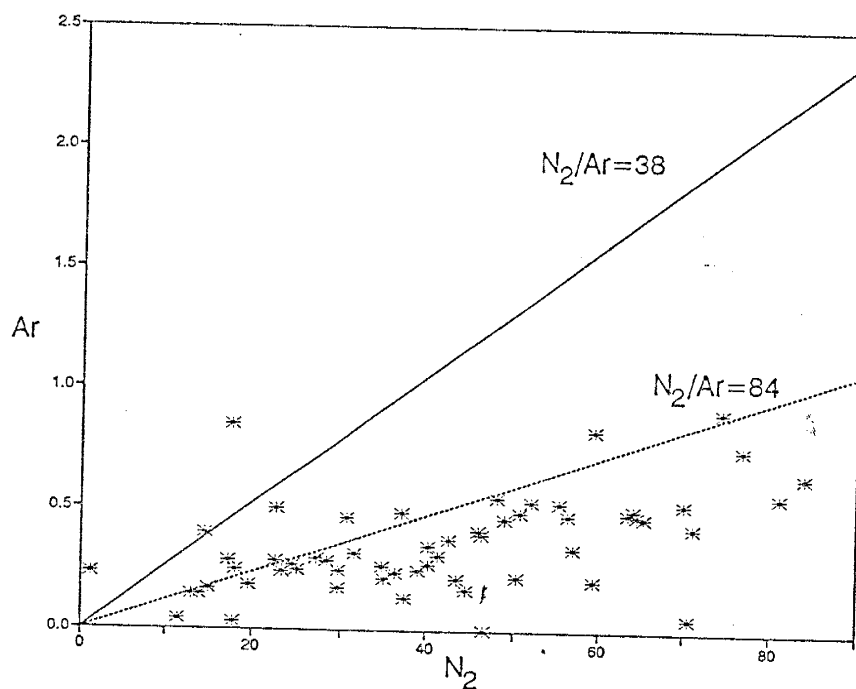
FIGURE 7. Scatter plot of Ar and N_2 "dry gas" concentrations from Steeple Rock fluid inclusion gas analysis. The N_2/Ar ratios of 38 and 84 correspond to N_2/Ar ratios in air-saturated-meteoric water and air respectively.

that the measured N_2 and Ar is affected by air contamination even after subtraction of N_2 and Ar using the air subtraction factor derived in the previous section. Samples from Steeple Rock can be placed into two groups: those samples with bladed quartz after calcite, or sulfide bearing samples. The S/CO_2 ratios of the two groups are plotted for comparison (Fig. 8). The ranges of the two groups have significant overlap, however, the median values are distinct from each other with S/CO_2 median ratio for sulfide bearing samples greater by a factor of 2 than the S/CO_2 ratios in samples with quartz after bladed calcite. Discriminant analysis of these two groups indicate CH_4 to be the most important factor followed by SO_2, H_2S, C_nH_n, H_2O, N_2, and CO_2 in decreasing order of importance. A scatter plot of SO_2 vs CH_4 helps to illustrate the difference between the two sample groups (Fig. 9). The two groups plot as separate as a group, have greater amounts of SO_2 and less CH_4 than samples containing quartz after bladed calcite. Many of the unclassified data are CH_4-rich and SO_2-poor relative to both of the above considered sample groups.

Ternary composition plots are useful for showing bivariate data trends. Fluid inclusion gas compositions from Steeple Rock are plotted on ternary composition plots in Figures 10a - 10d. All data plotted on ternary composition plots are multiplied by the indicated factor and normalized to 100 %. In Figure 10a, data are plotted on a
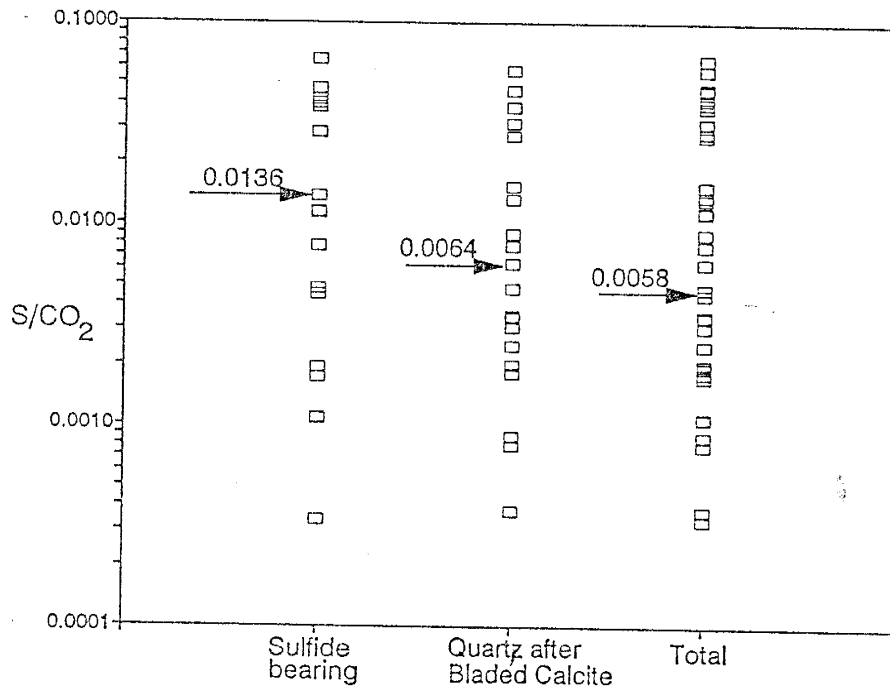
FIGURE 8. Total S/CO_2 is plotted against samples grouped as sulfide bearing, quartz after bladed calcite, and all samples. The arrows point to median values. The sulfide bearing samples have a median S/CO_2 ratio greater by a factor of 2 than the median value for quartz after bladed calcite samples.
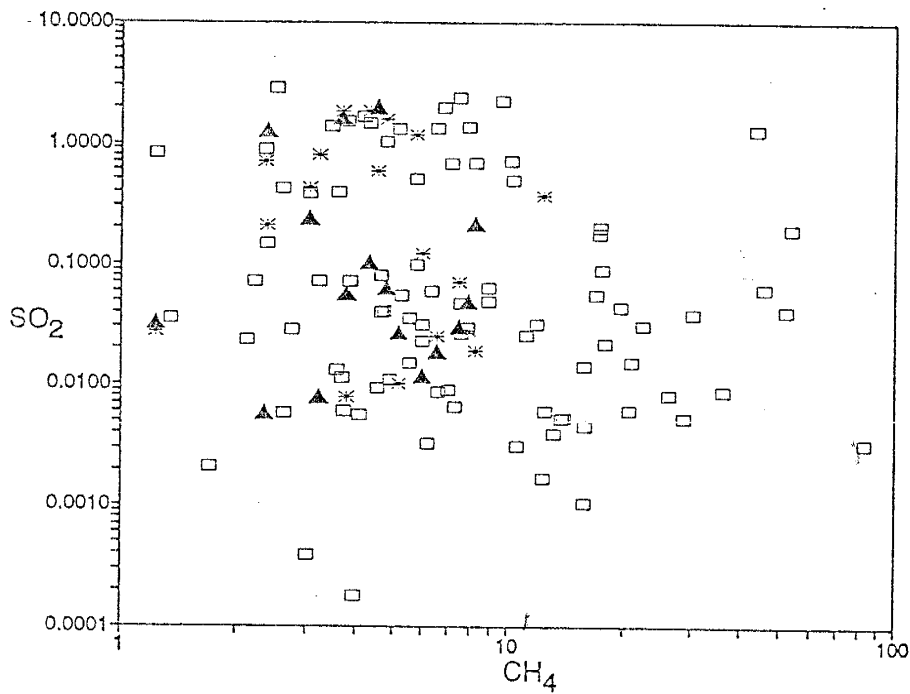
FIGURE 9. Scatter plot of SO_2 vs CH_4 "dry gas" concentrations. The asterisks are the sulfide bearing samples; filled triangles are the quartz after bladed calcite; and the open squares are the unclassified samples. Two data groups can be discerned: an SO_2-rich group and a SO_2-poor, CH_4-rich group.

clusters with some intermixing. The sulfide bearing samples, CO_2-10*CH_4-100*S ternary plot that shows groupings of data such that CH_4-rich samples are relatively S-poor and CH_4-poor samples are relatively S-rich. In Figure 10b, data are plotted on a H_2S-CO_2/100-SO_2 ternary composition plot. The data are distributed from the CO_2/100 apex toward the H_2S apex with a distinct group of CO_2-poor samples that are SO_2-rich relative to H_2S. The apparent linear boundary for minimum CO_2 concentrations in Figure 10b may be an artifact from normalizing compositions to 100%. The ternary plot shown in 10c plots H_2O against 10*CO_2 and 1000*S. In this plot the data defines two distribution trends from the H_2O apex toward the 10*CO_2 and 1000*S apexes with most of the data distributed between the H_2O and 10*CO_2 apex. In Figure 10d, data are plotted on a CO_2/10-CH_4-10*C_nH_n ternary composition plot with C_nH_n representing mostly C_3H_8 and C_4H_{10}. Most of the data are distributed linearly between CH_4 apex and the CO_2/10 apex with only a few samples deviating from this trend toward the 10*C_nH_n apex.

The systematic sampling of most outcropping mineralization on a district-scale facilitates the contouring of fluid inclusion gas data. The spacial distribution of samples is controlled by vein occurrences such that interpretation of contours must consider sample control. Contour plots for the following gas species and gas ratios are presented in Figures 11a - 11i respectively:
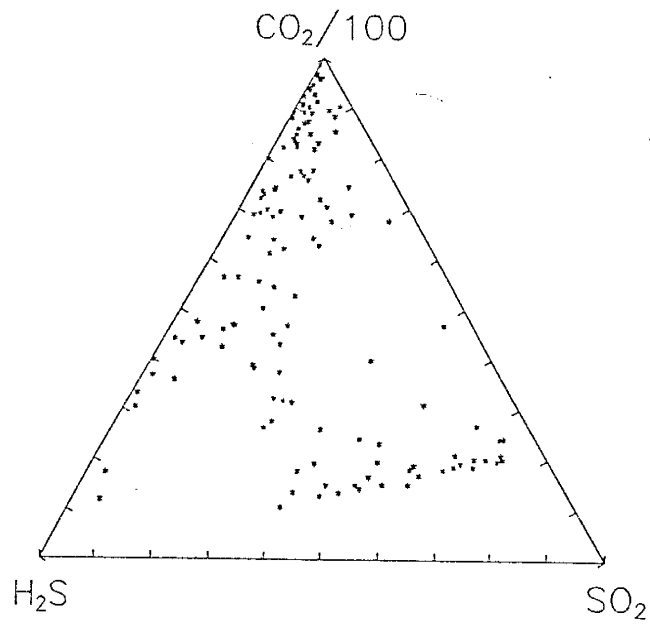
FIGURE 10a. Ternary composition plot of CO_2-10*CH_4-100*H_2S for Steeple Rock analyses.
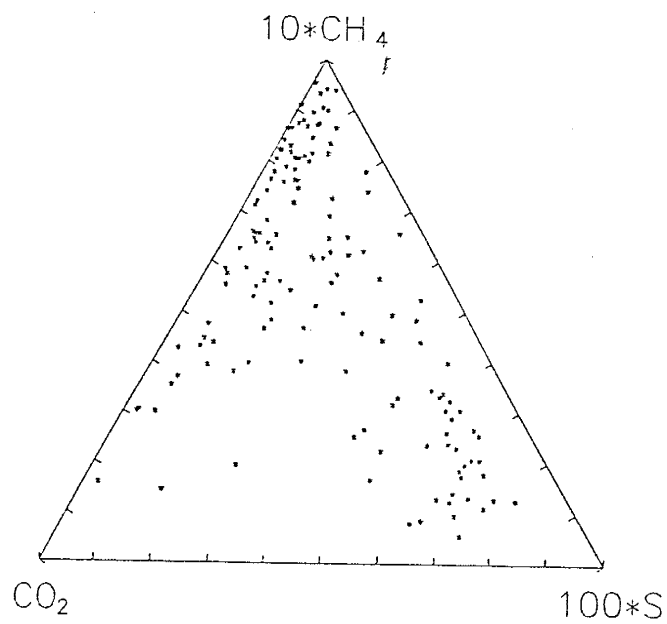
FIGURE 10b. Ternary composition plot of H_2S-CO_2/100-SO_2 for analyses from Steeple Rock.

H₂O
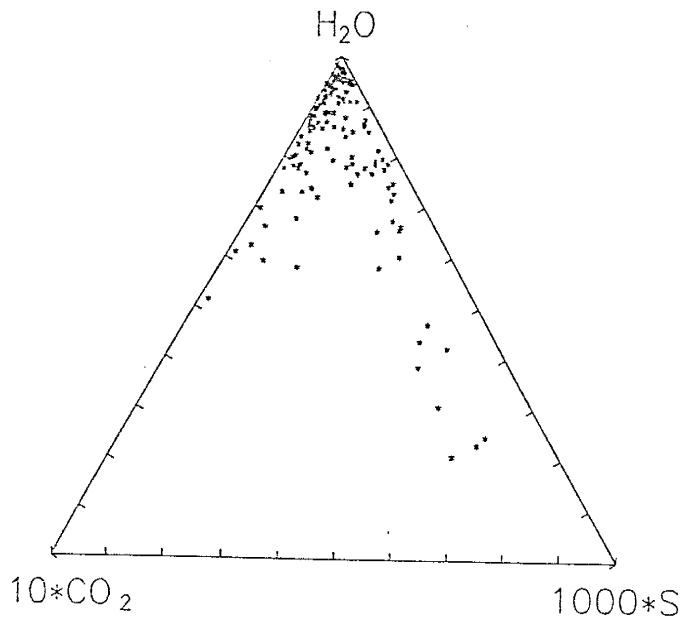
10*CO₂   1000*S

FIGURE 10c. Ternary composition plot $10*CO_2-H_2O-1000*S$ for Steeple Rock analyses.

CH₄
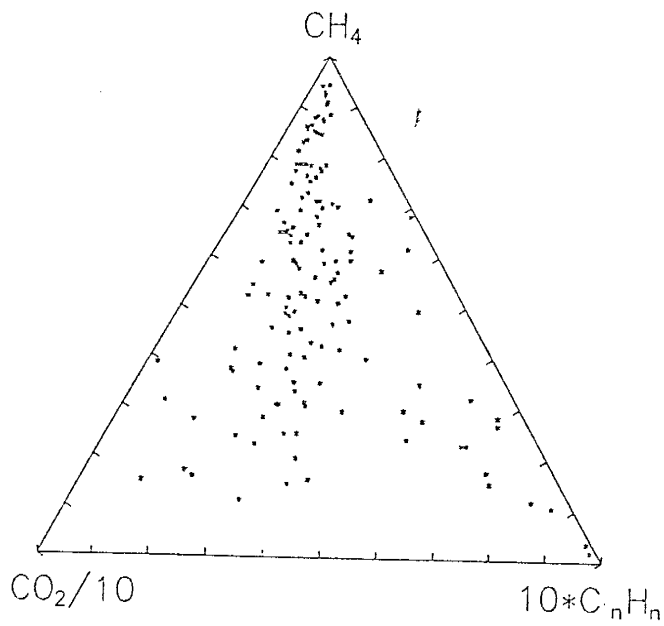
CO₂/10   10*CₙHₙ

FIGURE 10d. Ternary composition plot of $CO_2/10-CH_4-10*C_nH_n$ for Steeple Rock analyses.

log CH_4, % gas ("dry gas" mole %), N_2, log H_2S, log C_nH_n, CO_2, log SO_2, log S/CO_2, and log CH_4/CO_2 - log S/CO_2. All gas species and gas ratios are "dry gas" concentrations. Contour intervals are chosen for simplicity and discrimination of anomalies. Log CH_4 values are contoured in Figure 11a. Methane concentrations are bimodal (Fig. 5a), however the contour plot does not display broad anomalies or significant anomaly contrast. Negative CH_4 anomalies are small, localized, and appear as spot anomalies. In Figure 11b, % "dry gas" is contoured. This plot shows the highest gas concentrations are found away from the central part of the district in the northwest, southeast, and the west-central edge of the district defined as areas > 6.2 mole % "dry gas". The 3.2 mole % "dry gas" contour is the most discriminating and defines variations in concentrations in the central part of the district with areas > 3.2 mole % including the Summit Mine, Alabama Mine and vicinity, and part of the East Camp Mine group.

Carbon dioxide and N_2 are well correlated with a correlation coefficient of -0.81 resulting in inversely related contour plots (Figs. 11c and 11g). In Figure 11g, CO_2 concentrations display a district-scale zonation of low CO_2 concentrations of 30 mole % in the center of the district outward toward greater concentrations of 50 mole % or greater. Nitrogen and CO_2 are the major gas species in all analyses, and thus residual N_2 from air contamination

CH4
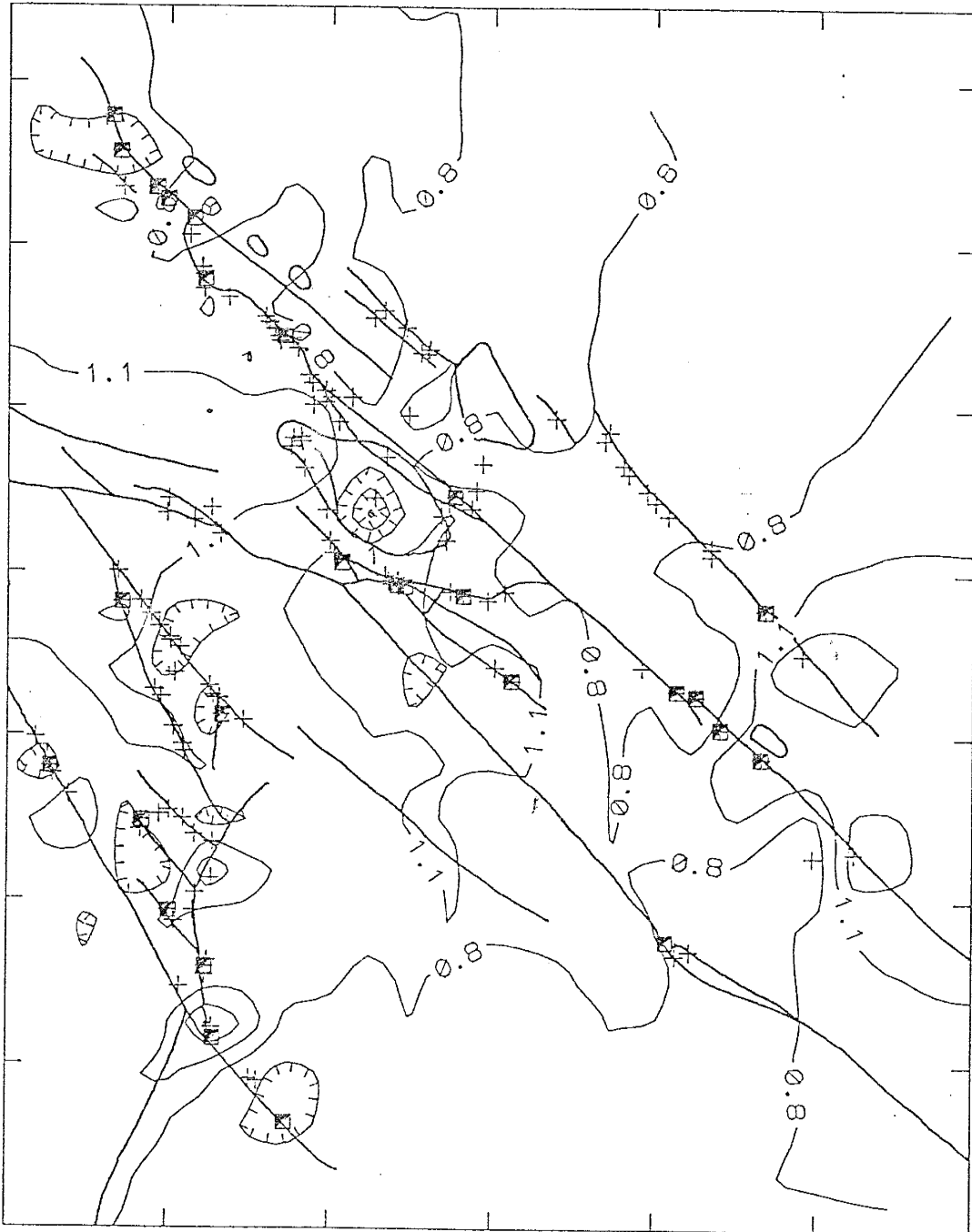
FIGURE 11a.   Log CH₄ concentrations contour plot.   Contour interval is 0.3 log units.   Note the negative localized anomalies.

% Gas
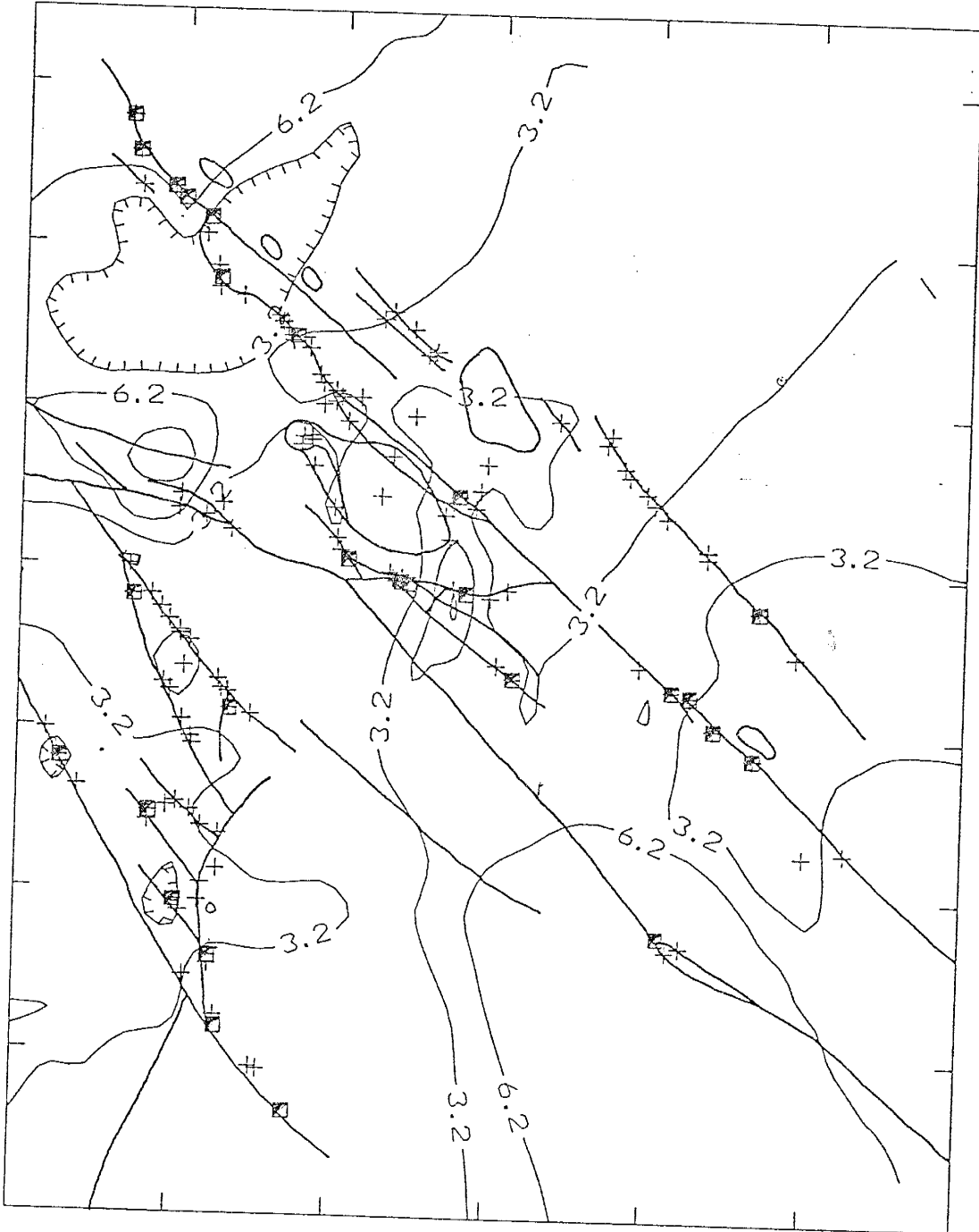
FIGURE 11b. "Dry gas" mole % contour plot.   Contour
interval is 3 mole %.

N2
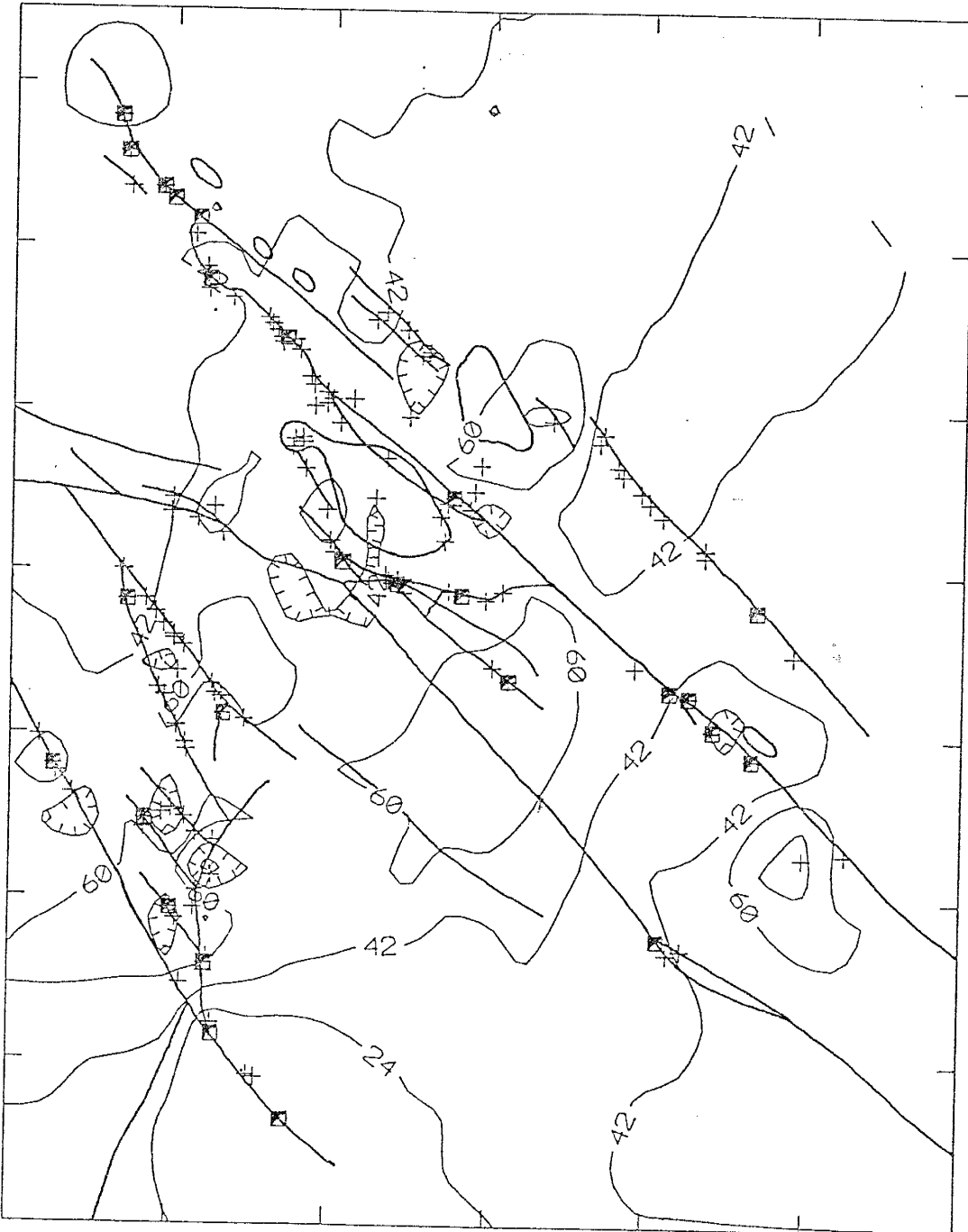
FIGURE 11c. Mole % N_2 concentration contour plot. Contour interval is 18 mole %. Note the high concentrations occur in the center of the district.

H2S
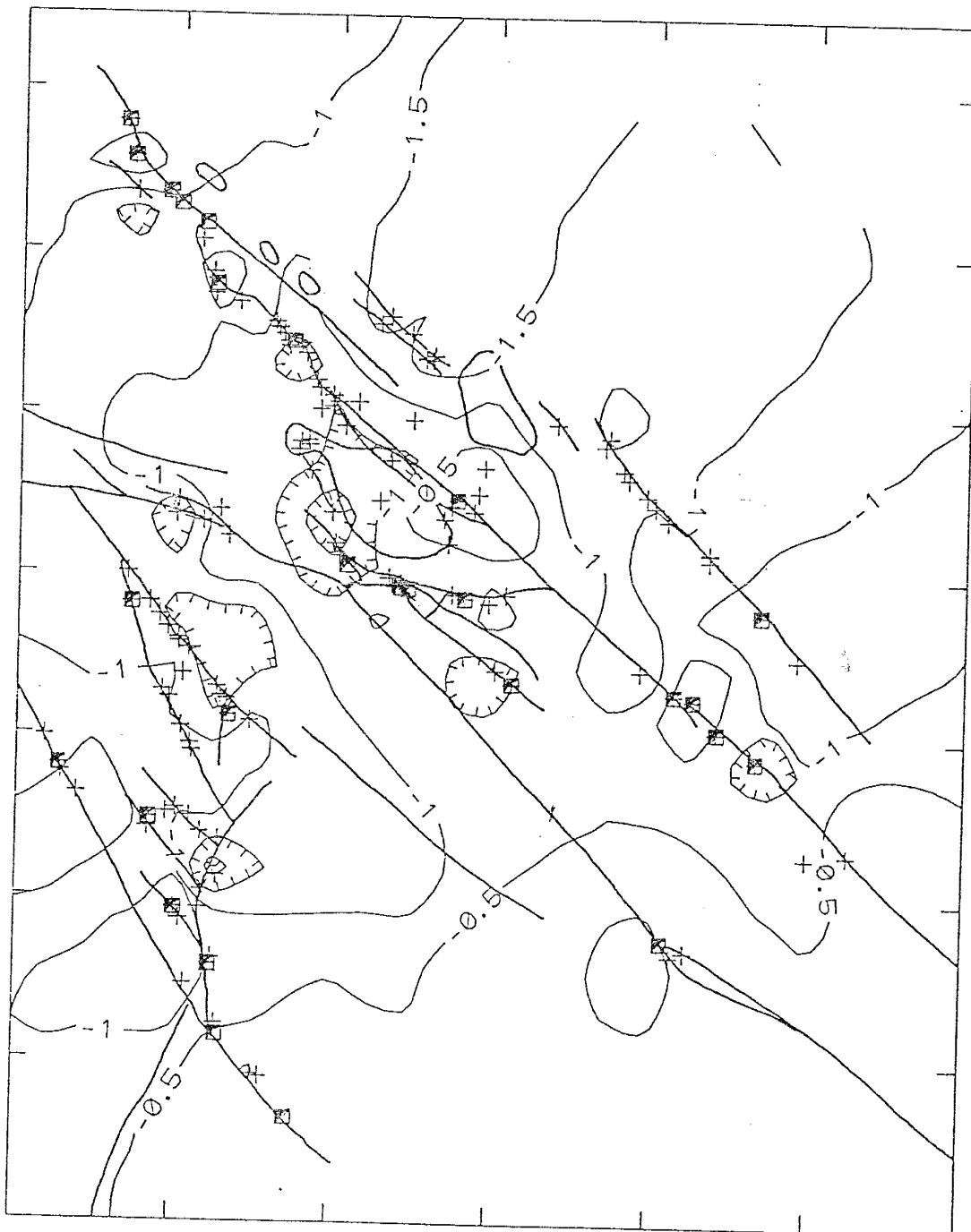
FIGURE 11d. Log mole % H₂S concentrations. Contour
interval is 0.5 log units. Note the localized positive and
negative anomalies.

$C_n H_n$
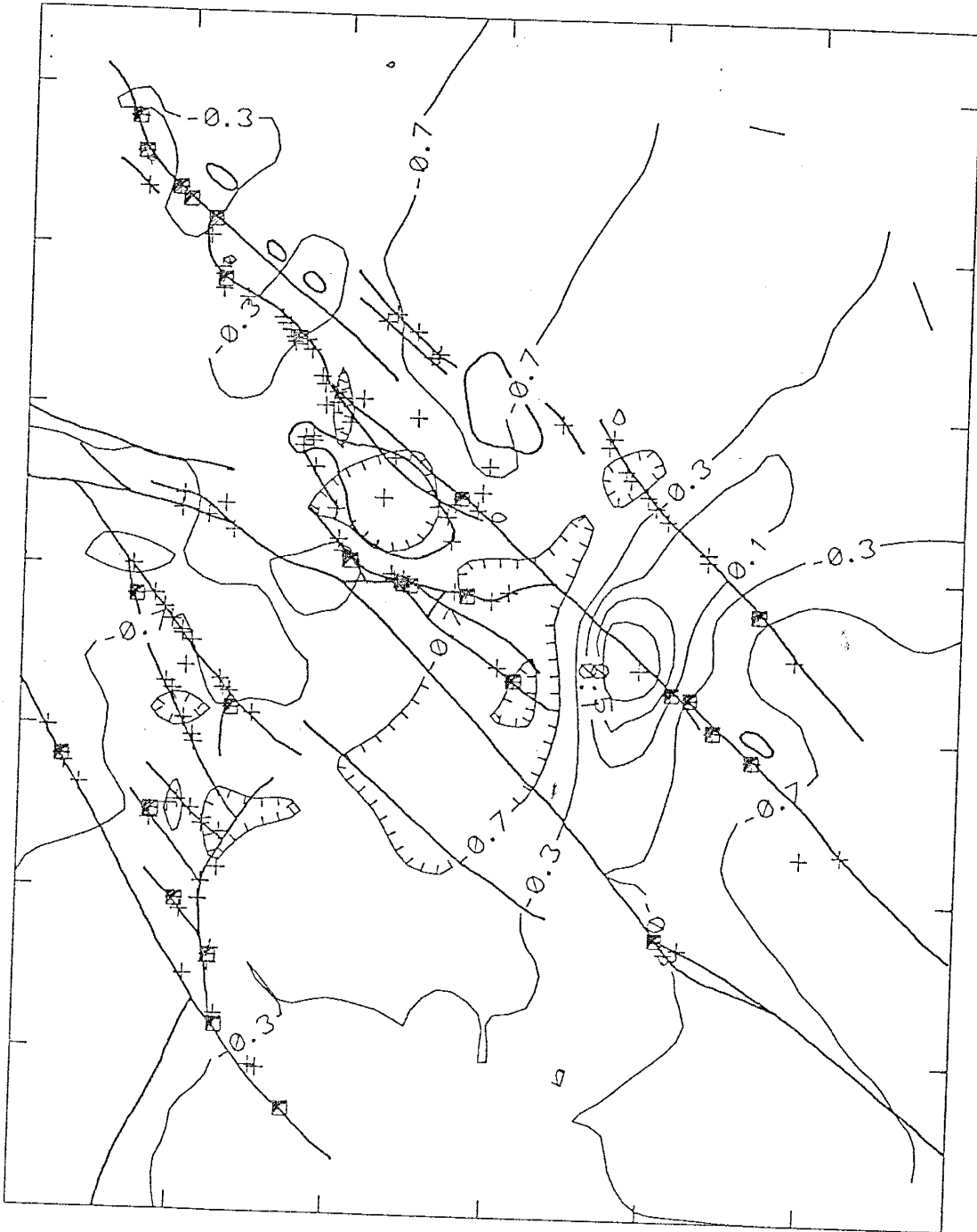
FIGURE 11e. Mole % log C_nH_n contour plot. Contour interval is 0.4 log units. Contours lack systematic variations.

CO2
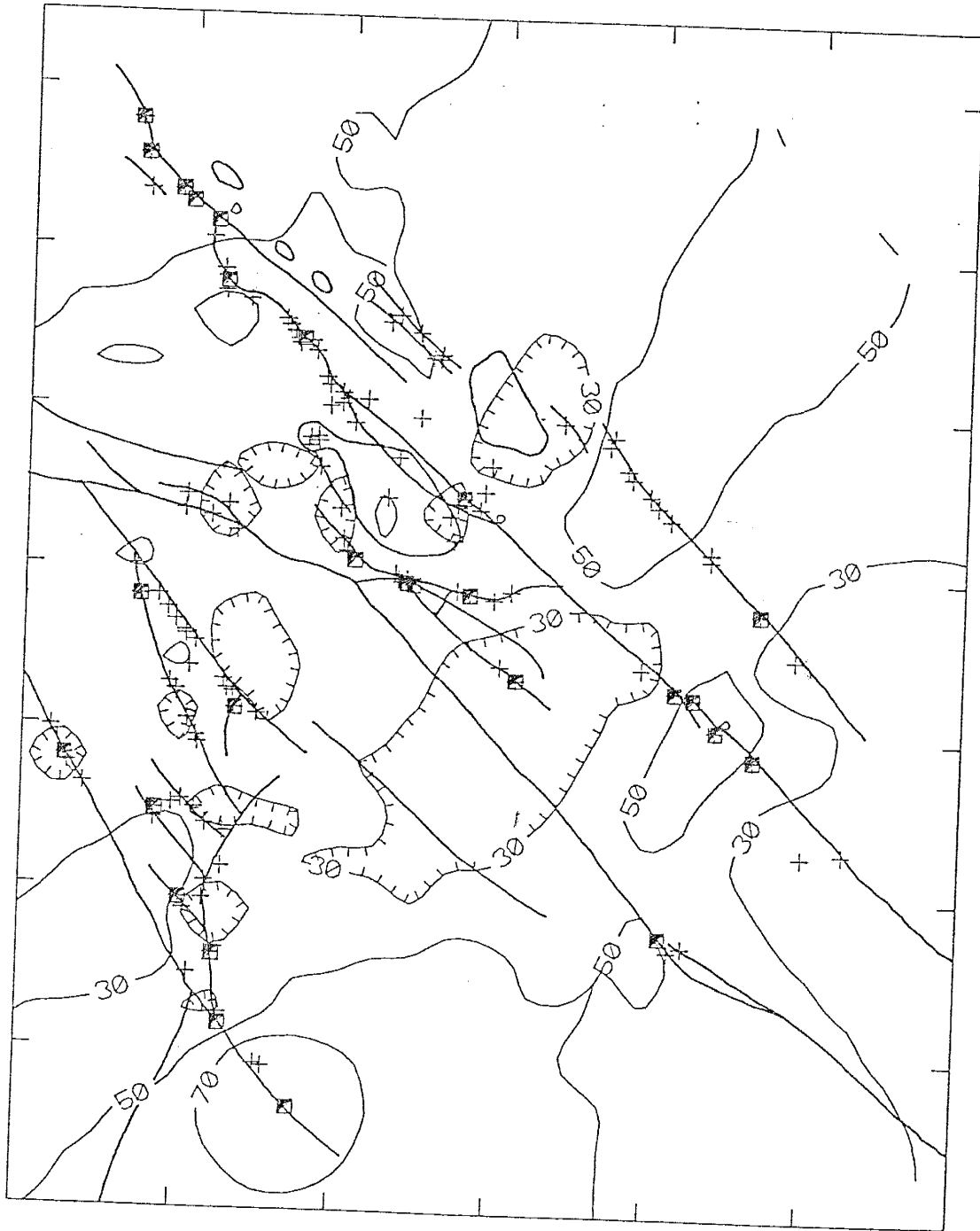
FIGURE 11f. Mole % CO_2 contour plot. Contour interval is 20 mole %. Note the district-scale zonation of CO_2 concentrations from the center of the district outward toward greater concentrations.

SO2
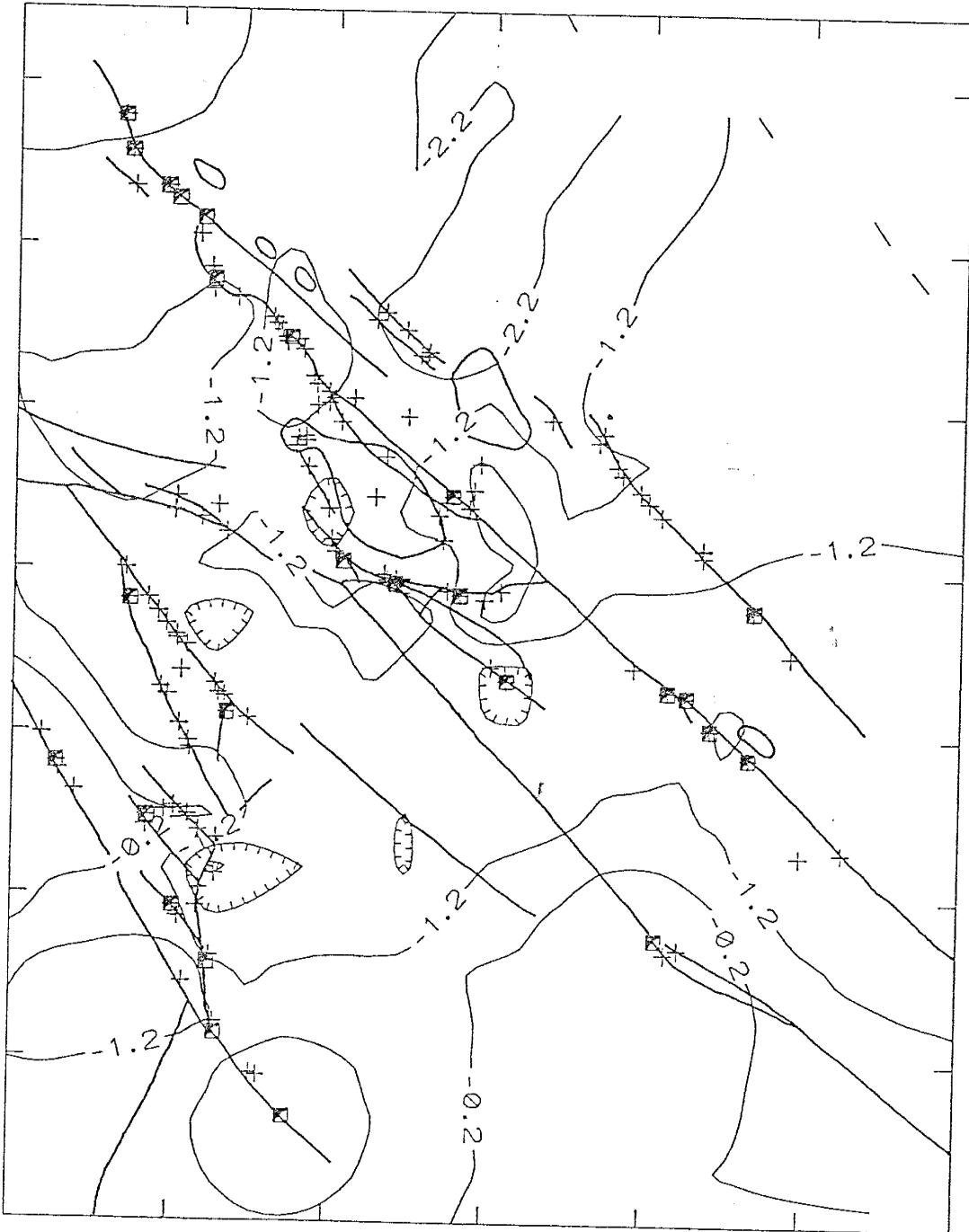
FIGURE 11g.   Log mole % SO_2 contour plot.   The contour
interval is 1 log unit.   Note localized anomalies.

S/CO2
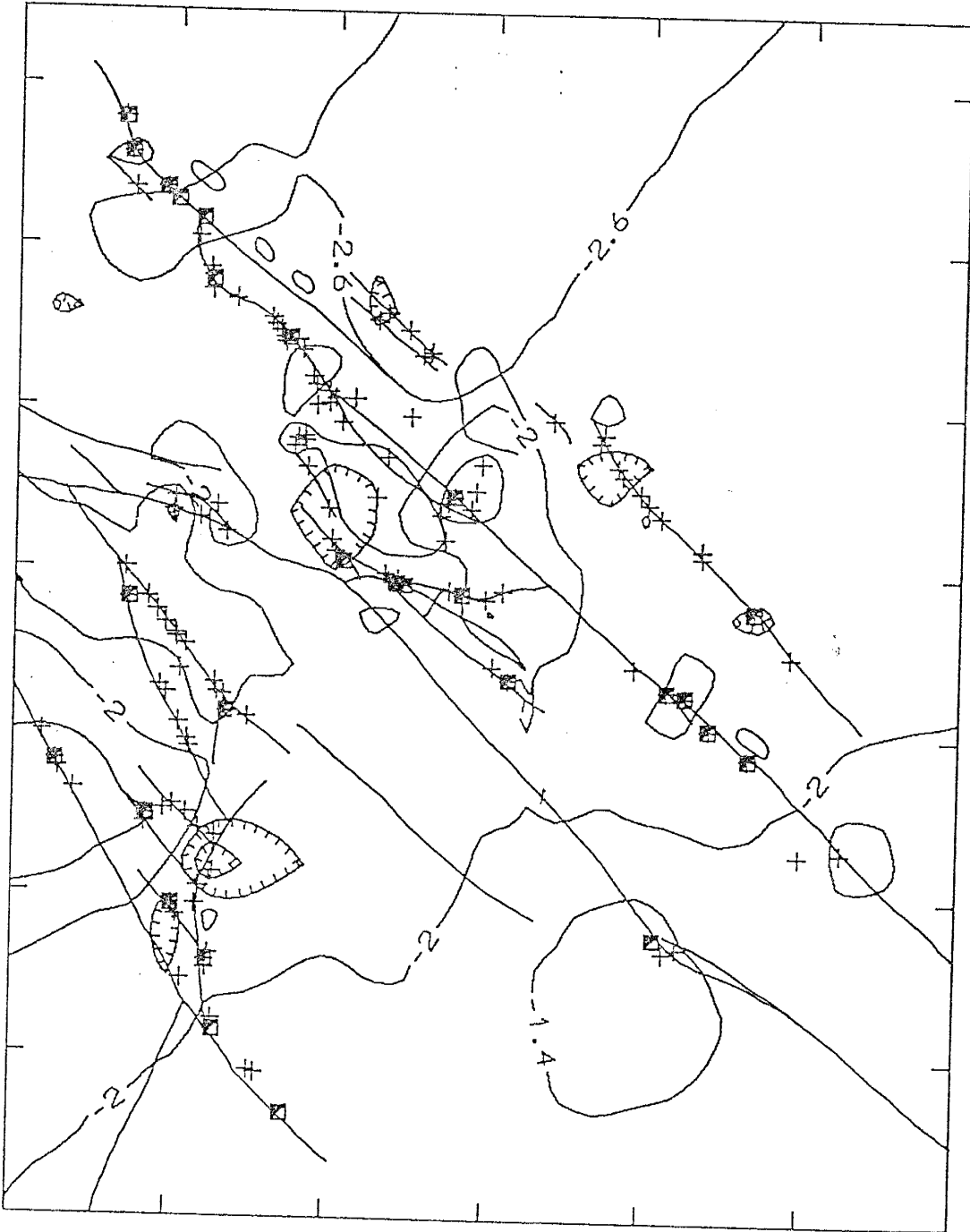
FIGURE 11h. Log S/CO_2 ratio contour plot. Contour interval is 0.6 log units. This contour plot shows well defined anomalies. Note the paired relationship between positive and negative anomalies.

CH4/CO2 - S/CO2
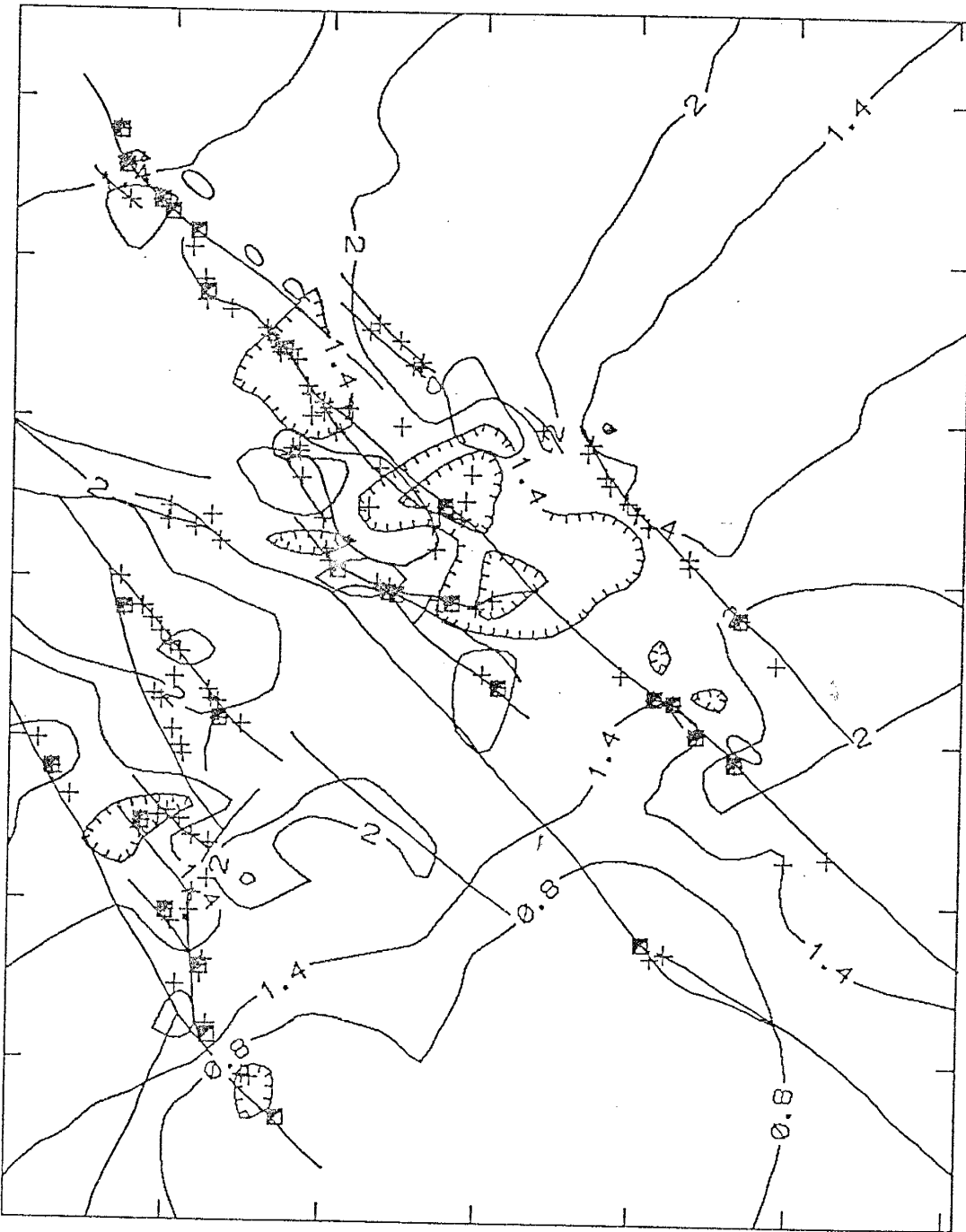
FIGURE 11i. Log CH_4/CO_2 - log S/CO_2 contour plot. Contour interval is 0.8 log units. Anomalies plot as depressions located along the Summit-East Camp fault and the Alabama mine area.

could affect CO_2 concentrations. Air contamination is most likely related to textural and mechanical sample attributes and unrelated to fluid inclusion chemistry, and as such would be randomly distributed with respect to sample location. However, the district-scale zonation of CO_2 concentrations suggests that N_2 air-contamination effects on CO_2 concentrations are not observed and that regional trends of CO_2 concentrations represents geologic zonation.

In Figure 11d, log H_2S mole % is contoured with the -1 contour discriminating the greatest number of samples. The central part of the district has log H_2S concentrations > -1 with localized and pared negative (-1.5) and positive (-.5) anomalies superposed. Similar pared anomalies occur at the East Camp mine and also at the Alabama Mines area in the western part of the district.

Sulfur dioxide is correlated with H_2S (see Table 2) with a correlation coefficient of 0.73 and would be expected to display contour features similar to the H_2S contour plot. The SO_2 contour plot (Fig. 10h) does display similarities with the H_2S contour plot, however, more local variability is apparent as localized anomalies in the central part of the district. The log -1.2 and greater contours define anomalous areas and include the Summit mine, Raeburn Hills, and East Camp mine which are all located along the Summit-East Camp fault. A positive anomaly in the western part of the district is also defined. Negative SO_2 anomalies are

not as pronounced as the negative H_2S anomalies.

A contour plot of C_nH_n concentrations shows a positive spot anomaly just north of the East Camp mine with the rest of the district at much lower concentrations. The contour log -0.7 discriminates many of the samples in the central part of the district. The histogram of C_nH_n concentrations (Fig. 5) and ternary plot of $CO_2/10-CH_4-10*C_nH_n$ (Fig. 10d) shows that concentrations do not range widely or display a distinct data trend and thus contouring does not reveal much anomaly contrast.

The histogram and probability plot of log S/CO_2 (Fig. 5) suggests a bimodal distribution. In addition, the ternary plots $10*CO_2-H_2O-1000*S$ (Fig. 10c) and $H_2S-CO_2/100-SO_2$ (Fig. 10b) each display discrete S-rich and CO_2 rich sample groups. To discriminate these data on a contour plot the ratio log S/CO_2 is contoured in Figure 11i. Anomalous areas are clearly defined by the -2 contour line that defines anomalies along the Summit-East Camp fault near the Summit mine, Telephone Ridge-Raeburn Hills, and the East Camp mine. These anomalies are well constrained and have adjacent low or negative anomalies (< -2.6). The anomaly contrast over a 5 km distance that includes the Telephone Ridge-Raeburn Hills area is 1.2 log units. The Alabama mine area in the western part of the district are also anomalous.

The ternary plot $CO_2-10*CH_4-100*S$ (Fig. 10a) shows samples that are relatively CH_4-rich and S-poor and another

sample group that is CH_4-poor and S-rich with data
distributed between. This is a bivariate data trend that
can be contoured by using the two ratios log CH_4/CO_2 and log
S/CO_2. Figure 11i is a contour plot that represents the
difference between the contoured log CH_4/CO_2 surface and the
contoured log S/CO_2 surface. Methane is much more abundant
than S and thus samples with high S/CO_2 ratios and low
CH_4/CO_2 ratios reduce the difference and plot as depressions
where the differences are minimized. Anomalies, represented
as depressions, are clearly defined and constrained and are
most prominent at Telephone Ridge - Raeburn Hills area and
the Summit mine area. Smaller anomalies occur near the East
Camp mine and at the Alabama mine in the western part of the
district. The log CH_4/CO_2 - log S/CO_2 contour plot displays
the best defined anomalies.

In this study significant amounts of SO_2 are measured
in fluid inclusions and several samples have SO_2/H_2S ratios >
5 (Fig. 6). The stability of SO_2 in fluid inclusions at low
temperatures is uncertain. Crushing and measuring SO_2 in
real-time immediately after release and in a high-vacuum
should minimize secondary or analytical sources for SO_2.
The SO_2/H_2S ratios in HF-1 are significantly less than the
SO_2/H_2S ratios in the Steeple Rock samples even though the
HF-1 samples are H_2S rich relative to Steeple Rock samples.
This supports the conclusion that SO_2 is present in
inclusions and is not an analytical product of H_2S. In

addition, SO_2/H_2S ratios from Steeple Rock are not constant, with the more S-rich samples having higher SO_2/H_2S ratios (Fig. 6).

INTERPRETATIONS

DATA DISTRIBUTIONS

The uncertain precision of the analytical method (see Table 1) can be overlooked if the sample to sample compositional range is much greater than the greatest estimate for precision. For example, the greatest estimate for SO_2 precision of about ±100 % would still allow placement of an analysis within one of the populations of SO_2 concentrations that are separated by > 1 order of magnitude. Histograms of gas concentrations for all measured gas species display ranges of 1 to 2.5 orders of magnitude (Fig 5). Methane and SO_2 concentrations display lognormal, bimodal distributions that suggests the analytical method is discriminating two populations (Fig. 5). The modes on the histograms for CH_4 and SO_2 are separated by factors of 4 and 10 respectively which is much greater than the precision listed in Table 1. Data distributions on ternary composition plots (Figs. 10a - 10d) define trends and groupings that suggest that results from crush analysis of fluid inclusion gases provides systematic variations. Contour plots of fluid inclusion gas

compositions show systematic groupings of high and low values (e.g. Fig. 11f for CO_2, and Fig. 11d for H_2S) in geologic space. These systematic variations are repeated by more than one gas species suggesting that fluid inclusion gas analysis data is representing geologic variations of gas compositions in an epithermal environment. Log S/CO_2 and log CH_4/CO_2 - log S/CO_2 contour plots provide the best defined anomalies (Figs. 11h, 11i). Processes or fluid interactions acting in the epithermal environment must have discriminated between H_2S and SO_2, CO_2, and CH_4. This is supported by a bimodal log S/CO_2 distribution, and trends on ternary composition plots that feature discrete S-rich and CO_2-rich sample groups (Figs. 10a, 10c).

In the shallow parts of geothermal systems, deep upwelling fluids boil and mix with shallow fluids (Hedenquist, 1989, 1991; Henley, 1984; Glover, 1970). Boiling can have a dramatic effect on dissolved gas compositions as the more volatile gases (i.e. CH_4) partition to the vapor phase at greater rates than the more soluble gases (i.e. H_2S, and SO_2) (Henley, 1984). The effect of boiling on dissolved gases can be modelled by using volatility ratios derived by Giggenbach (1980). Figure 12 is a ternary composition plot of CO_2-10*CH_4-100*S with data from Steeple Rock plotted along with a modelled fluid composition of a boiling fluid over the temperature interval 270° C to 250° C. The boiling model assumes continuous steam
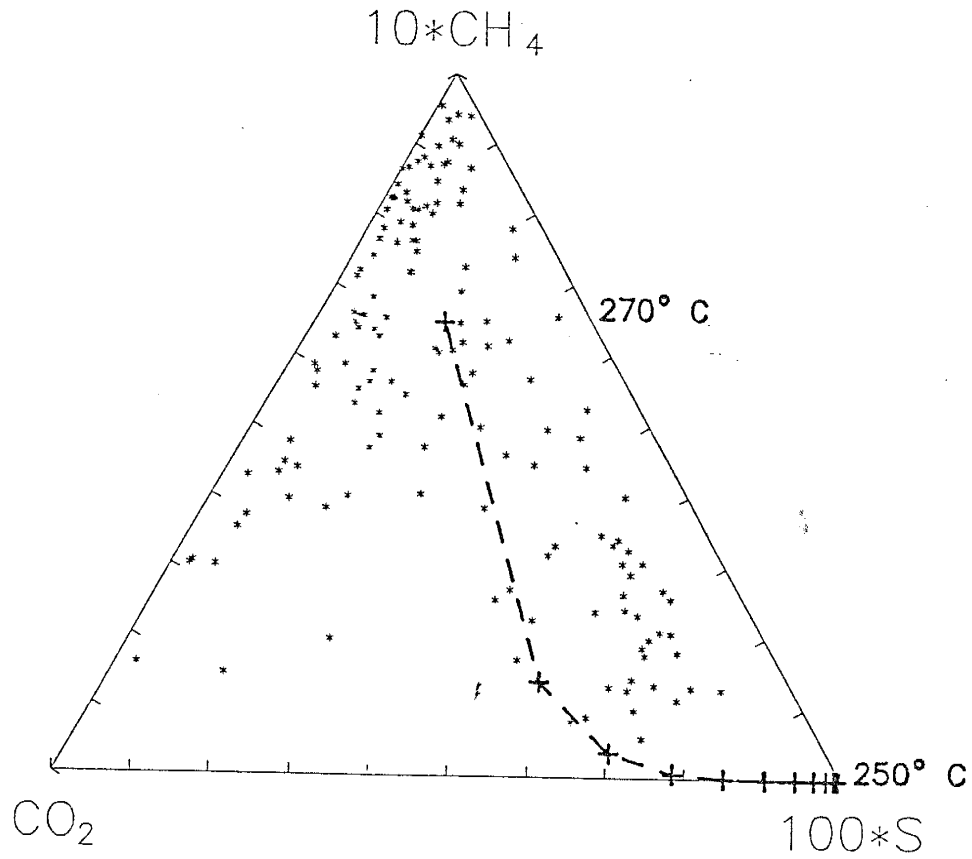
FIGURE 12. Ternary composition plot of CO_2-10*CH_4-100*S with data from Steeple Plotted as asterisks. The bold line and crosses represent the boiling model described in the text. This model illustrates that boiling can produce the data distribution observed.

separation and results in a cumulate steam fraction of 0.06.
The fluid composition is recalculated in two degree
increments. If hydrostatic pressure conditions are assumed
the corresponding depth interval would be 440 to 300 m. The
composition of the deep reservoir fluid is unknown and thus
a reasonable initial fluid composition is chosen to be 6.6%
CH_4, 19% CO_2, and 0.017% S (0.085% H_2S and 0.085% SO_2). The
modelled fluid path shows that initial boiling rapidly
partitions CH_4 into the vapor phase which causes the fluid
composition to move away from the 10*CH_4 apex. Carbon
dioxide is more volatile than H_2S or SO_2 such that with
continued boiling the fluid becomes S-enriched relative to
CO_2. The modelled fluid path serves to illustrate the
dramatic gas composition changes that may occur over a 20° C
boiling interval. The actual boiling conditions in a
epithermal environment are probably not represented by
continuous steam separation and most likely include mixing
between fluids. Giggenbach and Glover (1992) plot CH_4, CO_2,
and H_2S concentrations from the Rotorua Geothermal system,
New Zealand on a similar ternary composition plot that
displays data trends similar to those observed at Steeple
Rock. Giggenbach and Glover (1992) suggest the data
distribution represents relatively unboiled or "early vapor"
from CH_4-rich fluids and transitional compositions to a S-
rich fluid that is relatively degassed and would produce a
"late vapor". As the boiling model suggests, initial

boiling would produce CH_4-rich vapor that could be trapped as vapor-filled inclusions, however the positive correlation between H_2O and CH_4 does not support the presence of CH_4-rich vapor-filled inclusions. Upon further boiling, CO_2 partitions to the vapor phase resulting in a S-rich fluid. Data from Steeple Rock display groupings of S-rich and CO_2-rich fluids and is demonstrated by the bimodal distribution character of the log S/CO_2 ratios (Figs. 5). In addition, the ternary plot of CO_2-H_2O/100-S shows that gas-rich samples tend to be either S-rich or CO_2-rich (Fig. 10c). The contour plot of log S/CO_2 ratios shows positive log S/CO_2 anomalies are commonly flanked by negative log S/CO_2 anomalies (Fig 11h). This relationship is observed in the upper parts of active geothermal systems that have S-rich, degassed, reservoir fluids in upflow zones with marginal CO_2-rich fluids (Hedenquist, 1991; Henley, 1984; Glover, 1970). The partial pressures (P) of dissolved gases are related to their mole fraction (X) by Henry's Law Coefficient (K_H).

$$P = K_H * X$$

Figure 13 is a plot of ln K_H vs Temperature for five gases in H_2O. Note that the K_H for CO_2 passes through a maximum at about 175° C. Thus in the cooler marginal fluids of a hydrothermal system CO_2 is more soluble which may help explain the bimodal nature of the S/CO_2 ratios.

Sulfur dioxide is more soluble than H_2S and in degassed
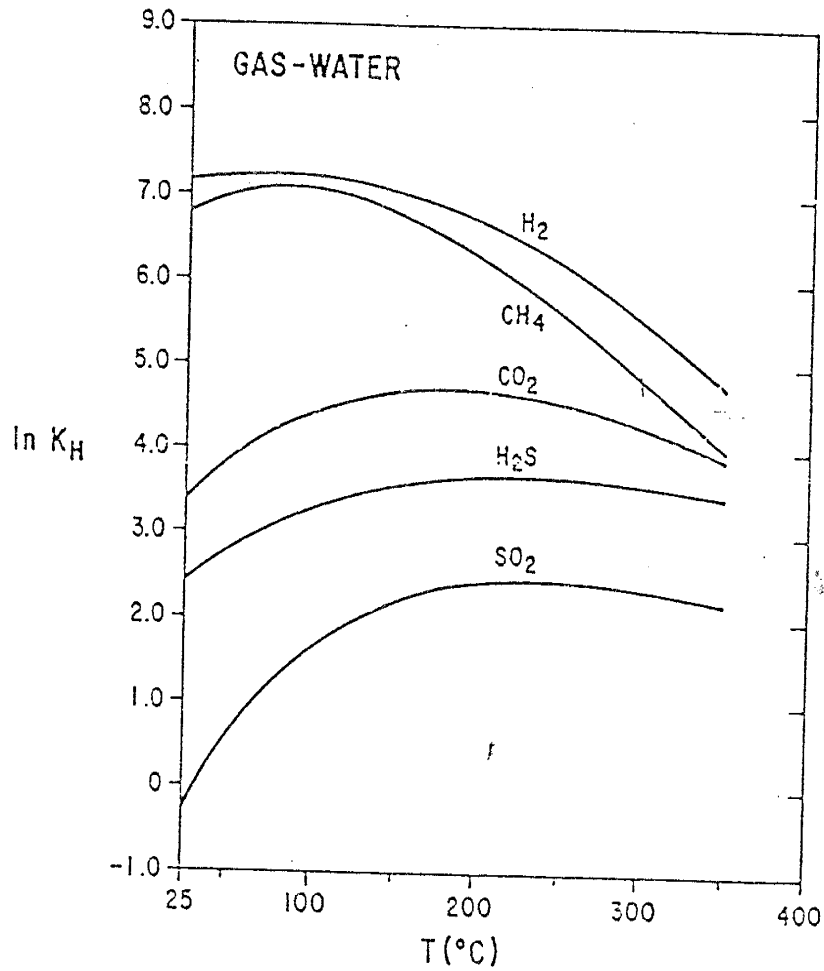
FIGURE 13. Plot of ln K_H against Temperature (from Drummond, 1981). Greater ln K_H values represent less solubility in water. Note the maximum solubility of CO_2 at about 175° C.

fluids could become enriched relative to H_2S. A boiling model of fluid gas compositions is plotted on a H_2S-CO_2/10-SO_2 ternary plot along with data from Steeple Rock (Fig. 14). The same parameters are used for this model that are used in the model depicted in Figure 12 and an initial fluid composition of 7% CO_2, 0.018% H_2S, and 0.012% SO_2. This model suggests boiling is capable of enriching a fluid in SO_2.

The contour plot of log CH_4/CO_2 - log S/CO_2 shows well-defined anomalies (Fig 11j). The modelled boiling path in Figure 12 is bivariate with initial loss of CH_4 resulting in decreasing CH_4/CO_2 ratios and with continued boiling increasing S/CO_2 ratios. This suggests the well defined anomalies that occur as depressions because CH_4 is always much greater than S, on the log CH_4/CO_2 - log S/CO_2 contour plot represent the various degrees to which a fluid has boiled with the center of the anomalies representing the most boiled fluid. The above discussion favors a boiling process for distribution of fluid-gas regimes at Steeple Rock, mixing however, almost certainly occurred. Data that may represent a mixing trend are found on the CO_2-10*CH_4-100*S ternary composition plot as data between the S-rich samples and the CH_4-rich samples (Fig. 12).

RELATION OF FLUID INCLUSION GAS ANOMALIES TO MINERALIZATION

The best defined fluid inclusion gas anomalies utilize
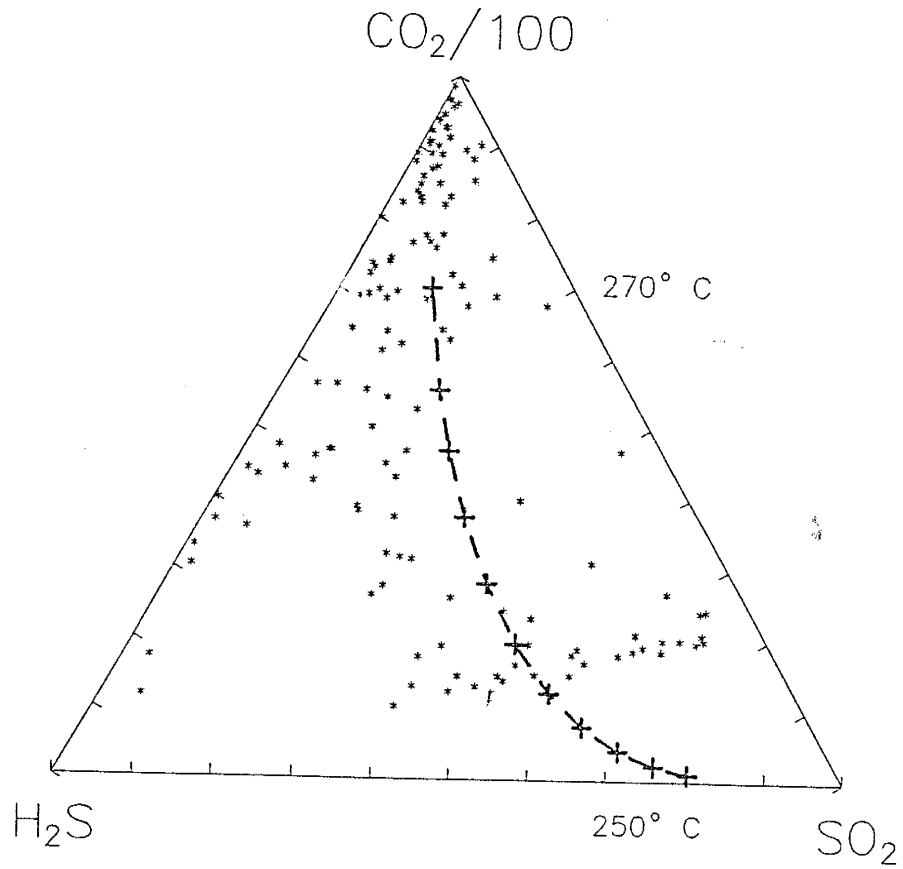
FIGURE 14. Ternary composition plot of H_2S-CO_2/100-SO_2. The asterisks are data from Steeple Rock and the bold line and samples represents to boiling model described in the text. This model shows that SO_2 can be enriched relative to H_2S through boiling.

S/CO_2 and $CH_4/CO_2 - S/CO_2$ ratios. Where these anomalies are coincident they appear to represent S-rich boiling fluids which is a favorable setting for ore deposition (Figs. 15, 16). Four significant anomalies are recognized and ranked according to their areal size, intensity, and sample control and are: 1) the Telephone Ridge - Raeburn Hills area, 2) the Summit mine area, 3) Alabama mine, and 4) the East Camp mine area (see Figs. 15, 16). The anomalous samples in the southern part of the district are unconstrained. Three of the four anomalies listed occur along the Summit-East Camp fault which also localizes mineralization on a district scale.

The Telephone Ridge - Raeburn Hills anomaly is the largest and best defined anomaly and occurs in the center of the district on the Summit - East Camp structure. This anomaly does not feature known mineralization and lacks large quartz ± adularia veins. The Summit mine area has the second most prominent fluid inclusion gas anomaly. The ore mineralization reported by Biron Bay Resources Ltd. - Nova Gold occurs on the north margin of this anomaly.

The third most prominent anomaly occurs at the Alabama mine in the western part of the district. At the Alabama mine has historic production of Au-Ag-Cu ore in rhyolite dike margins. Drilling by Great Lakes Exploration drilled at the Alabama mine in 1991 did not encounter ore-grade mineralization. The fourth ranked anomaly occurs at the

FIGURE 15 (next page). Log S/CO_2 contour plot with
constrained anomalies > -2 shaded. See Figure 2 for
abbreviations. This contour plot shows the best anomaly
contrast and paired positive and negative anomalies. The
following four anomalies are recognized: The Telephone Ridge
- Raeburn Hills anomaly, Summit mine anomaly, Alabama mine
anomaly, and the East Camp mine anomaly based on anomaly
contrast, size, and constraint.

Scale

Steeple Rock
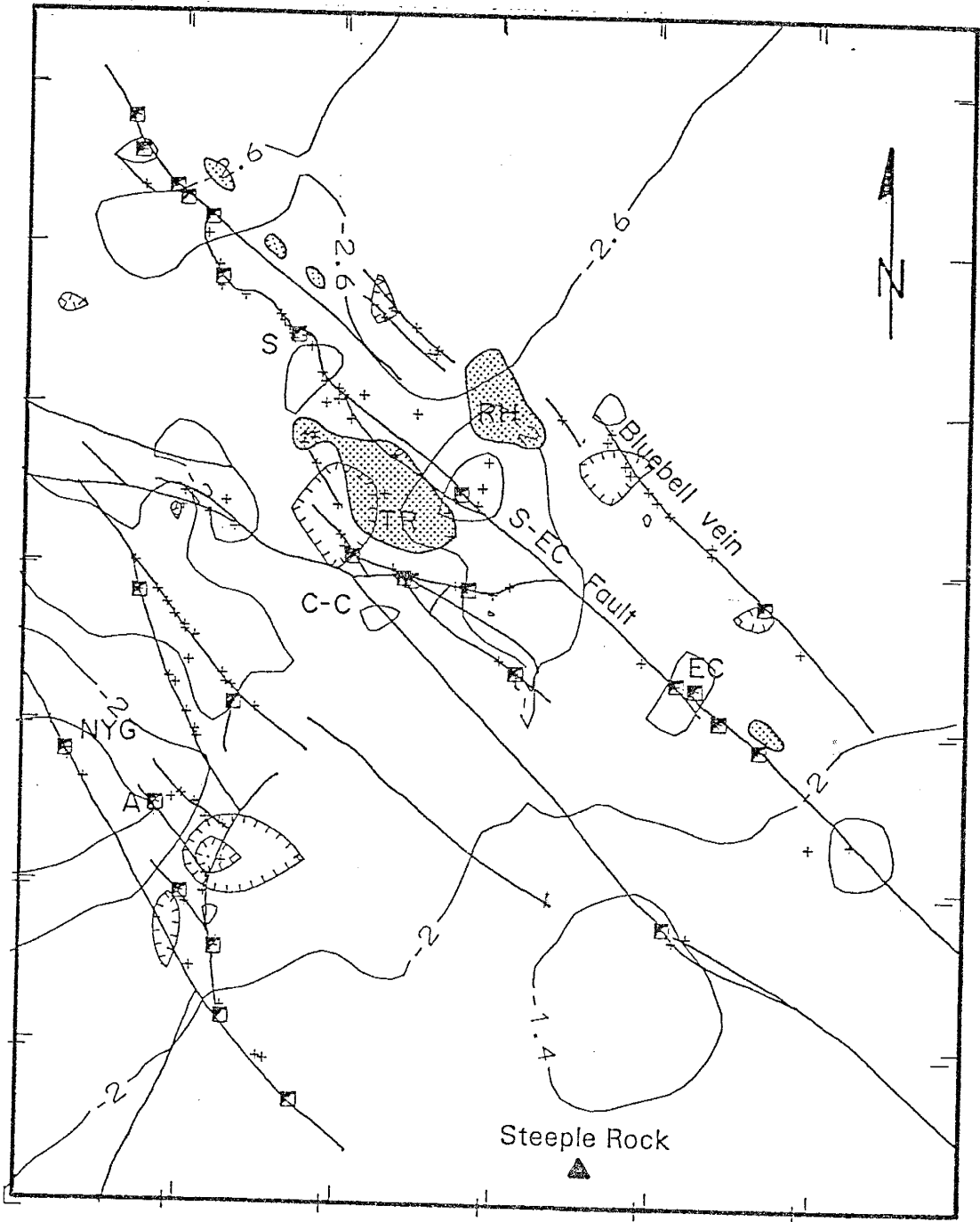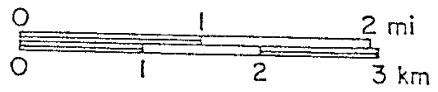
FIGURE 16 (next page). Log CH_4/CO_2 - log S/CO_2 contour plot with anomalies < 1.4 highlighted. See Figure 2 for abbreviations. The following four anomalies are recognized: The Telephone Ridge - Raeburn Hills anomaly, the Summit mine anomaly, the Alabama mine anomaly, and the East Camp mine.
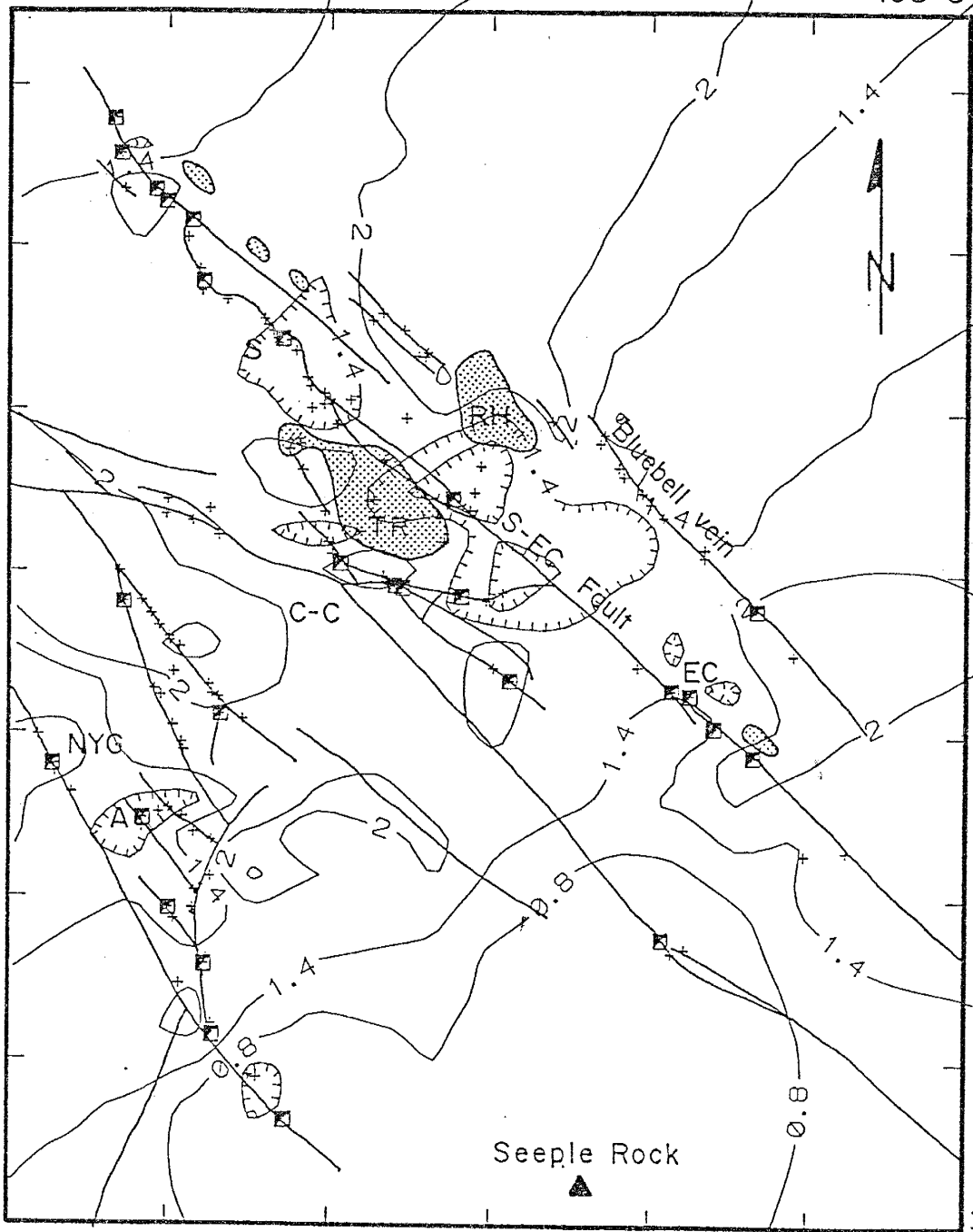
Legend

⟍ Fault
▨ Mine
+ Sample Location
⬡ Acid Sulfate Alteration

Scale

0 — 1 — 2 mi
0 — 1 — 2 — 3 km
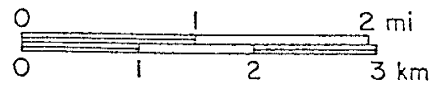
East Camp Mine. The East Camp mine has been one of the largest Au-Ag producers in the district.

The three largest known ore occurrences at Steeple Rock are the Center-Carlisle mines, the East Camp mines, and the Summit mine. Two of these areas have proximal or coincident fluid inclusion gas anomalies with the notable exception of the Carlisle - Center mine. The Carlisle - Center mines have been the most prolific metal producers in the district. The Center-Carlisle Mine group lies between the Center-Carlisle Mine group positive S/CO_2 anomaly and a adjacent negative log S/CO_2 anomaly (Fig. 15). This different anomaly relationship for this ore locality may suggest a different fluid-gas regime. The Summit Mine, Center-Carlisle Mines, and the East Camp Mines all contain ore grade precious metals, however the Carlisle-Center mines are more base-metal rich than the Summit or East Camp Mines. A possible explanation for these different anomaly relations could be that different ore-forming processes occurred at the Carlisle-Center Mine Group. As fluids boil during their ascent, the loss of CO_2 and H_2S destabilize HS^- complexes, including Au resulting in Au precipitation (Drummond and Ohmoto, 1985; Reed and Spycher, 1985). Cooling or mixing, is more effective at precipitating Cl^- complexed base-metals (eg. Pb, Zn, Cu)(Reed and Spycher, 1985). It is possible that mixing was a more prominent process at the Center-Carlisle mine group than either at the Summit mine or East

Camp mine.

GENESIS OF ACID SULFATE ALTERATION AND RELATION TO ORE MINERALIZATION

Significant areas of acid-sulfate alteration and silicification occur in the vicinity of the Summit-East Camp fault and are cut by quartz ± adularia veins. These acid-sulfate altered areas have attracted exploration efforts for disseminated ore.

The presence of pyrophyllite at Telephone Ridge suggests equilibrium temperatures of 250° C or greater as does fluid inclusion homogenization temperatures. If hydrostatic pressure is assumed, a temperature of 250° C corresponds to a depth of about 300 m below the water table.

Acid sulfate alteration can form principally in three environments as summarized by Rye et al. (1992): 1) Hot spring environment in which H_2S is oxidized to SO_4^{2-} above the water table, 2) disproportionation of magmatic SO_2 into H_2S and SO_4^{2-} where magmatic volatiles condense and cool, and 3) a supergene effect caused by oxidation of sulfides. Holland (1965) was one of the earliest workers to propose disproportionation of SO_2 according to the following reaction:

$$4SO_2 + 4H_2O \longrightarrow H_2S + 3H_2SO_4$$
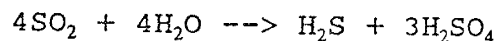
Stoffregen (1987) modelled the formation of deep acid-sulfate alteration in the epithermal environment at the

Summitville deposit, Colorado, using SO_2 disproportionation.
Utilizing sulfur isotope studies of alunite and pyrite, Rye
et al.,(1992) demonstrates a magmatic source for sulfur in
deep acid-sulfate alteration from several epithermal
deposits.

The temperatures of formation of acid-sulfate
alteration at Telephone Ridge of about 250° C suggests a
deep environment.   The condensation of acidic magmatic
volatiles at depths of 300-400m below the water table may
have been responsible for the acid sulfate alteration at
Telephone Ridge and other acid-sulfate altered areas at
Steeple Rock.   The Summit-East Camp structure may have
provided conduits for localized plumes of magmatic
volatiles.   Many acid-sulfate altered areas at Steeple Rock
are capped by stratiform silicified rocks.   Some of the
silicified rock on Telephone Ridge exhibit relict textures
suggesting a volcaniclastic host rock.   This volcaniclastic
unit may have been a deep aquifer in which acidic magmatic
fluids may have mixed and deposited quartz.   The acid
sulfate alteration is cut by quartz ± adularia veins which
hosts the known ore in the district.   This spacial
relationship between ore bearing quartz ± adularia veins and
acid sulfate alteration is found in many epithermal
districts such as the Comstock, NV (Vikre, 1989), and
Cactus, CA (Blaske, et al., 1991).   Vikre, et al., (1988)
dated (K-Ar) widespread acid-sulfate alteration and vein

formation at the Comstock District, and found most of the acid-sulfate alteration to be a close precursor, vein formation. If the SO_2 analyzed in fluid inclusions at Steeple Rock represents a magmatic gas component, the hydrothermal fluid depositing the quartz ± adularia veins may have entrained some magmatic volatiles.

EXPLORATION IMPLICATIONS

Potential ore-forming fluids in an epithermal environment should be H_2S-rich, ascending, and boiling and/or mixing. This study demonstrates fluid inclusion gas analysis can detect district-scale gas anomalies that reflect fluid-gas regimes. Potential ore-forming fluids are represented by positive log S/CO_2 anomalies. Boiling zones are more broadly represented by negative log CH_4/CO_2 - log S/CO_2 anomalies. The most prominent fluid inclusion gas anomalies occur along the Summit-East Camp structure which apparently controls hydrothermal fluid regimes on a district-scale at Steeple Rock. The Alabama Mine area in the western part of the district also has a significant log S/CO_2 anomaly. The largest and most promising negative log CH_4/CO_2 - log S/CO_2 and positive S/CO_2 anomalies occur at Telephone Ridge and Raeburn Hills altered areas. No ore mineralization has been found within the Telephone Ridge - Raeburn Hills anomaly, but this evidence suggests the Telephone Ridge - Raeburn Hills area has potential for blind

mineralization. Fluid inclusion gas analysis has also located areas of nonanomalous gas compositions suggesting low ore potential.

CONCLUSIONS

Fluid inclusion gas analysis utilizing a fast-scanning QMS and crush-release of fluid inclusion volatiles provides a relatively rapid method for analyzing fluid inclusion volatiles. Analytical considerations include absorption effects on H_2O concentrations and air contamination from absorbed and trapped air on sample surfaces. A correction factor for H_2O absorption is derived from repeat analyses of Hansonberg fluorite. Repeats of baked samples allow derivation of an air subtraction factor that removes most of the air component from analyses.

Analyses of 149 surface samples from the Steeple Rock and Duncan mining districts provide the following conclusions:

(1) A total of eight gas species were measured: CH_4, H_2O, N_2, H_2S, Ar, C_nH_n, CO_2, and SO_2. The most useful gas species for defining data distribution trends are CH_4, H_2S, CO_2, and SO_2.

(2) The ratio of total S/CO_2 ratios display a bimodal lognormal distribution with the modes separated by about one order of magnitude.

(3) Data distribution trends can be explained by invoking a boiling process that partitions the more volatile gases into the vapor phase.

(4) District-scale contour plots show that log S/CO_2 and log CH_4/CO_2 - log S/CO_2 produce the best defined anomalies and are coincident. These anomalies represent ascending and boiling fluids. The correlation of anomalous values in geologic space implies spacial relations dominate over paragenetic variability.

(5) The Summit-East Camp fault localizes fluid inclusion gas anomalies and appears to exert a district scale control on fluid-gas regimes. These anomalies are proximal to or coincident with known ore localities.

(6) The most prominent fluid inclusion gas anomaly occurs at the Telephone Ridge - Raeburn Hills area. This area includes acid-sulfate alteration but does not include known ore mineralization and is considered to have good exploration potential.

REFERENCES CITED

Analytical Methods Committee, Royal Soc. of Chem., Burlington House, Piccadilly, London W1V 0BN, UK, 1989. Robust statistics-How not to reject outliers, Part 1 Basic concepts. Analyst, v. 114, 1693-1697.

Blaske, A.R., Bornhorst, T.J., Brady, J.M., Marsh, T.M., and McKitrick, S.A., 1991. The Shumake volcanic dome-hosted epithermal, precious metal deposit, western Mojave Desert, California. Econ. Geol., v. 86, pp. 1646-1656.

Browne, P.R.L., Roedder, E & A., Wodzicki, (1976).
    Comparison of past and present geothermal waters from a
    study of fluid inclusions, Broadlands field, New
    Zealand, *in*: T. Cadek (editor), Proceedings
    International Symposium on Water-Rock Interaction,
    Czechoslovakia, 1974, Geol. Survey, Prague, pp. 140-
    149.

Chapin, C.E., and Seager, W.R., 1975. Evolution of the Rio
    Grande Rift in the Socorro and Las Cruces areas: New
    Mexico Geological Society Guidebook 26, pp. 297-322.

Drummond, S.E., and Ohmoto, H., 1985. Chemical evolution and
    mineral deposition in boiling hydrothermal systems.
    Econ. Geol., v. 80; pp. 126-147.

Drummond, S.E., 1981. Boiling and mixing of hydrothermal
    fluids: Chemical effects on mineral precipitation.
    Unpub. Ph.D. thesis, Pennsylvania State Univ., 380 pp.

Gerlach, T.M., 1980a. Investigation of volcanic gas analysis
    and magma outgassing from Erta'Ale Lava Lake, Afar,
    Ethiopia. Jor. Volcan. Geothermal Res., v. 7, pp. 415-
    441.

Gerlach, T.M., 1980b. Evaluation of volcanic gas analyses
    from Kilauea volcano. Jor. Volcanology and Geothermal
    Res., v. 7, pp. 295-317.

Gerlach, T.M., 1982. The chemical and isotopic composition
    of gas discharges from New Zealand andesitic volcanoes.
    Bull. Volcan., v. 45, pp. 253-256.

Giggenbach, W.F., 1980. Geothermal gas equilibria. Geochim.
    Cosmochim. Acta, v. 44, pp. 2021-2032.

Giggenbach, W.F., 1982. The chemical and isotopic
    composition of gas discharges from New Zealand
    andesitic volcanoes. Bull. Volcanolgy, v. 45, pp. 253-
    256.

Giggenbach, W.F. and Glover, R.B., 1992. Tectonic regime and
    major processes governing the chemistry of water and
    gas discharges from the Rotorua geothermal field, New
    Zealand. Geothermics, v. 21, pp. 121-140.

Glover, R.B., 1970. Interpretation of gas compositions from
    the Wairakei field over ten years. Geothermics, v. 2,
    pp. 1355-1366.

Graney, J.R., Kesler, S.E., and Jones, H.D., 1991.
Application of gas analysis of jasperoid inclusion
fluids to exploration for micron gold deposits, *in*:
S.E. Kesler (editor) Jorn. Geochem. Expl., special
issue; Fluid Inclusion Gas Analyses in Mineral
Exploration, v.42, pp 91-106.

Griggs, R.L., and Wagner, H.C., 1966. Geology and ore
deposits of the Steeple Rock mining district, Grant
County, New Mexico. U.S.G.S. Bull., 1222-E, 29 pp.

Hayashi, K., and Ohmoto, H., 1990. Solubility of gold in H_2S
and NaCl bearing aqueous solutions at 250° to 350° C.
(abs.) Proceedings Geol. Soc. Am. annual Meeting,
Dallas, TX, pp. A157.

Haynes, P.S., and Kesler, S.E., 1988. Analysis of fluid
inclusion gases in jasperoid as an exploration method
for micron gold deposits. Jor. Geochem. Explor., v. 30,
pp. 142-149.

Hedenquist, J.W., and Browne, P.R.L., 1989. The evolution of
the Waiotapu geothermal system, New Zealand, based on
the chemical and isotopic composition of its fluids,
minerals and rocks. Geochim. Cosmochim. Acta, v. 53,
pp.2235-2257.

Hedenquist, J.W., 1991. Boiling and dilution in the shallow
portion of the Waiotapu geothermal system, New Zealand.
Geochim. Cosmochim. Acta, v. 55, pp. 2753-2765.

Hedenquist, J.W., 1990. The thermal and geochemical
structure of the Broadlands-Ohaaki geothermal system,
New Zealand. Geothermics, v. 19, pp. 151-185.

Hedenquist, J.W., and Aoki, M., 1991. Meteoric interaction
with magmatic discharges in Japan and the significance
for mineralization. Geology, v. 10, p. 961-1056.

Hedlund, D.C., 1990a. Geologic map and sections of the
Steeple Rock quadrangle, Grant and Hidalgo Counties,
New Mexico. USGS, Open-file Rpt 90-0240.

Hedlund, D.C., 1990b. Geology and mineral deposits of the
Steeple Rock and Duncan mining districts, Grant and
Hidalgo Counties, New Mexico, and Greenlee County,
Arizona. USGS, Open-file Rpt. 90-0239.

Henley, R.W., 1984. Gaseous components in geothermal processes, *in*: J.M. Robertson (editor), Fluid-Mineral Equilibria in Hydrothermal Systems. Reviews in Economic Geology, v. 1, pp. 45-55.

Holland, H.D., 1965. Some applications of thermochemical data to problems of ore deposits, II. Mineral assemblages and the composition of ore-forming fluids. Econ. Geol., v. 60, pp. 1101-1166.

Jones, H.D., and Kesler, S.E., 1992. Fluid inclusion gas chemistry in east Tennessee Mississippi Valley-type districts: Evidence for immiscibility and implications for depositional mechanisms. Geochim. Cosmochim. Acta, v. 56, pp. 137-154.

Kesler, S.E., Haynes, P.S, Creech, M.Z., and Gorman, J.A., 1986. Application of fluid inclusion and rock gas analysis in mineral exploration. Jorn. Expl. Geochem., v. 25, pp. 201-215.

Knight, J.E., 1977. A thermochemical study of alunite, enargite, luzonite, and tennantite deposits. Econ. Geol., v. 72, pp. 1321-1336.

Landis, G.P., and Hofstra, A.H., 1991. Fluid inclusion gas chemistry as a potential tool: Case studies from Creede, CO, Jerritt Canyon, NV, Coeur d'Alene district, ID and MT, southern Alaska mesothermal veins, and mid-continent MTV's, *in*: S.E. Kesler (editor) Jorn. Geochem. Expl., special issue; Fluid Inclusion Gas Analyses in Mineral Exploration, v.42, pp 25-60.

Magro, G., and Pennisi, M., 1991. Noble gases and nitrogen: mixing and temporal evolution in the fumarolic fluids of Vulcano, Italy. Jor. Volcan. Geothermal Res., v. 47, pp. 237-247.

McIntosh, W.C., Chapin, C.E., Ratte', J.C., and Sutter, J.F., 1992. Time-stratigraphic framework for Eocene-Oligocene Mogollon-Datil volcanic field, southwest New Mexico. Geol. Soc. America Bull., v. 104, pp. 851-871.

Marty, B., and Giggenbach, W.F., 1990. Major and rare gases at White Island, New Zealand: Origin and flux of volatiles. Geophys. Res. Lett., v. 17, pp. 247-250.

McLemore, V.T., and Clark, K.F., 1993. Alteration and epithermal mineralization in the Steeple Rock mining district, Grant County, New Mexico, and Greenlee County, Arizona (Ext. Abs.). in: S.B. Romberger (editor), Proceedings from Integrated Methods in Exploration and Discovery, Soc. Econ. Geol., Denver, CO, 1993.

Norman, D.I., and Sawkins, F.J., 1987. Analysis of volatiles in fluid inclusions by mass spectrometry. Chem. Geol., v. 61, pp. 1-10.

Norman, D.I., Harrison, R.W., and Behr Andres, C., 1991. Geology and geochemical analysis of mineralizing fluids at the St. Cloud and U.S. Treasury mines, Chloride mining district, New Mexico, in: S.E. Kesler (editor) Jorn. Geochem. Expl., special issue; Fluid Inclusion Gas Analyses in Mineral Exploration, v.42, pp 61-90.

Osborne, M.A., 1987. Geology and alteration of a part of the Aurora mining district,Mineral County, Nevada in: J.L. Johnson (editor), Bulk Minable Precious Metal Deposits of the Western U.S., 1987, Guidebook, Geol. Soc. of Nevada, pp. 245-249.

Putnam, B.R.III, Norman, D.I., and Smith, R.W., 1983. Mississsppi valley-type lead-fluorite-barite deposits of the Hansonburg mining district, in: New Mexico Geol. Soc. Guidebook, 34th Field Conference, Socorro Region II, 1983.

Ratte', J.C., Cather, S.M., Chapin, C.E., Duffield, W.E., Elston, W.E., and McIntosh, W.C., 1989. Excursion 6A: Eocene-Miocene Mogollon-Datil volcanic field, New Mexico, in: C.E. Chapin and J. Zidek (editors), Field Excursions to Volcanic Terranes in the Western United States, Volume I: Southern Rocky Mountain Region, pp. 43-120. IAVCEI General Assembly, Santa Fe, NM, 1989, New Mexico Bureau of Mines and Mineral Resources, Bulletin 137, 192 pp.

Reed, M.H., and Spycher, N.F., 1985. Boiling, cooling, and oxidation in epithermal systems: A numerical modelling approach, in: B.R. Berger and P.M. Bethke (editors), Geology and geochemistry of epithermal systems. Reviews in Economic Geology, v. 2, pp. 249-270.

Rye, R.O., Bethke, P.M., and Wasserman, M.D., 1992. The stable isotope geochemistry of acid-sulfate alteration. Econ. Geol., v. 87, pp. 225-262.

Spycher, N., and Reed, M., 1989. Evolution of a Broadlands-type epithermal ore fluid along alternative P-T paths: Implications for the transport and deposition of base, precious and volatile metals. Econ. Geol., v. 84, pp. 328-359.

Stoffregen, R., 1987. Genesis of acid-sulfate alteration and Au-Cu-Ag mineralization at Summitville, Colorado. Econ Geol. v. 82, pp. 1575-1591.

Sverjensky, D.A., 1987. The role of migrating oil field brines in the formation of sediment-hosted Cu-rich deposits. Econ. Geol., v. 82, pp. 1130-1141.

Simmons, S.F., and Christensen, B.W., 1990. Platy calcite as an indicator of boiling in epithermal deposits: Evidence from New Zealand geothermal systems (abs.). Geol. Soc. of America annual meeting, Dallas, TX, v. 22, p. 42.

Taguchi, S., and Hayashi, M., 1982. Application of the fluid inclusion thermometer to some geothermal fields in Japan. Geothermal Resources Council Trans., v. 6, pp. 59-62.

Vikre, P.G., McKee, E.H., and Silberman, M.L., 1988. Chronology of Miocene hydrothermal and igneous events in the western Virginia Range, Washoe, Storey and Lyon Counties, Nevada. Econ. Geol., v. 83, pp. 864-874.

Vikre, P.G., 1989. Fluid mineral relations an the Comstock Lode. Econ. Geol., v. 84, pp. 1574-1613.

Wahl, D.E., Jr,. 1980. Mid-tertiary volcanic geology in parts of Greenlee County, Arizona, Grant and Hidalgo Counties, New Mexico. Tempe, Arizona State University, Ph. D. dissertation, 147 p.

Wahl, D.E., Jr,. 1983. Comments on economic volcanology between Redrock, New Mexico, and Clifton, Arizona (abs.). New Mexico Geology, V. 5, p. 67.

APPENDIX A
DESCRIPTION OF COMBINED CRACKING OUTLINES AND SENSITIVITY MATRIX

Matrix algebra is used to solve a series of linear equations in the data reduction routine. The necessary equation to solve is;

Intensity (I) = Partial pressure (P) x Sensitivity (S)

Table A1. This table is the sensitivity matrix that is used to solve the analyses after inversion and multiplication with a column matrix of AMU intensities.

	CH_4	H_2O	N_2	O_2	H_2S	Ar	C_nH_n	CO_2	SO_2
15	.801	0	0	0	0	0	0	0	0
18	0	.678	0	0	0	0	0	0	0
28	0	0	.871	0	0	0	0	.120	0
32	0	0	0	.862	.136	0	0	0	.126
34	0	0	0	0	.029	0	0	0	0
40	0	0	0	0	0	.929	0	0	0
43	0	0	0	0	0	0	1.66	0	0
44	0	0	0	0	0	0	.055	.795	0
64	0	0	0	0	0	0	0	0	.918

Table A2 lists the cracking profiles fro the measured gases. For each gas species the number represents the % intensity of the major peak.

	CH_4	H_2O	N_2	O_2	H_2S	Ar	C_nH_n	CO_2	SO_2
15	85.8	0	0	0	0	0	0	0	0
18	0	100	0	0	0	0	0	0	0
28	0	0	100	0	0	0	0	0	0
32	0	0	0	100	44.4	0	0	0	0
34	0	0	0	.4	100	0	0	0	0
40	0	0	0	0	0	100	0	0	0
43	0	0	0	0	0	0	100*	0	0
44	0	0	0	0	0	0	0	100	0
64	0	0	0	0	0	0	0	0	100

(*) At AMU 43 C_4H_{10} is 100% and C_3H_8 is 22.3%.

Table A2 illustrates that the major peaks were measured for all gas species with the exception of CH_4 in which the major peak at AMU 16 has interference from a secondary H_2O peak.

APPENDIX B

ABSORPTION TESTS AND H_2O CORRECTION FACTOR

Two examples of absorption tests are shown in Figure B1 and B2.   If the assumption that gas ratios released by crushing are constant regardless of sample size, a positive slope on a sample size vs. gas species/CO_O plot (Figure B1) would indicate absorption effects relative to CO_O.   Figure B1 plots H_AS/CO_O ratio against sample size with the bulk of the data vertically distributed suggesting very little absorption effects. Figure B2 plots the H_O/CO_O ratio against sample size and illustrates a crud linear distribution suggesting a greater proportion of released H_2O is absorbed from the smaller sample sizes.

Figure B1.

HF−C TEST
Absorbtion vs Sample Size
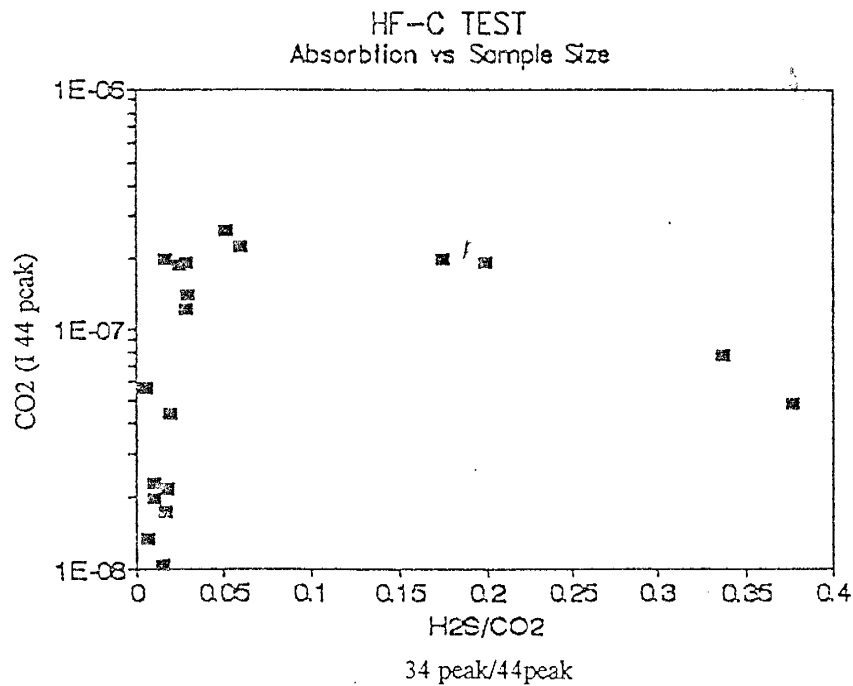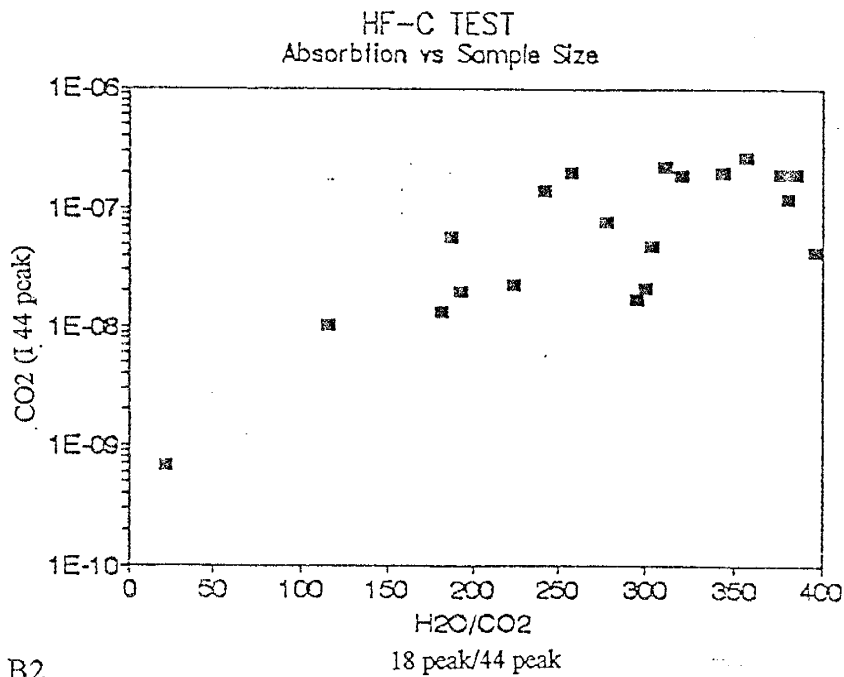
Figure B2.

A correction factor for absorption effects on H_2O is derived from repeated crushes of Hansonberg Fluorite (HF-1) with variable gas yields. The results are plotted on a CO_2 vs. H_2O plot in Figure B3 as crosses. The solid squares represent constant CO_2/H_2O ratios taken from the largest sample sizes and projected to the smaller sample sizes. The difference between the two slopes is used as a correction factor for H_2O absorption in the data reduction program in which H_2O is incrementally added to the smaller samples.

HF-C TEST
Absorbtion vs Sample Size
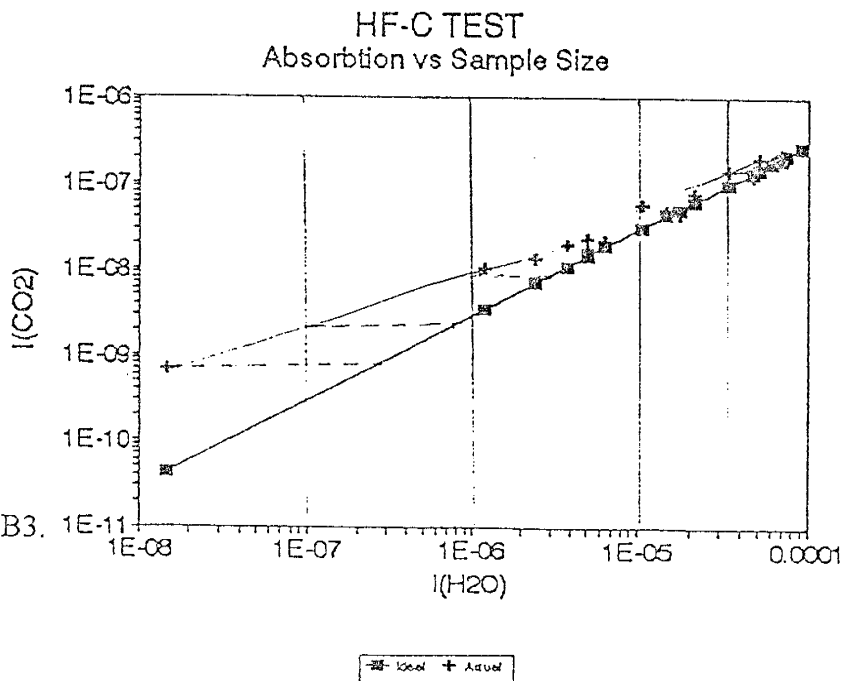
Figure B3.

APPENDIX C

DERIVATION OF AIR CONTAMINATION FACTOR

Two samples from Steeple Rock, SR-83 and SR-87B, contained anomalous amounts of N_2 and O_2 in their analyses. Splits from these two samples were repeated after bake-out at 100° C overnight under a high vacuum. Table C1 compares the analyses from the baked samples with the unbaked samples. The gas concentrations are in mole % of the dry-gas composition.

Table C1.

	Unbaked	Baked	Unbaked	Baked
	83B (2807)	83B (4016)	87 (2813)	87 (4017)
He	n.m.	0.296	n.m.	0.009
CH_4	4.99	5.59	2.23	2.36
% Gas	8.87	0.90	8.50	16.42
N_2	81.16	40.23	79.53	39.45
O_2	6.15	1.88	8.98	2.44
H_2S	0.0170	0.2731	0.0244	0.0229
Ar	n.m	0.267	n.m.	0.227
C_nH_n	0.069	0.468	0.072	0.291
CO_2	7.61	50.95	9.12	55.17
SO_2	0.0005	0.0477	0.0185	0.0115

The bargragh below (Figure C1) plots the data listed above in Table C1. Note the two Y-axes at different scales.
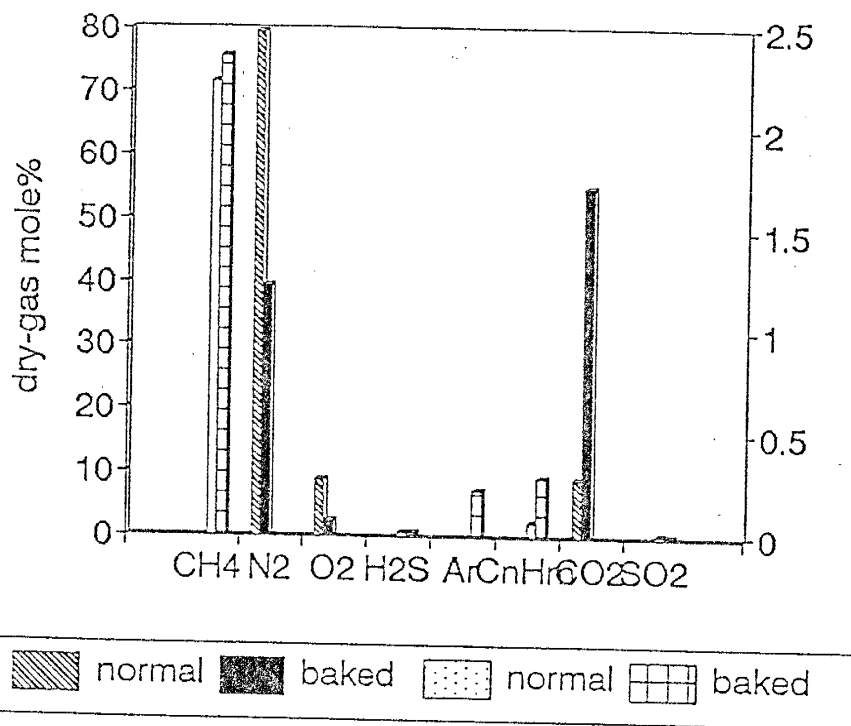
Figure C1.

These results suggest absorbed air was degassed by the bake-out process. From these results an air contamination factor was derived based on the ratios of N_2 to O_2 and N_2 to Ar for the degassed air fraction. AMU peak 32 was monitored in all analyses and where measured is assumed to be entirely from air contamination. The O_2 concentrations are then used to subtract N_2 and Ar according to:

Air component $N_2 = $ (mole % O_2) * (6)

Air component Ar = (mole % O_2) * (0.05)

APPENDIX D

DATA TABLES

On pages D2-D5 all analyses from Steeple Rock are listed. The section column indicates the section number for the sample site prefixed by the quadrant of the section (i.e. sw-36 is southwest quadrant of section 36). The x and y column are distance coordinates for each sample with the southwest corner of the Steeple Rock quadrangle the origin. These coordinates are in cm and 6.7 cm = 1 mile. Columns labeled sulf, Lat cc, and ore correspond to sulfide bearing, quartz after bladed calcite, and proximity to a productive mine site (< 100 ft). Gas concentrations are average mole % from multiple analyses for each sample (analyses/sample column). For data evaluation, He was subtracted and each analysis was renormalized. The column labeled I is the sum of ion intensities and represents sample size.

ʄ

Steeple Rock Data Base of Fluid Inclusion Gas Analysis

Sample averages sample #	section	x	y	analysis/sample	1=yes 0=no Sulf	Lat ca	Ore	He	CH4	H2O	N2	H2S	Ar	C2H6	CO2	SO2	I
1	no-10	1.85	36.82	7	avg	0	0	n.m	0.066659	98.5251	1.103302	0.003739	n.m.	0.002425	0.284044	0.008648	3.13E-06
2	nw-14	5.6	36.28	6	avg	0	0	n.m.	0.015506	98.32784	1.391599	0.005077	0	0.003123	0.425051	0.015145	1.19E-06
3	nw-14	5.65	36.65	6	avg	0	0	n.m.	0.084541	98.52968	0.795709	0.043257	n.m.	0.003207	0.566411	0.017143	7.00E-07
4	no-1	15.15	49.05	3	avg	0	0	n.m.	0.036909	97.00903	1.119181	0.002932	n.m.	0.002742	1.928329	0.000023	1.06E-06
5	so-5	29.11	47.5	3	avg	0	1	0.001181	0.390399	95.26019	2.014137	0.003603	0.017802	0.013300	2.29933	0.000901	7.1E-07
5b	so-5	29.11	47.5	8	avg	0	1	n.m.	0.152801	97.97775	1.214123	0.003139	n.m.	0.124700	0.544496	0.001426	3.97E-06
6	so-5	29.1	47.8	3	avg	0	1	n.m.	0.11529	97.77643	1.501152	0.001343	n.m.	0.304205	0.305278	0.305278	6.03E-07
7	so-5	29.12	47.05	3	avg	0	1	n.m.	0.414113	91.31703	3.823965	0.103307	n.m.	0.02714	4.175772	0.137078	1.03E-07
7b	so-5	27.35	49.15	6	avg	0	0	n.m.	0.434828	93.304401	1.82075	0.003077	n.m.	0.097078	4.277181	0.00168	1.03E-06
8	so-5	26.0	49.7	3	avg	0	1	0.001815	0.175309	95.29507	1.450591	0.006079	0.009016	0.023719	3.009817	0.007409	3.20E-07
55	nw-5	26.45	50.15	4	avg	0	0	0.001674	0.003163	95.55562	0.904228	0.003648	n.m.	0.021403	2.394688	0.007171	1.91E-06
10	nw-5	25.65	50.85	3	avg	0	0	0.002091	0.092091	97.58366	0.912944	0.001569	n.m.	0.000431	1.425513	0.305274	1.09E-07
11	nw-5	25.45	51.2	3	avg	0	0	n.m.	0.050414	98.47947	0.375733	0.009554	n.m.	0.002601	1.000028	0.000192	3.62E-08
12	nw-5	24.85	52.55	6	avg	0	1	n.m.	0.226048	94.76998	0.786685	0.014091	n.m.	0.008654	4.092307	0.009307	9.34E-07
13	nw-5	24.65	52.2	3	avg	0	0	0.001815	0.316482	93.91556	4.300985	0.001487	0.009016	0.045496	1.428538	0.000017	1.73E-07
14	nw-20	9.15	62.59	3	avg	0	0	n.m.	0.002745	98.95562	0.455807	0.001397	n.m.	0.023524	0.473107	0.000291	8.91E-07
15	so-30	13.4	53.95	3	avg	0	1	n.m.	0.104233	93.63112	5.273134	0.01229	n.m.	0.005107	0.356902	0.02711	5.33E-07
16	so-30	13.15	54.2	3	avg	0	1	n.m.	0.166496	95.5478	1.149104	0.047713	n.m.	0.000195	0.123713	n.m.	1.23E-08
17	sw-30	12.0	54.5	3	avg	0	1	n.m.	0.035039	94.47929	1.152206	0.002049	n.m.	0.002125	0.317892	0.010003	1.95E-06
18	sw-30	12.45	54.85	6	avg	0	0	0.001319	0.081319	98.64156	0.307372	0.001789	n.m.	0.002694	0.894432	0.001605	2.8E-06
19	sw-30	12	55.95	6	avg	0	0	n.m.	0.269865	97.82672	1.110729	0.000809	n.m.	0.004159	0.779688	0.007069	1.91E-07
20	sw-30	11.8	56.38	6	avg	0	0	n.m.	0.054378	99.12448	0.340047	0.002049	n.m.	0.005046	0.521302	0.01875	1.26E-06
21	sw-36	11.3	56.25	6	avg	1	0	n.m.	0.225425	98.47142	1.8765	0.006672	n.m.	0.005468	0.41922	0.0002	1.8E-07
22	sw-36	11.25	56.45	3	avg	0	0	n.m.	0.092178	97.751	1.530762	0.020048	n.m.	0.064599	0.532512	n.m.	4.32E-06
23	nw-30	11.05	56.75	6	avg	0	0	0.002003	0.084180	98.46467	0.815633	0.007292	n.m.	0.034606	0.592653	0.000503	2.27E-06
24	nw-30	10.65	57	9	avg	0	1	n.m.	0.62957	92.152	3.557747	0.021474	0.021474	0.038977	4.539917	0.010591	5.31E-07
25	nw-30	10.7	57.25	3	avg	0	1	n.m.	0.075223	98.04908	0.753001	0.001162	n.m.	0.014822	0.500907	0.000401	7.01E-08
26	c-8	20.25	42.92	3	avg	0	1	n.m.	0.007324	98.29908	0.853912	0.000031	n.m.	0.354410	0.421381	0.000459	2.14E-08
27	c-8	27.7	41.05	3	avg	1	0	n.m.	0.061057	99.54311	0.225051	0.001103	n.m.	0.015015	0.120112	0.000293	1.02E-06
28	c-8	26.5	41.75	6	avg	1	0	n.m.	0.060474	99.45717	0.04629	0.04629	n.m.	0.002247	2.322511	0.000665	2.2E-06
29	so-23	10.15	26.1	6	avg	1	0	n.m.	0.22829	94.128808	0.313501	0.007553	n.m.	0.041173	5.176407	0.096371	1.21E-06
30	so-23	10.45	26	3	avg	0	1	n.m.	0.048695	97.90794	0.475303	0.000799	n.m.	0.01122	1.619508	0.027475	3.95E-06
31	so-23	8.55	28.19	3	avg	0	0	n.m.	0.006002	98.49205	0.204306	0.004033	n.m.	0.003083	0.414518	0.00849	4.20E-08
32	nw-23	7.2	29.85	3	avg	1	0	0.000794	0.159185	97.58805	1.530608	0.000031	n.m.	0.01122	0.707901	0.00168	2.2E-07
33	no-23	8.25	30.31	9	avg	0	0	0.001192	0.257928	96.21217	2.136115	0.004102	0.018078	0.010165	1.363109	0.003904	1.59E-06
34	no-23	8.25	30.65	3	avg	0	0	0.001295	0.057741	97.82111	1.605225	0.003102	n.m.	0.038977	0.484515	0.000594	1.79E-06
35	nw-14	8.35	30.9	2	avg	0	0	0.009990	0.050317	99.73165	0.060912	0.001494	0.024064	0.001104	0.140308	0.000104	9.93E-08
36	nw-23	6.75	32.95	3	avg	0	0	0.00752	0.110407	98.70647	2.759935	0.004604	0.024064	0.022044	0.292373	0.00757	5.73E-08
37	nw-23	9.5	32.5	6	avg,alt x	0	0	0.001841	0.091278	97.80301	1.304187	0.011034	0.004569	0.159000	0.708472	0.010997	2.16E-08
38	no-23	7.75	32.95	3	avg	1	1	0.000401	0.070736	96.71602	7.480002	0.130033	0.001787	0.159009	5.157095	0.010437	9.06E-07
39	so-14	7.85	33.7	3	avg	0	0	n.m.	0.13316	95.4191	3.567153	0.018392	n.m.	0.037374	0.02428	0.000538	3.06E-07
40	sw-6	10.1	48.1	3	avg	0	0	n.m.	0.657009	94.70214	3.25300	0.003010	n.m.	0.008760	1.19005	0.000104	4.2E-08
41	nw-6	17.02	48.1	3	avg	0	0	n.m.	20.303007	0	1.147932	1.147932	n.m.	0.103502	11.21004	0.071447	4.30E-08
42	nw-6	10.22	49.65	9	avg	0	0	0.001841	0.091278	97.80301	1.304187	0.011034	0.004569	0.708472	0.708472	0.010997	2.1E-06
43	nw-6	10.40	49.9	3	avg	1	0	0.00018	0.20732	96.716002	7.480002	0.130033	n.m.	0.159009	5.157095	1.05E-07	7.6E-07
44	nw-6	10.05	51.25	3	avg	0	0	n.m.	0.327574	90.62452	6.067244	0.04207	n.m.	0.015510	2.062073	0.003001	1.84E-07
45	sw-6	10.2	49.41	2	avg	0	0	n.m.	0.062076	99.64793	0.059903	0.003908	0	0.002032	0.214537	0.000209	2.72E-08
46	nw-6	19.4	50.15	9	avg	0	0	n.m.	0.095244	98.84925	1.902275	0.00508	n.m.	0.012703	1.040400	0.000109	2.07E-08

Steeple Rock Data Base of Fluid Inclusion Gas Analysis

Sample averages

sample #	section	x	y	analysis/sample	Sulf 1=yes 0=no	Lat co.	Ore	He	CH4	H2O	N2	H2S	Ar	Celta	CO2	SO2	1
47	nw-7	20.0	45.85	3	0	0	1	n.m.	0.152355	98.70288	2.02218	0.008147	n.m.	0.006027	0.075020	0.033183	5.05E-07
48	nw-7	19.80	45.85	3	0	0	1	n.m.	0.185002	98.4715	0.755535	0.008405	n.m.	0.001594	0.578105	0.0202200	4.52E-07
40	nw-7	18.85	45.85	3	0	0	1	n.m.	0.126828	94.88740	3.202250	0.002054	n.m.	0.005487	1.005002	0.000594	7.40E-07
60	nw-7	18.3	40	3	0	0	1	n.m.	0.091340	99.4171	0.143007	0.001000	n.m.	0.002248	0.210070	0.000076	7.30E-04
63	ne-20	27.7	31.15	3	0	0	0	n.m.	0.093512	98.93387	0.305202	0.001808	n.m.	0.000118	0.545657	0.010144	4.22E-04
64	ne-20	29.26	31.35	0	0	0	0	n.m.	0.104208	97.21304	1.437248	0.018280	0.000111	0.000128	1.413305	0.011303	4.07E-04
65	ne-10	1.05	38.02	0	0	0	0	0.003411	0.012714	99.75000	0.127151	0.000725	n.m.	0.000008	0.005510	0.000510	7.04E-09
56	ww-10	1.25	40.01	3	1	0	0	n.m.	0.248828	97.4242	1.300483	0.003057	n.m.	0.003001	0.035502	0.033052	8.91E-08
57	ne-15	2.65	37.68	3	0	0	0	n.m.	0.2250622	99.23150	0.235002	0.000229	n.m.	0.001074	0.320070	0.011200	1.20E-08
58	nw-14	8.35	38.80	3	0	0	0	n.m.	0.790774	99.05841	0.018300	0.000453	n.m.	0.035770	0.100078	0.003033	3.07E-07
59	nw-14	8.74	37.05	3	1	1	0	0.00003	0.198340	98.93051	0.431701	0.021012	n.m.	0.024130	0.721471	0.231471	8.55E-08
66	nw-14	7.31	36.72	3	0	0	1	n.m.	0.11338	98.37800	1.050015	0.01459	n.m.	0.001028	0.419531	0.014484	1.2E-07
61	ww-30	8.01	53.05	2	0	0	0	0.001437	0.2100002	95.87251	2.007875	0.004270	0.02348	0.001411	0.000202	0.001070	5.05E-07
62	ww-11	8	41.88	3	0	0	0	n.m.	0.471032	98.10788	0.41904	0.002041	n.m.	0.001105	0.380640	n.d.	2.32E-08
63	nw-11	8.35	41.05	3	0	0	0	0.001403	0.037590	90.73104	0.003358	0.000008	0.000711	0.001314	0.530774	0.000104	8.1E-07
64	ww-2	4.98	46.02	3	0	0	0	n.d.	0.103340	98.83051	0.43701	0.000043	n.m.	0.003051	0.172447	2.60E-05	5.74E-07
65	ww-2	4.05	45.05	3	0	0	0	0.00003	0.740088	98.09032	0.460046	0.001301	0.000058	0.003425	0.84021	0.000437	3E-08
66	nw-11	9.01	45.8	2	0	0	0	n.m.	0.1046	99.16840	0.550058	0.004270	n.m.	0.001411	0.165151	0.000206	9.18E-08
67	nw-11	8	45.05	3	0	0	0	n.m.	0.364443	94.395453	7.376E-05	0.000274	n.m.	0.001105	0.386640	n.d.	2.32E-08
68	nw-11	8.35	44.55	3	0	1	0	n.d.	0.403004	98.78305	0.823874	0.000070	0.000711	0.003121	0.530774	0.000181	8.5E-07
69	nw-11	8.77	44.1	3	0	0	0	n.d.	0.11293	83.86279	13.388005	0.000000	n.m.	0.002250	0.812075	2.50E-05	8.74E-07
70	nw-11	8.8	43.05	3	0	0	0	0.007051	0.007051	98.37077	0.871590	0.000003	0.000005	0.004013	0.855127	4.42E-05	1.27E-08
71	nw-11	7.2	43.7	3	0	0	0	n.m.	0.71603	95.77803	2.463007	0.000027	n.m.	0.003008	1.037035	8.0E-05	3.90E-08
72	nw-11	8.05	42.05	3	0	0	0	0.000051	0.076243	98.35010	0.013712	0.000010	0.000017	0.007761	0.345047	0.001184	4.05E-07
73	ww-2	7.75	41.04	3	0	0	0	0.000851	0.078243	98.35010	0.013712	0.000504	0.000017	0.004328	0.250018	2.40E-05	8.1E-07
74	ww-2	8.05	48.35	3	0	0	1	n.m.	0.042035	98.84001	0.154044	0.001100	0.000711	0.003002	0.195554	1.05E-08	1.4E-08
76	ww-1	13.5	47.50	3	0	0	1	n.m.	0.417083	97.35505	1.453230	0.000001	n.m.	0.001933	0.737304	0.000228	3.2E-08
77	ww-2	8.7	40.70	3	0	0	0	n.m.	0.148181	90.51103	0.050445	0.002714	n.m.	0.00111	0.208751	0.000002	8.02E-08
78	ww-2	8.92	40.2	2	0	0	0	n.m.	0.302	94.54207	0.000183	0.000010	n.m.	0.001602	0.345047	8.40E-07	3.44E-08
79	ww-2	8.45	40.45	2	0	0	0	n.m.	1.050300	93.35000	4.903107	0.000504	n.m.	0.00101	0.50018	8.1E-07	1.31E-08
80	ww-11	8.81	41.83	3	0	0	0	n.m.	0.340737	95.37073	2.054185	0.000748	n.m.	0.003320	1.31534	2.20E-08	2.20E-08
81	ww-11	8.55	41.75	3	0	0	1	n.m.	0.180107	92.77800	8.348975	0.007205	0.005903	0.003233	0.802277	0.023129	3.02E-08
82	ww-11	8.42	42.12	3	0	0	0	n.m.	0.583818	94.60780	3.307320	0.002272	n.m.	0.003084	1.200804	0.000221	8.02E-08
83	ww-11	8.92	40.44	3	0	0	0	n.m.	0.034704	95.31644	3.202242	0.004455	n.m.	0.004480	0.535000	8.40E-07	3.44E-08
83A	ww-11	8.92	40.45	6	0	0	0	n.m.	1.007004	94.48101	3.562325	0.000010	n.m.	0.00003	0.804702	n.m.	8.72E-08
83B	ww-11	8.92	40.46	4	0	0	0	0.000208	0.290430	97.98006	2.055348	0.002035	0.001580	0.005320	0.500500	0.001101	3.73E-08
84	ww-11	7.26	30.76	3	0	0	0	n.m.	0.039088	96.30848	0.205100	0.010003	n.m.	0.005301	0.278737	0.010101	2.51E-07
85	ww-14	7.37	39.45	3	0	0	0	n.m.	0.127340	99.27400	0.314821	0.000000	n.m.	0.002308	0.278786	0.000205	3.5E-07
86	ww-11	8.65	40.73	3	0	0	0	n.m.	0.180011	94.22331	1.098008	0.002010	n.m.	0.004270	0.405053	0.000205	4.58E-07
87	ww-11	8.92	40.93	2	0	0	0	0.017803	0.303120	91.80424	2.001032	0.005063	0.017803	0.027033	5.008415	0.001181	1.00E-07
87A	ww-14	8.5	34.28	2	0	0	1	n.m.	0.012941	97.91804	0.284050	0.000112	0.000002	0.000802	0.880100	2.20E-08	2.20E-08
88	ww-14	8.55	35.78	3	0	0	0	n.m.	0.45014	92.84704	4.505811	0.004240	n.m.	0.005501	2.132903	n.d.	4.05E-08
89	mw-14	7.8	36.07	3	0	0	0	n.m.	0.531719	88.37127	10.881E	0.007074	n.m.	0.015303	2.304005	n.d.	1.00E-07
90	mw-1	13.35	40.60	3	0	0	1	n.m.	0.16809	97.31128	1.804005	0.011058	n.m.	0.010452	2.222228	0.078730	8.97E-08
91	sw-1	13.21	40.93	3	1	1	1	n.m.	0.71094	98.02275	8.713002	0.000007	n.m.	0.002744	1.034004	3.45E-05	3.70E-08
92	sw-1	12.3	40.35	2	0	0	0	n.m.	1.153022	92.84428	4.112044	0.000607	n.m.	0.010103	2.133703	5.01E-08	5.01E-08
93	sw-1	11.75	51.05	2	0	0	0	0.037002	0.037002	98.31312	n.d.	0.001020	n.m.	0.001040	0.149040	n.m.	9.71E-09

Steeple Rock Data Base of Fluid Inclusion Gas Analysis

Sample average

sample #	section	x	y	analysis/sample	1=yes 0=no Buff	Let cc	Ore	He	CH4	H2O	N2	H2S	Ar	C2H6	CO2	SO2	1
94	sw-1	11.85	52.27	3				0.001309	0.800005	01.00208	8.900088	0.000350	0.017708	0.181844	1.157759		3.55E-08
95	sw-1	12.05	53.82	5				n.m.	0.002421	90.43192	0.060402	0.010242	n.m.	0.002075	0.825022	0.004805	2.30E-08
96	nw-1	12.15	52.35	2				n.m.	2.040002	95.53348	n.d.	0.011034	n.m.	0.011884	0.377837	0.011884	3.00E-08
97	nw-1	12.2	52.15	13				n.m.	0.243013	88.48021	5.722836	0.015524	n.m.	0.012115	2.000018	0.001705	2.87E-07
98	nw-1	13.7	52.05	5				0.001158	0.815205	84.21458	1.708116	0.008820	0.021123	0.037405	3.330327	0.000373	1.80E-07
99	sw-38	13.15	53.75	3		0		n.m.	0.860020	98.03114	1.151208	0.003362	n.m.	0.002472	0.825022	0.000304	1.87E-08
100	ne-1	16.52	53.21	3	0		0	0.000700	0.129032	90.20214	0.305200	0.001074	0.002277	0.017074	2.108671	0.000527	1.30E-07
101	ne-1	15.6	51.5	8	0		0	0.001234	0.302487	84.02207	3.211157	0.001408	0.001818	0.290014	3.90040	0.000208	8.3E-07
102	sw-31	17.3	53.7	3	0		0	0.000268	0.405044	97.5146	3.8278e	0.001453	0.044030	0.000814	1.737050	0.000311	3.12E-08
103	sw-31	16.4	56.8	3	0		0	0.000278	1.290479	07.27053	1.302504	0.000547	n.m.	0.002553	1.353481	9.11E-05	5.52E-08
104	sw-38	15.5	57.5	3	0		0	0.000103	0.396304	84.5487	2.953434	0.001002	n.m.	0.000203	0.553303	0.00011	1.40E-08
105	sw-38	15.1	57.2	3	0		0	n.m.	0.80057	84.03207	3.151208	n.m.	n.m.	0.002472	2.104345	0.000202	3.33E-08
106	sw-31	17.4	55.0	3	0		0	n.m.	0.190134	94.79361	1.101102	0.001108	n.m.	0.017074	2.108671	0.000527	1.87E-08
107	sw-38	17	55.75	3	0	1	0	n.m.	0.202705	84.1783	3.8278e	0.001453	n.m.	0.001453	3.90040	0.000311	8.3E-07
108	c-18	33.3	53.25	3	0		0	0.00103	0.209205	96.25001	1.302504	0.001200	0.044030	0.002533	2.624004	0.002233	3.12E-08
109	c-18	35.1	35.4	3	0		0	0.0007785	0.210205	03.20048	5.056030	0.008705	0.043374	0.000255	0.794004	0.001162	2.13E-07
110	sw-8	31.15	30.25	3	0		0	0.007769	0.010602	84.73762	0.870108	0.01301	n.m.	0.002203	0.301743	0.000508	1.30E-08
111	sw-8	20.5	40.42	3	0		1	0.00076	0.180547	90.23405	0.227290	0.00058	n.m.	0.001893	0.346803	0.000423	2.50E-07
112	sw-8	32.85	43.45	3	0		1	0.000076	0.301090	97.11834	0.000033	0.007674	n.m.	0.002450	2.462330	0.002057	5.47E-07
113	sw-8	31.3	46.3	3	0		1	0.000278	0.04237	97.27053	1.300235	0.001300	n.m.	0.011822	0.420105	0.0011001	1.77E-08
114	ne-8	22.65	53.1	8	0	1	1	0.000763	0.785063	81.7244	8.721277	0.002518	n.m.	0.048061	4.020327	0.004931	1.03E-07
115	c-7	20.9	42.35	3	0	1		0.000579	0.481479	90.31118	2.745465	0.003101	n.m.	0.002450	0.712064	0.001172	4.21E-08
116	c-7	20.2	42.68	3	0			0.000208	0.08554	98.081e2	0.200043	0.000103	n.m.	0.002227	0.421283	0.000103	3.11E-08
117	sw-1	18.05	46.47	2	0		0	0.00059	0.593392	93.3730	1.90077	0.001275	n.m.	0.003274	0.543308	0.000183	2.85E-08
118	ne-15	21.0	35.68	3	1	1	0	0.000335	1.040018	93.73730	4.737082	0.002518	n.m.	0.004421	1.202008	0.000303	1.52E-07
119	nc-15	21.03	35.71	2	0		0	0.000014	0.10024	95.07418	2.093060	0.021402	0.021402	0.000108	0.956201	0.000189	2.35E-08
120	nc-15	21.3	35.7	3	0	1	0	0.000807	0.052044	90.55007	0.074314	0.002057	0.001004	0.033418	0.284076	0.001817	2.9E-08
121	ne-15	18.0	38.3	2	0		0	0.000003	0.461000	97.73730	0.817500	0.002726	0.003310	0.005820	0.852003	0.000370	3.76E-08
122	ne-15	18.0	36.33	2	0		0	0.000000	0.377004	98.1708e	0.220043	0.000103	0.002040	0.014220	1.180311	0.000020	1.07E-07
123	sw-10	20.78	36.62	2	0		0	0.000014	0.040445	95.08774	0.001091	0.001004	0.000037	0.014570	0.160001	0.000400	1.03E-05
124	sw-10	20.76	35.55	3	0		0	0.000014	0.10024	93.23100	1.131524	0.00069	0.07212003	0.053004	0.163008	0.000207	8.4E-07
125	nw-10	22.8	42.7	3	0		0	0.001157	0.152042	90.78012	0.072004	0.001306	0.001257	0.002285	0.253064	0.000530	3.03E-08
126	nw-10	22.31	42.9	2	0		0	0.000204	0.045229	90.05078	0.047107	0.001102	0.011105	0.001925	0.100264	0.000350	1.59E-07
127	nc-0	28.48	43.8	2	0		0	0.00221	0.055078	90.89107	n.d.	0.001557	0.00052	0.001523	0.000058	0.000051	5.25E-08
128	nc-0	28.5	43.0	2	0		0	0.001608	0.048135	90.72108	0.052281	0.00203	0.02574	0.002084	0.242704	0.001108	4.07E-04
129	nc-4	26.3	40.05	3	0	1	0	0.00104	0.055412	90.57305	0.115795	0.001306	0.00004	0.002500	0.160021	0.003007	3.40E-05
130	nc-4	28.4	40.07	3	0		0	0.00047	0.05022	90.7612	0.072004	0.001740	0.001257	0.001823	0.500034	0.000008	1.05E-08
131	ne-4	27.35	47.8	3	0		0	0.000002	0.279103	04.50460	3.865739	0.000000	0.02e614	0.01823	1.002200	0.001431	1.0E-05
132	ne-4	27.3	45.35	3	0		0	0.000805	0.05784	94.4780	0.101737	0.000755	0.025743	0.014240	0.347724	0.000014	7.54E-04
133	ne-4	27.3	45.38	3	0	1	0	0.00104	0.10704	90.21202	0.378042	0.0008	0.0008	0.002430	1.270003	0.000033	1.75E-04
134	nc-35	26.15	58.05	3	0	1	1	0.002040	0.058000	90.76244	0.00727	0.001441	n.d.	0.001208	0.050007	0.000063	3.27E-04
135	nc-35	8.1	59	3			1		0.14810	90.41701	1.103409	0.00202	0.0301	0.002030	0.152020	0.000205	3.05E-07
136	nc-35	8.1	58.4	3	0	1	1	0.00186	0.150003	00.82101	0.320371	0.0002	0.02043	0.042230	0.280902	0.000484	5.22E-07
137	ne-35	8	59.3	3	0	0	1	0.004035	0.210518	08.17854	0.020371	0.001855	0.001010	0.01823	0.541051	0.000400	8.80E-08
138	ne-35	8	50.3	3	1	0	0	0.00104	0.112112	90.17854	0.101737	0.001504	0.0001855	0.01823	0.347724	0.000040	8.54E-04
139	cp	60.82		2	0			0.001735	0.049025	00.12008	1.462810	0.001054	0.092000	0.01823	0.074023	0.000014	1.75E-04
140	cp	62.50		3		0		n.d.	0.200002	07.22181		0.003007	0.00322	0.001103	0.074023	0.000123	2.42E-07
141	cp	64.05		3	1	1	0	0.001008	0.200002	04.82256	2.9030	0.001034	0.01148	0.017302	2.339507	0.000200	4.81E-07
142	cp	64.03		3		1											
143	cp	65.0		3													

Steeple Rock Data Base of Fluid Inclusion Gas Analysis
Sample averages

sample #	section	x	y	analysis/sample	1=yes 0=no Sulf	La1 co	Ore	He	CH4	H2O	N2	H2S	Ar	Cn/n	CO2	SO2	
144	cp	4.30	85.52	3	0	0	0	0.002374	0.045868	99.62303	n.d.	0.004200	n.d.	0.003108	0.318141	0.00254	3.00E-05
145	ss-1	15.83	48.33	3	0	0	0	0.001008	0.055823	99.7880	n.d.	0.002870	n.d.	0.002332	0.148023	0.001513	7.57E-08
146	ss-1	15.68	48.44	3	0	0	1	0.001807	0.040560	99.82041	0.030304	0.002041	0.000404	0.002218	0.000078	0.002342	8.00E-08
147	ss-1	15.4	48.04	3	1	0	1	0.000332	0.418478	84.29437	0.710159	0.000190	0.000190	0.003205	0.625500	n.d.	5.50E-08
148	ss-1	15.55	48.68	3	1	0	1	0.000279	0.122224	99.25121	0.981208	0.000205	0.001758	0.002198	0.342440	0.04E-05	1.80E-07

This thesis is accepted on behalf of the faculty
of the Institute by the following committee:

Donald L. Norman
_____
Adviser

_____

_____

_____

Sept. 16, 1993
_____
Date